Performance Evaluation of Hybrid and Predictive Controllers In Remote Surgery

Vivian Chai

Thesis submitted to the University of Ottawa
in partial Fulfillment of the requirements for the
Master's in Applied Science degree in Mechanical Engineering

Department of Mechanical Engineering
Faculty of Engineering
University of Ottawa

Abstract

Telerobotics are becoming increasingly more prevalent in the medical field due to the many advantages they have over standard methods. In particular, their use in surgical procedures provides benefits such as safer operations and greater health care access, among others. However, there are drawbacks that dissuade telerobotic usage and aspects that can still be improved upon. Examples of these include the inevitable impact of time delay and the existence of disturbances, such as patient-manipulator contact. These factors can result in system destabilization and ultimately task failure, discouraging the usage of telerobotics in these settings.

This thesis investigates the effects of time delay and contact disturbances on telerobotic performance in a surgical setting. In this work, different methods of improving telerobotic performance such as using hybrid controllers and predictive technology are explored. The goal is to investigate options for mitigating the negative effects of these elements while improving overall telerobotic performance.

Dedication

This work is dedicated to my family and friends who have supported me through these difficult times. I am forever grateful to the people who didn't lose faith in me and continued to encourage me throughout.

Acknowledgements

This thesis could not have been possible without the help and support of the people around me who have, in many ways, contributed to the completion of this study.

First, I would like to express my sincere gratitude to my supervisor, Dr. Dan-Sorin Necsulescu, who gave me the opportunity to research this topic. His expertise, guidance, and time have been invaluable in helping me to refine and finish this work. I have learned so much from him and it is with his help that this journey has been made possible.

I am grateful to my friends who have supported me throughout this entire endeavor. A special mention to my best friend who has been with me for many years and has been a source of mental strength. I could not ask for better people to be on my side during these challenging times.

Finally, I'd like to acknowledge my family, my parents and siblings, for everything they've done for me. To my parents, thank you for giving birth to me and raising me with love and care. And to my siblings, thank you for your life lessons, which have helped me to be who I am today. Special thanks to my sister who has always believed in me, even when I lost confidence in myself.

It is because of all these people that I was able to complete this degree successfully and I would like to express my deepest appreciation for all of them.

Table of Contents

List of Figures

List of Tables

Abbreviations

CAD – Computer-Aided Design

DOF – Degree of Freedom

dVRK – da Vinci Research Kit

MIS – Minimally Invasive Surgery

MPC – Model Predictive Controller

MTM – Master Tool Manipulator

PID – Proportional-Integral-Derivative

PSM – Patient Side Manipulator

1. Chapter 1: Introduction

Medical telerobotics refers to a medical treatment performed by bypassing an obstruction via a communication network [1]. These treatments are carried out using a user-controlled master console and a slave console, a semi-autonomous robot that moves based on directions given from the master. There are two types of telerobotics: short-distance, where the consoles are close to one another and the barrier is physical, and long-distance, where the barrier represents a significant distance between the two consoles. For some long-distance telerobotics, an external location for communication transmissions may be established. Telerobotics are beneficial, as they enable procedures without direct contact between patient and surgeon.

At present time, telerobotic surgery is a major topic of interest for medical treatments. Generally, robotic surgeries are less invasive than regular surgeries, reducing patient recovery time, blood loss and other surgical complications [2]. In addition, they are suitable for procedures where the transmission of diseases is possibility [1]. Robots can also provide a greater range of motion when compared to a surgeon's hand [3]. Furthermore, specialized surgical procedures can be carried out in areas that would not otherwise have access to these treatments and groups of specialists can be gathered for operations [4]. These advantages encourage the technological advancements of robotics in this field.

Today, many teleoperated robots are designed for minimally invasive surgery (MIS), for procedures where versatile tools are inserted into small incisions in the patient's body [5]. These robots have various sensors for relaying crucial information, such as position and force feedback, to the master controller. Furthermore, competent MIS robotic systems have complex and capable setups to improve the hand-eye coordination, giving the operator the feeling of being at the surgical site. A few telerobotic MIS systems are described below.

1.1 Existing Minimally Invasive Surgical Systems

1.1.1 SOFIE System

The SOFIE (Surgeon's Operating Force-Feedback Interface Eindhoven) is a short-distance teleoperated robot, developed by Dr. Ir. Linda van den Bedem in fulfillment of her doctoral degree. It is the first medical telerobotic system capable of sending force feedback data to the operator [6]. The master console consists of a series of joysticks on a control panel, while the slave console is a multi-DOF manipulator shown in Figure 1. Information from sensors, located at the slave console, is relayed back and processed to generate counter-pressure forces in the master console. These forces increase and decrease the resistance in the joysticks to mimic contact with a surface. Compared to other existing medical telerobotics, the SOFIE system may not be as well known, however, it serves as an important technological advancement and provided a foundation for developing more realistic operating conditions for surgeons.

Figure 1: SOFIE Robot. [1]

1.1.2 RAVEN System

Another research-based MIS system is the RAVEN, a two-armed surgical system designed for long-distance operations [1][7][8]. Components at the surgeon site include two PHANTOM Omni controllers, one for each arm, a foot pedal for camera control, a display, and a user interface. At its slave site, there are various sensors and a camera, which are used in collaboration to relay signals, haptic and visual, via a communication network. Developed in the United States of America, these robots are open-source and can be found in various educational institutions across the country, with the purpose of furthering research in the field. The main objective for its development was to improve collaborative efforts between multiple surgeons, located in different areas, by using more than one RAVEN system at a surgical site [9], as shown in Figure 2.

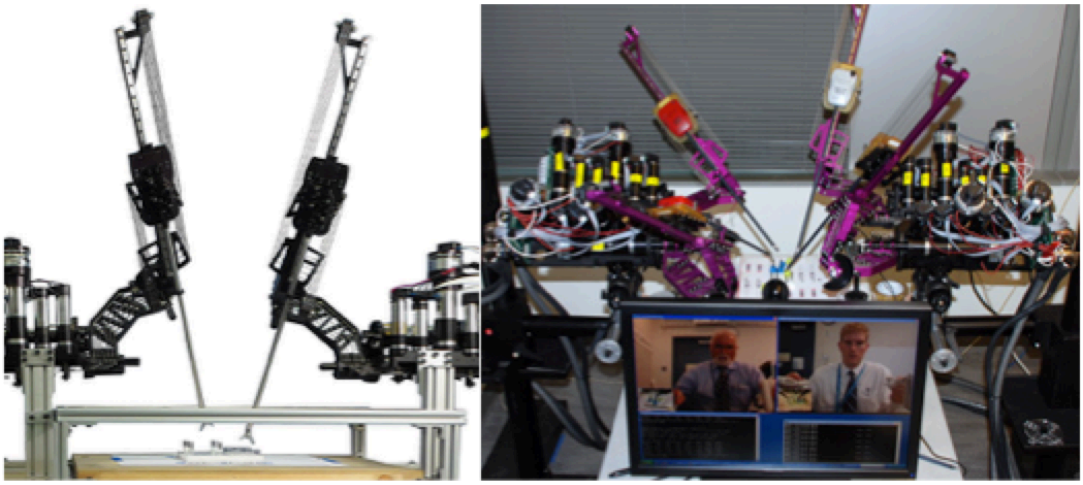

(a) **(b)**

Figure 2: RAVEN (a) Arms at Surgical Site (b) Collaborative Efforts between Two Systems. [8][9]

1.1.3 ZEUS Surgical System

The ZEUS surgical system is one of the most renowned medical robots, as it successfully performed the first telerobotic surgery in 2001 [10]. The procedure, called the Lindbergh operation, was a gall bladder removal operation with the patient lying in France and the surgeon operating from New York.

The ZEUS robot consists of two operating arms, each with 5-DOF, and an endoscope arm for viewing. A user interface, with various handles for moving the arms, and a high-quality video display are located at the operator site. Years after its development, the ZEUS surgical system was used in combination with the AESOP (Automated Endoscopic System for Optimal Positioning) system, a voice-controlled computer used for endoscope manipulation. This pairing effectively reduced the amount of controls required by the surgeon for operating [11]. Figure 3 shows the original ZEUS robot setup as well as the AESOP unit that was implemented later.

(a) (b)

Figure 3: (a) ZEUS Surgical Robot (b) AESOP Endoscope Voice Control Unit. [12][13]

Although the ZEUS system is no longer used today, it serves as a major landmark, as it marks the first time the effects of communication latency were overcome in a surgery.

1.1.4 Da Vinci Surgical System

Perhaps the most well-known and advanced telesurgical robot to date is the da Vinci robot, created by Intuitive Surgical. Currently, it is the only general MIS robot that is available for commercial purchase [14]. The da Vinci robot is a surgical system that sports four arms at its slave site, three 7-DOF arms for operating and one for camera control [11]. At the operator site, the surgeon has a console, with two 8-DOF joystick arms and foot pedals for arm control, as well as a separate imaging console. To operate the system, the surgeon manually controls the joysticks arms at the operator site, and the movement is reflected in the motion of the arms at the slave site. Training is extensive

and includes studying the technical aspects of the system, simulation-based training, as well as observing, shadowing, partaking in supervised operations, and more [15][16].

The da Vinci system can be used for both regular robotic surgeries, by connecting the units with electric cables, or short-distance telerobotic operations, with consoles in the same room but separated by a physical barrier. Long-distance applications are not viable, likely due to the complexity of the robot.

Figure 4 below shows the three units of the da Vinci system: the master console, the slave console, and the imaging unit.

Figure 4: The da Vinci Robot Master Console, Slave Console, and Imaging Unit. [14]

1.2 Latency Issues

Even with today's advancements in technology, telerobotic surgeries still have many problems that have yet to be resolved. One of these issues is the latency in the

information transmission between sites, an unavoidable element in any telerobotic procedure. When comparing the effects of different time delays, studies have shown that processes with shorter time delays yield better performance than those with longer delays [17][18]. As surgeries require high performance results, limiting the effects of latency is crucial.

However, different methods of reducing latency can also have repercussions that negatively affect telerobotic surgery. One such case is using velocity control in attempts to negate time delay. From a study, it was found that latency effects can be reduced by lowering the velocity of the telerobotic slave manipulator [19]. While this may be a viable solution for some applications, in the case of surgeries, where procedures are time-sensitive, this approach is neither practical nor efficient.

Another example of these unfavorable effects is shown in the trade-off between time delay and the frequency bandwidth size, which also determines the amount quantity of information transferred. Short delays require to smaller bandwidths, resulting in less data needed to be transferred between slave and master. On the contrary, long delays require larger bandwidths, resulting in more information transfer [20]. For telerobotic surgeries, this trade-off is not beneficial, as large quantities of data, in the form of audio, visual, and haptic signals, are required for the surgeon to have a complete understanding of the environment. Furthermore, it was found that telerobotic procedures with acceptable time delays have a bandwidth frequency of only a few hertz, whereas humans are able to perceive up to 1000 hertz at a time [21]. Thus, when comparing a telerobotic operation to

an in-person operation, there is a significant lack of information. Without sufficient information from the surgical site, telerobotic surgeries can be very dangerous.

Alternatively, a possible method for reducing the effects of time delay is to modify or improve the equipment used for telerobotic procedures. This method was implemented in an experiment involving a long-distance telerobotic surgery between Japan and Thailand [4]. A new low latency CODEC system, developed by a Japanese research team, focused on increasing the compression speed for the images being relayed back to the operator. The results of the experiment showed a reduced time delay for longer distances, when compared to standard telerobotic procedures, while maintaining sufficient information to complete the operation.

Predictive control is also an attractive option used to compensate for latency problems. This type of technology implements a system model in the master side control to predict the response of a system without delay. In one study, a series of recurrent neural networks were used to generate the plant model [22]. Using the recursive behaviour of these networks, the controller makes linear estimations of the current dynamics of a non-linear system. The results of the neural network were satisfactory, with predictions being very similar to the actual output results, and improved as the simulation time increased. Other predictive control methods include prediction using a Smith predictor setup as well as model predictive control (MPC). Overall, predictive controllers appear to show promising results.

1.3 Objectives

The main objective of this work is to explore various scenarios that may affect telerobotic MIS performance. These scenarios will be performed in Matlab™ and Simulink™ and include: end effector contact with a tissue-like surface, the use of hybrid control, and implementation of corrective predictive control. Simulations with these effects will be subjected to varying degrees of time delay and performance will be compared and discussed. Conclusions taken from the simulation results will be used to devise next steps for future work.

1.4 Thesis Structure

This thesis consists of seven chapters, which look into the effects of different surgical considerations on the performance of MIRS systems. In particular, three scenarios are simulated and the control framework and environmental setup of each is covered. The chapters covering these simulations are adapted from previous papers, [23], [24], and [25], presented at the ICINCO 2021, MMAR 2021, and MMAR 2022 conferences respectively.

Chapter 1 begins with an introduction, outlining prominent telerobotic MIRS systems and discussing related latency issues. The objective of this work is also described in this chapter.

Chapter 2 provides a literature review of all topics needed to have a full understanding of the performed experiments. These topics include: time delay, various controllers and their setups, soft tissue behaviours, and manipulator models used in the simulations.

Chapter 3 covers the system kinematics and dynamics that are used to move and the simulation manipulators.

Chapter 4 contains the first set of simulations, which aim to explore the effects of contact with a tissue-like surface. For these simulations, the manipulator model engages with a soft tissue model, both lightly and heavily, and performance is examined.

Chapter 5 features the second set of simulations, which look into hybrid position-force control. Two types of hybrid controller setups, one with PID controllers and the other with MPC, are compared and results are discussed.

Chapter 6 focuses on the final set of simulations involving predictive control, namely using the Smith predictor and model predictive control. Results of these predictor simulations are compared and analyzed.

Chapter 7 closes out the work, drawing conclusions from all simulations and stating recommendations for possible future work.

2. Chapter 2: Literature Review

Presently, telerobotic surgery is a topic of interest that is actively being pursued, with various institutions and corporations working together to develop it. One corporation in particular is Intuitive Surgical, the creators of the da Vinci surgical system. They have provided an open-source platform, which contains models, electronics, and software of the da Vinci robot, to a number of research facilities and universities across the globe [26]. The aim is to have collaborative research efforts from around the world and encourage growth in the field.

A main area of current research for telerobotic surgery is the effect of time delay, as standard surgeries are not subjected to it. This delay negatively impacts system performance and represents one of its major disadvantages. Other subjects that may be further explored include the effects of different controllers and setups, as well as the impact of external disturbances on the system.

For simulation-based research, it is important to consider models for the both the robot and the environment. In surgery, this would be the robotic slave manipulator and the patient's body tissues respectively. Given their purpose, it is crucial that these models accurately capture the properties and behaviours of the components.

This chapter covers different topics pertaining to factors that affect telerobotic performance. This includes the effects of different lengths of time delay on performance and details about different types of controllers and setups. Furthermore, models for both

parts of the simulations will be described and presented. The goal is to develop a better understanding of the elements that must be considered when operating surgical robots.

2.1 Time Delay

All telerobotic operations have time delays, due to a combination of delays from image capturing, communications, signal processing for the controllers and many more factors, which cannot be prevented [19][27]. In particular, the image and audio processing, for visual and audio information transmission generates the majority of the delay [4]. From various studies, it has been shown that as the time delay increases, the number of moves required and the time to complete the task, as well as the number of errors all increase [28][29][30][31][32][33]. Furthermore, issues such as packet loss can increase time delay if the information must be sent again [4]. Table 1 below shows different time delays and their performance effects on the system gathered from various papers [28][34][35][36].

Table 1: Performance Effects of Various Time Delays.

Delay Length	**Performance**
No Time Delay	No effect.
< 300ms	Task duration increased, no performance effects.
300ms-500ms	Task duration increased, increase in errors.
500ms-700ms	Possible task failure, increase in errors.
700ms+	Task failure, error in every task.

It should be noted that tasks with time delays between 500ms - 700ms rely heavily on the operator's experience. More experienced operators may have less errors and succeed in tasks that inexperienced ones would fail [37].

From Table 1, it can be said that a telerobotic task is expected to be successful when the delay is 500ms or less, as the task is completed. With a greater delay, there is a chance of failure, and at a delay of 700ms or greater, the task is expected to fail.

2.2 Controllers

A controller is uses a combination of feedback signals, reference values, and internal operations to generate an ideal plant signal for completing a specified task. A variety of controllers and controller setups will be tested and compared in this thesis. These include the PID controller, MPC, hybrid controllers, the Smith predictor, and adaptive MPC. Descriptions of these controllers are provided below.

2.2.1 Proportional-Integral-Derivative Controller

The first controller discussed in this work is the Proportional-Integral-Derivative (PID) controller. It is the most commonly used controller for a variety of reasons, such as its ease of use and implementation, as well as its efficiency [38]. PID controllers are used for over 90% of applications in process industries, such pulp and paper, chemical, and refining industries [39][40].

The PID controller employs three different gain values, the proportional, integral, and derivative gains, and applies them to errors from the feedback. Each gain is applied to its corresponding error operation and the summation of these amplified errors is then used to generate an ideal actuating signal. Equation (1) below shows the general PID equation and Figure 5 shows the implementation of the controller setup in a system.

$$PID = K_P e(t) + K_I \int_0^t e(\tau)d\tau + K_D \frac{de(t)}{dt} \quad (1)$$

Where:

- K_P is the proportional gain
- K_I is the integral gain
- K_D is the derivative gain
- $e(t)$ is the error with respect to time

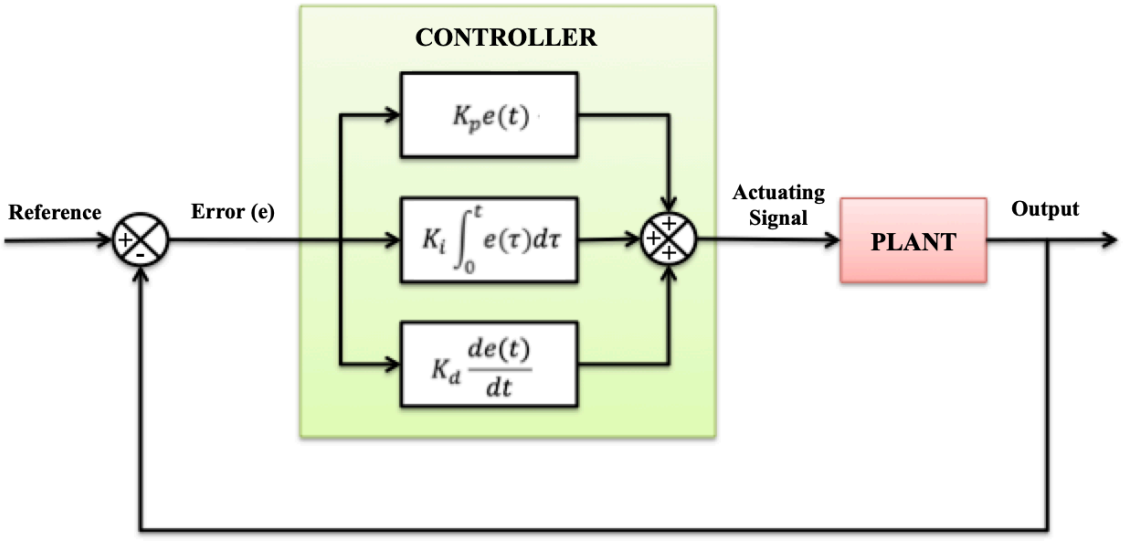

Figure 5: General PID Controller Setup.

The proportional gain acts to amplify or minimize the unaltered error using a tuned constant, with a value greater than 1 resulting in larger corrective actions and a value less than 1 resulting in smaller corrective actions [41][42]. This gain component leads to efficient minimization of large errors, however, is not very effective for correcting small errors. As the proportional gain affects only the current error from the feedback, it is often interpreted as the signal generated by looking at the present state of the system.

For the aforementioned small errors, the integral component is useful for reducing or eliminating them. From Equation (1), it can be seen that the integral term corresponds with the integrated errors, that is, the summation of errors from the start of the process to the current process time. Thus, the integral component is often interpreted as examining all past errors to generate an appropriate control signal [41][42]. As the summation of errors grows with each time step, it allows for corrective action even for small errors. This term will stabilize once the errors are no longer increasing, giving a constant steady-state error correction. However, its nature of using past values means that the integral component will react slowly to the current error, and therefore, cannot be used alone. In addition, the accumulated error acts to slow down the system, which worsens with the larger integral gain values, resulting in a longer response time.

Opposing the integral control, the derivative control is interpreted as looking at possible future errors, based on the error's rate of change. This component aims to minimize the rate of change, which would reduce oscillation and allow the system to stabilize faster [41][42]. However, oversaturation is a major concern for derivative control and can occur

when the error changes too rapidly. These changes result in large control efforts, making the system to become unstable [43].

As PID controllers use a combination of three gains to generate a single signal, it is important to consider the advantages and disadvantages of each, when tuning, and balance all three components to achieve the best system performance.

2.2.2 Model Predictive Controller

Another type of controller discussed in this work is the model predictive controller (MPC). MPCs are designed to reduce or negate latency by using a built-in plant state-space model to predict the expected state of a system when it is not subjected to time delay. The MPC state and output equations for the plant model are defined in Equations (2) and (3), while the general controller setup, with equation numbers, is shown in Figure 6 below.

$$x_{k+1} = A_k x_k + B_k u_k + w_k \tag{2}$$

$$y_k = C x_k + D u_k \tag{3}$$

Where:

- x_k is the predicted state for the current time step
- x_{k+1} is the predicted state for the next time step
- u_k is the current control signal
- y_k is the output of the system
- w_k is the process noise

- A_k is the state matrix
- B_k is the input matrix
- C is the output matrix
- D is the feedforward matrix

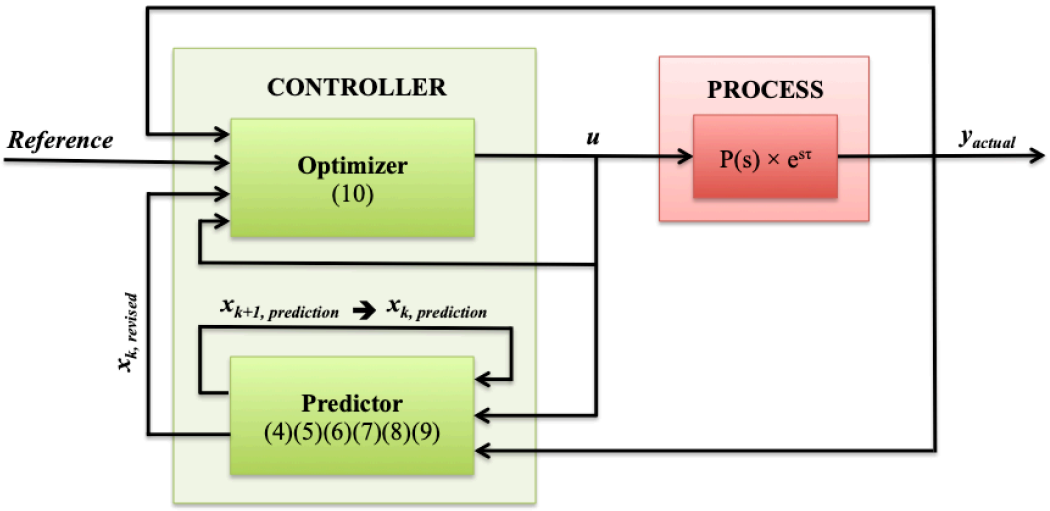

Figure 6: General Model Predictive Controller Setup.

From Figure 6, the MPC shows two distinct components: the predictor and optimizer.

During the predictor stage, possible output trajectory paths are generated over a specified number of time steps into the future, called the prediction horizon [44]. These trajectory paths are created using a combination of past-predicted values, as well past and current feedback and control signals. Comparing the input reference trajectory and predicted output trajectory, a control signal for each time step of the prediction horizon is created. Figure 7 below shows the MPC prediction process for a single trajectory output prediction at time step *k*. It can be noted that with each iterated time step, the new predicted value becomes more accurate and closer to the desired trajectory.

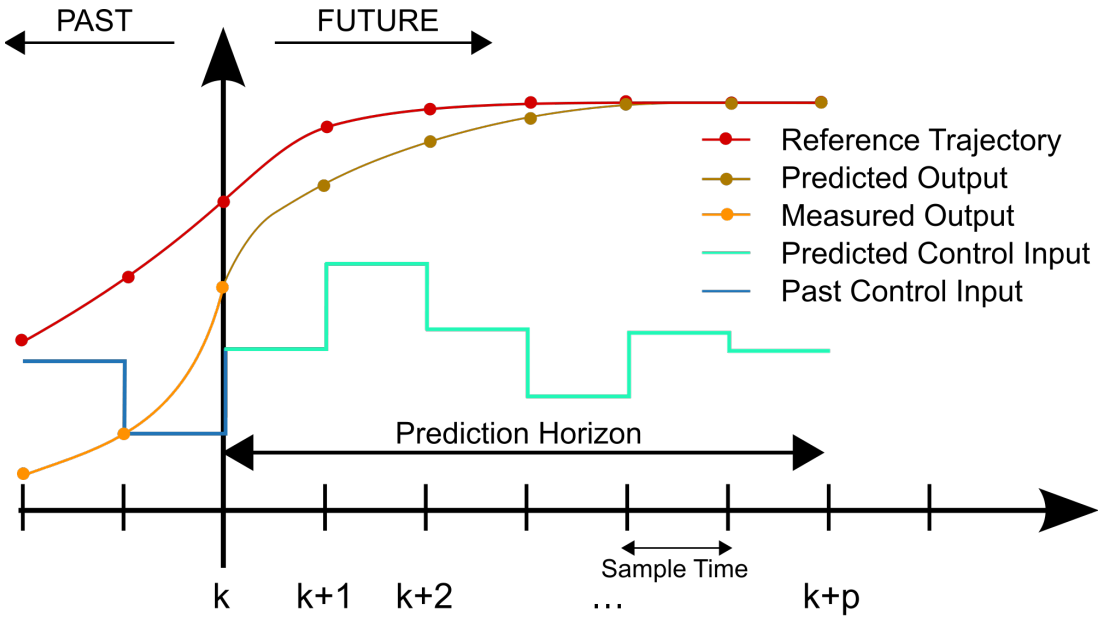

Figure 7: MPC Trajectory Output Prediction. [45]

In Matlab, the MPC state predictions for each subsequent time step *k* are calculated using Kalman filtering, an iterative process designed to reduce or eliminate noise in a system [46]. In Kalman filtering, a calculated gain value is applied to and affects estimates by giving more weight to either the predicted values or the measured values from the feedback. A Kalman gain value closer to 0 gives more weight to the predicted values, while a gain closer to 1 gives more weight to new measurements. Ideally, the calculated gain will reduce the effects of measured noise from the feedback, while also revising predictions to be more accurate.

In addition to estimating system states, the MPC also predicts the estimate covariance. The estimate covariance compares the estimate to the actual state and indicates how the accurate it is. Equations (4) and (5) below show the predictor equations for state estimate and the covariance respectively [47].

$$x_{k+1} = A_k \tilde{x}_k + B_k u_k + w_k \tag{4}$$

$$P_{k+1} = A_k \tilde{P}_k {A_k}^T + Q \tag{5}$$

Where:

- $\tilde{x}_k$ is the revised, predicted, current state for the current time step
- $\tilde{P}_k$ is the revised, predicted, current estimate covariance for the current time step
- P_{k+1} is the predicted estimate covariance for the next time step
- Q is process noise covariance, assumed to be white noise

Note that the state estimate, Equation (4), is the plant model state equation from Equation (2), but with a revised term, $\tilde{x}_k$. Likewise, the estimate covariance, Equation (5), also contains the revised term $\tilde{P}_k$. This revision involves applying the Kalman gain, shown in Equation (6) below, as well as adjusting the state estimate based on the measurement error, also called the innovation, shown in Equation (7).

$$K = \frac{P_k {C_k}^T}{C_k P_k {C_k}^T + R} \tag{6}$$

$$e_k = y_k - C x_k \tag{7}$$

Where:

- K is the Kalman gain
- P_k is the predicted estimate covariance for the current time step
- R is the measurement noise covariance
- e_k is the innovation

Thus, the revised state and estimate covariance are given as follows:

$$\tilde{x}_k = x_k + Ke_k \tag{8}$$

$$\tilde{P}_k = (1 - K)P_k \tag{9}$$

Note that a small innovation or Kalman gain value would indicate that the current predicted values are very close to the actual measurements.

Once updated, the predictions for the next time step, from (4) and (5), then become predictions for the current time step. The entire predictive process is then repeated for each time step along the entire length of the prediction horizon.

From the series of trajectories predicted via Kalman filtering, the best output trajectory is selected using optimization of a cost function [48]. The standard cost function employed in Matlab, shown by Equation (10) below, is the summation of four different costs that are minimized.

$$J = J_Y + J_{\Delta U} + J_U + J_\varepsilon \tag{10}$$

Where J is the total cost function.

The first cost variable of Equation (10), J_Y, represents the difference between the predicted output value and the desired value, the reference. Ideally, the magnitude of

these values will be the same, but factors such as noise can affect predictions. Variables $J_{\Delta U}$ and J_U both relate to the manipulated variable, the control signal. $J_{\Delta U}$ is defined as the difference between the previous and current control signal. This signal should not fluctuate significantly to prevent sudden movements of the system. The cost variable J_U compares the manipulated variable with the specified target. Generally, this cost will only affect systems that have more inputs than outputs or systems, as different combinations of inputs can produce the same output. With the implementation of a target value, these combinations would have the different costs, even with the same output. Finally, J_ε factors in the constraint limitations, such as restrictions due to singularities, or violation costs. The total cost includes summation of the costs for all the predicted outputs across the entire prediction horizon.

After selecting the best-predicted trajectory, based on the optimization cost formula, the control signal associated with the trajectory is generated. However, only the control signal at time *k* is applied to the plant, as the actual system state will change and may not follow the predicted trajectory. The MPC will then repeat the process for the next time step, computing various trajectories and optimizing at time *k*+1. This iterative process continues until the system completes its designated task.

However, as the plant model cannot account for external disturbances at the slave location, the prediction and actual feedback is expected to have disparities. These disparities are even more evident in systems with multiple outputs, such as a robotic arm in a telerobotic surgery, due to the effects of the estimates on one another.

2.2.3 Smith Predictor and PID Controller Setup

Predictors can also be implemented with other controllers to reduce or negate the effects of time delay on the system performance. In particular, the Smith predictor, which pairs a predictive plant model with a PID controller, is a frequently used setup that has shown promise in improving performance capabilities [49][50]. Figure 8 shows the general controller arrangement, which consists of two feedback loops: one with a plant model and the other with the actual process plant [51][52].

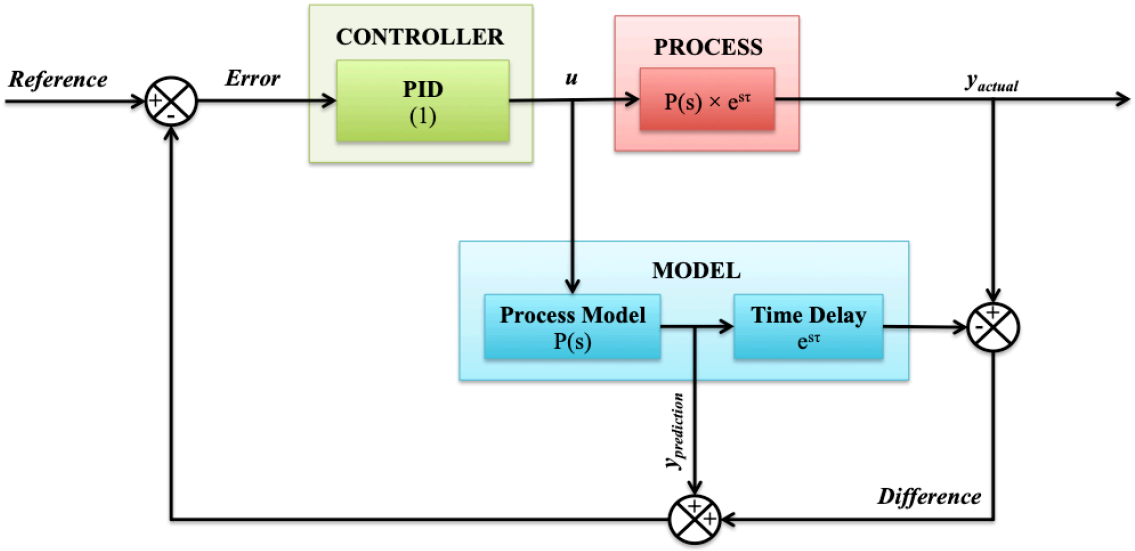

Figure 8: Smith Predictor Setup with Plant Model and PID Controller.

The outer loop acts as a standard feedback control loop, containing the process plant and providing the actual state of the system. For standard telerobotic operations, information from the regular feedback loop is delayed, thus the controller is does not receive up-to-date information about the state of the system. In the Smith predictor, the inner loop, which is not subjected to delays, generates and relays predictions to the controller,

allowing it to use up-to-date approximations of the plant with the intent of achieving a more accurate actuating signal. Ideally, the predictions and outputs from the two loops will be the same, but this idealized scenario is often not the case as factors such as external disturbances or noise may be difficult to account for.

To compensate for this error, the difference between the predicted output, implemented with a delay, and the actual output is calculated and summed with the current model prediction. This delay, shown on the right side of the blue model block in Figure 8, is an artificial delay applied to the non-delayed predictions from the inner loop of the Smith predictor. It is set to match the length of the actual delay from the outer loop process allowing comparison between the output values at the same time step. The summation of the error and prediction is considered the revised prediction and is the estimate of the current state with errors. Thus, the controller is able to correct for these past errors while also using approximate current states to generate more accurate control signals.

2.2.4 Adaptive Model Predictive Control

Adaptive model predictive control expands on the standard capabilities of MPCs by allowing the controller to adjust to changing system dynamics. This adaptation process uses adaptive gain values that are modified with each time step iteration [53]. In particular, adaptive control is beneficial for improving performance in environments with external forces or disturbances.

In Matlab, the adaptive MPC uses two adaptive gain values, one which is the Kalman gain, and the other which affects the two estimates, x_{k+1} and P_{k+1}. The new gain, L_k, is mathematically defined by Equation (11) below:

$$L_k = \frac{A_k P_k {C_k}^T + N}{C_k P_k {C_k}^T + R} \tag{11}$$

Where N is the covariance matrix between the process noise and measurement noise. The estimates x_{k+1} and P_{k+1} are then adjusted as follows:

$$x_{k+1} = A_k \tilde{x}_k + B_k u_k + L e_k + w_k \tag{12}$$

$$P_{k+1} = A_k P_k {A_k}^T - \left(A_k P_k {C_k}^T + N\right) {L_k}^T + Q \tag{13}$$

The remaining general equations MPC are the same as those used in standard MPC applications, as shown in Equations (6), (7), (8), and (9). In this way, adaptive control is easily implemented into MPC design but can greatly improve system performance.

2.2.5 Hybrid Controller

For cases where more than one state is observed and controlled, hybrid control is an attractive option. In a hybrid controller, the actuating signals are generated using two different laws, one for each state [54]. The laws can be formulated with different controllers, such as using PIDs or MPCs. Each degree of freedom (DOF) is associated with one of the laws and the summation of the signals is used as the final output of the

controller and input into the plant [55]. A common hybrid controller combination is the hybrid position-force controller, where the joints are assigned either a position control law or a force control law. Figure 9 below shows the basic formulation for a hybrid position-force controller.

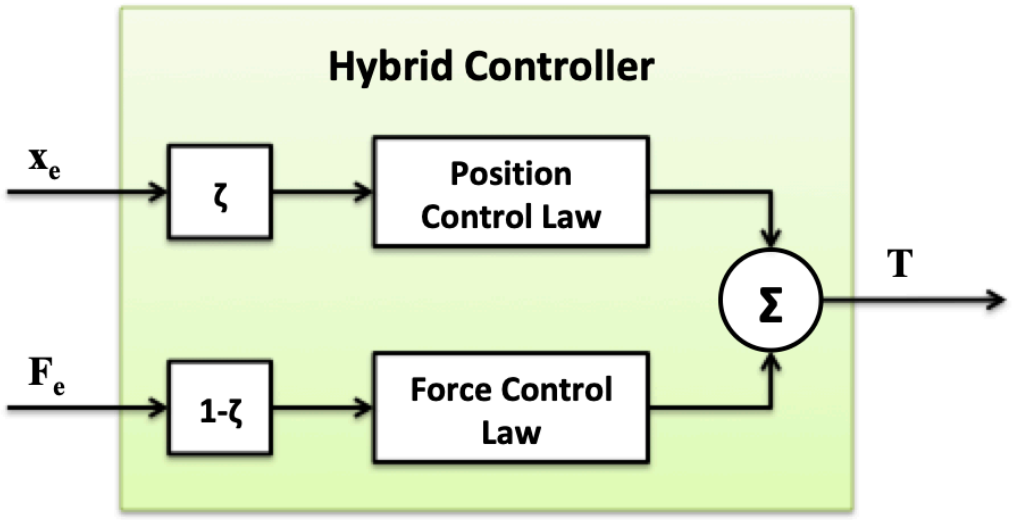

Figure 9: General Hybrid Position-Force Controller Setup.

The controller inputs are the respective errors and ζ is the compliance selection vector. This vector is a binary diagonal $n \times n$ matrix where n is the number of DOFs. A diagonal value of 1 designates position control, while a value of 0 would designate force control. The binary nature of the compliance values indicates that each DOF is entirely dependent on its associated law.

Although hybrid control is a relatively simple method of control, it allows the system to consider and control the effects of multiple states on the system performance.

2.3 Soft Tissue

To accurately simulate robotic surgery, the environment, namely the patient's body, must be modeled. However, the soft tissues that make up the body exhibit various behaviours, making it difficult to develop accurate mathematical equations to represent the tissues. Required information related to tissue modeling, such as soft tissue behaviour, current methods of modeling, and tissue force limitations are discussed below.

2.3.1 Soft Tissue Behaviour

The difficulties in modeling soft tissues stem from a variety of unique characteristics such as tissue hyperelasticity, viscoelasticity, and composition.

Soft tissues are hyperelastic materials, which means they have a non-linear stress-strain relationship derived from their non-linear strain-energy density functions [56]. A study, summarized in [57], showed that the derived stress-strain relationship for soft tissues is linear only if strain is within 1-2%, then becomes non-linear with increased strain. Thus, deformations do not occur uniformly. Figure 10 below shows general stress-strain tissue behaviour of hyperelastic materials, using test points and a curve of best fit to outline curvature. Various models, such as the Ogden, Yeoh, and Arruda-Boyce models [58], have been developed in attempts to capture this complex property of soft tissues.

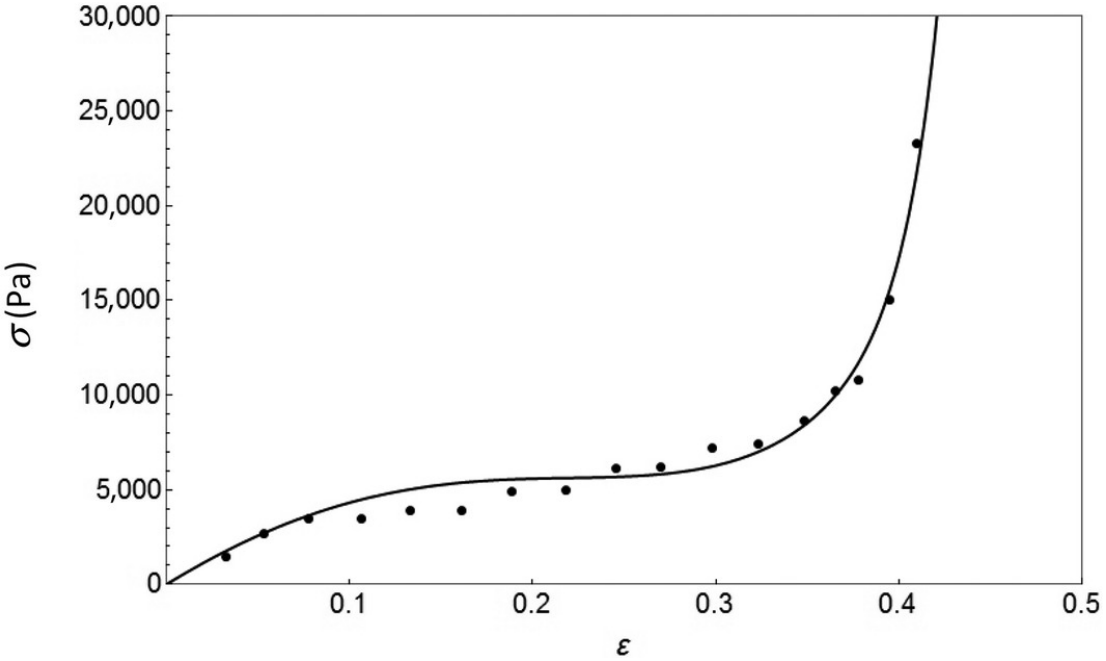

Figure 10: General Hyperelastic Soft Tissue Behaviour. [59]

Soft tissues also exhibit viscoelastic behaviour: with the 'elastic' term indicating that the tissues will return back to their original form after deformation and the 'viscous' term indicating that stress increases with strain [60]. The combination of these two properties causes a phenomenon known as hysteresis, where the material experiences energy loss and is slow to return back to its original form [61]. Figure 11 below shows the hysteresis process, with both loading and unloading processes, with the area between the curves shows the dissipated energy.

The compositions of tissues also affect the soft tissue behaviour. Tissues are made of different quantities of cells, elastin, collagen, and other components, set in different arrangements and at different orientations [62]. These quantities, arrangements, and orientations can change how the material reacts to various forces applied to it.

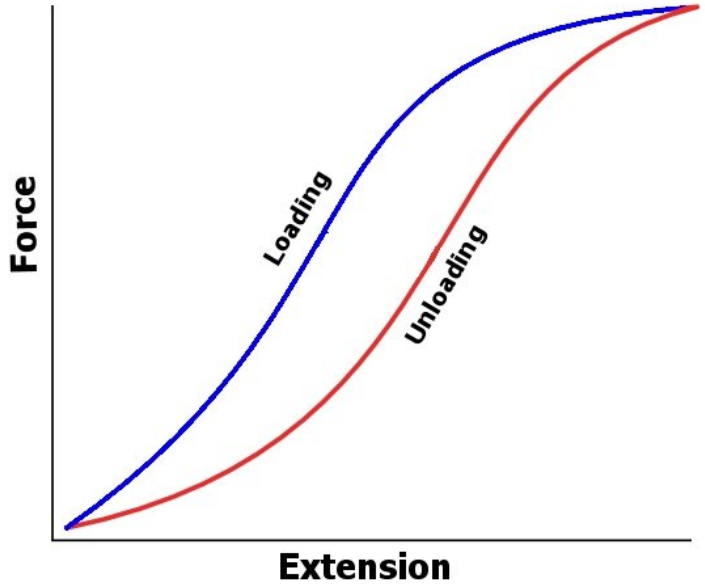

Figure 11: Hysteresis Plot with Loading and Unloading Processes. [63]

In addition, tissues also have general properties that influence their behaviours and interactions. These include elements such as frictional coefficients, tissue density, and more. Table 2 presents a list of general properties for skin tissues, which will be used in this thesis [64][65].

Table 2: Skin Tissue Parameters and Magnitudes.

Parameters	**Magnitudes**
Coefficient of Static Friction	0.52
Coefficient of Kinetic Friction	0.36
Skin Density (kg/m3)	1020

The combination of these factors, as well as many others, must be considered for simulating reactions with tissues. Furthermore, soft tissue properties differ depending on

the type of tissue (epithelial, muscle, etc.) and from patient to patient, adding more difficulty in predicting and modeling tissue behaviour.

2.3.2 Soft Tissue Force Limitations

In addition, tissue behaviour can change due to permanent damage when subjected to forces or pressures beyond their limitations. Even with its elasticity, soft tissues experience tears or plastic deformation once a specified threshold has been surpassed. A study on the mechanical properties of human skin indicate that skin tissue is able to resist a pressure of approximately 21.5 MPa before yielding [66]. Knowing this, the maximal, safe contact force on skin tissue can be resolved with Equation (14) below.

$$P(t) = \frac{F(t)}{A} \tag{14}$$

Where:

- $P(t)$ is the pressure on the surface with respect to time
- $F(t)$ is the force on the surface with respect to time
- A is the area of contact

As operations involve different movements, such as cutting through or holding skin tissues, the aspect of controlling the applied forces and pressures must be considered.

2.3.3 Soft Tissue Modeling

There have been many attempts to model soft tissue, most of which can be divided into three types: heuristic, continuum-mechanical, and hybrid models [62]. Heuristic models are composed of different arrangements and combinations of springs and dampers while continuum-mechanical models are derived from continuum mechanics laws. The last of these models, the hybrid model, combines aspects of both heuristic and continuum-mechanical models.

Of the three types of models, heuristic models, which are also called mass-spring-damper models, are considered the most basic. There are many varieties of these models, but the most popular ones include the Maxwell model, the Kelvin-Voigt model, and the Kelvin-Boltzmann (or Zener) model [57][67]. The arrangement of these models is shown in Figure 12 below and corresponding equations are shown in Equations (15), (16), and (17) respectively.

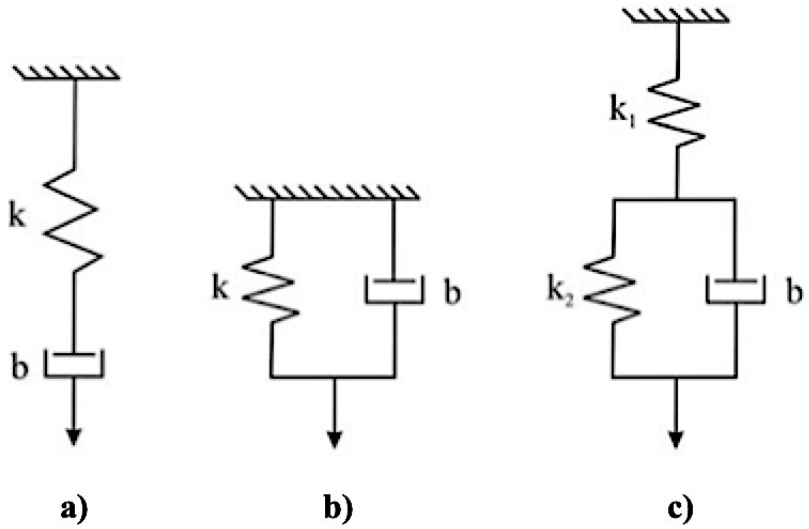

Figure 12: a) Maxwell Model b) Kelvin-Voigt Model c) Kelvin-Boltzmann Model. [57]

$$F_M(t) = b\frac{d}{dt}x(t) - \frac{b}{k}\frac{d}{dt}F_M(t) \tag{15}$$

$$F_{KV}(t) = kx(t) + b\frac{d}{dt}x(t) \tag{16}$$

$$F_{KB}(t) = \frac{k_1 k_2}{k_1 + k_2}x(t) + \frac{bk_2}{k_1 + k_2}\frac{d}{dt}x(t) - \frac{b}{k_1 + k_2}\frac{d}{dt}F_{KB}(t) \tag{17}$$

Where:

- $F_M(t)$ is the force applied by the Maxwell model with respect to time
- $F_{KV}(t)$ is the force applied by the Kelvin-Voigt model with respect to time
- $F_{KB}(t)$ is the force applied by the Kelvin-Boltzmann model with respect to time
- $x(t)$ is the displacement with respect to time
- k is the spring constant
- b is the damping coefficient

The parameters k and b are obtained from experimental trials and will differ depending on tissue type and composition. Table 3 presents a list of parameters for each of the models, obtained experimentally from in-vitro animal tissue relaxation tests via robot-tissue interactions [68].

Of the three models, studies have shown that the Kelvin-Boltzmann representation is the most accurate and produces behaviours that are closest to that of real soft tissues [57][67][69]. However, all presented models are limited by their linearity and fail to capture certain aspects of the tissue.

Table 3: Experimental Parameters for Various Tissue Models Obtained from In-Vitro Animal Tissue Tests.

Model	**Parameter**		
	$\boldsymbol{b}$	$\boldsymbol{k}$ $(\boldsymbol{k_1}\|\boldsymbol{k_2})$	
Maxwell	349.58	1294.74	
Kelvin-Voigt	112.72	629.11	
Kelvin-Boltzmann	198.83	805.92	3017.69

A non-linear model, called the Hunt-Crossley, was developed to improve upon the performance of the existing heuristic models. While this model resembles the Kelvin-Voigt design, the calculated force is exponentially proportional to the displacement of the tissue [68]. Figure 13 below shows the Hunt-Crossley model with its corresponding equation shown in Equation (18).

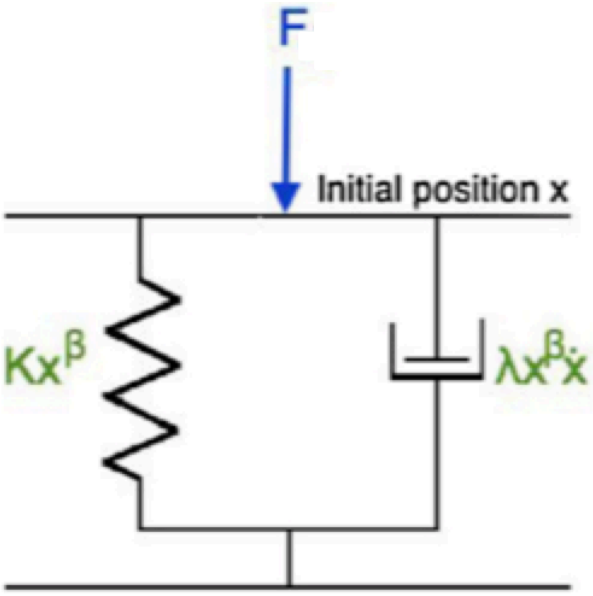

Figure 13: Hunt-Crossley Model. [68]

$$F_{HC} = Kx^{\beta}(t) + \lambda x^{\beta}\dot{x}(t) \tag{18}$$

Where:

- K is the spring constant
- λ is the damping coefficient
- β is the displacement exponential factor

These parameters, K, λ, and β, are all obtained experimentally and can vary significantly between different tissue type and composition. In particular, the variable β gives the model its non-linear component, allowing the Hunt-Crossley method to capture more characteristics of the soft tissue behaviour while still being considered a simple model [68]. Table 4 below shows the Hunt-Crossley parameters for skin tissue, obtained by taking the average value from five experimentation trials [70].

Table 4: Experimental Hunt-Crossley Parameters and Magnitudes for Skin Tissue.

Hunt-Crossley Skin Tissue Parameters	**Magnitude**
$K\ \left(\frac{N}{m}\right)$	5.5432
$\lambda\ \left(\frac{Ns}{m^2}\right)$	0.1496
β	1.5826

On the contrary, continuum-mechanical models are much more complex. These models assume soft tissue is a continuous matter by deriving its behavioural, mathematical equations from well-known laws, such as the conservation of mass, the conservation of momentum, and the conservation of energy [71][72][73]. In this way, continuum-

mechanical models are able to capture aspects that heuristic models cannot, for example, the tissue changes due to the growth of new cells [74].

Due to their complexity, continuum-mechanical models use a variety of different methods to analyze material behaviour [62]. One of the most frequently used methods, called the finite element analysis (FEA), uses a mesh model that divides a complete, continuous material into many small, discrete regions [69][75]. These sections each have individual models that represent the behaviour only within the boundaries of the region. Boundary behaviours are obtained via interpolation of the equations describing the surrounding regions. In addition, the region boundaries and nodes are not fixed, and are able to move during simulation and analysis. This effect mirrors real tissue behaviour, as the model will change with any material changes, such as the reaction of tissue towards an external force.

Figure 14 below shows the use of finite element analysis on a femur bones, subjected to different loads. The divided regions with differing colours indicate the stress magnitudes calculated by the models in each region.

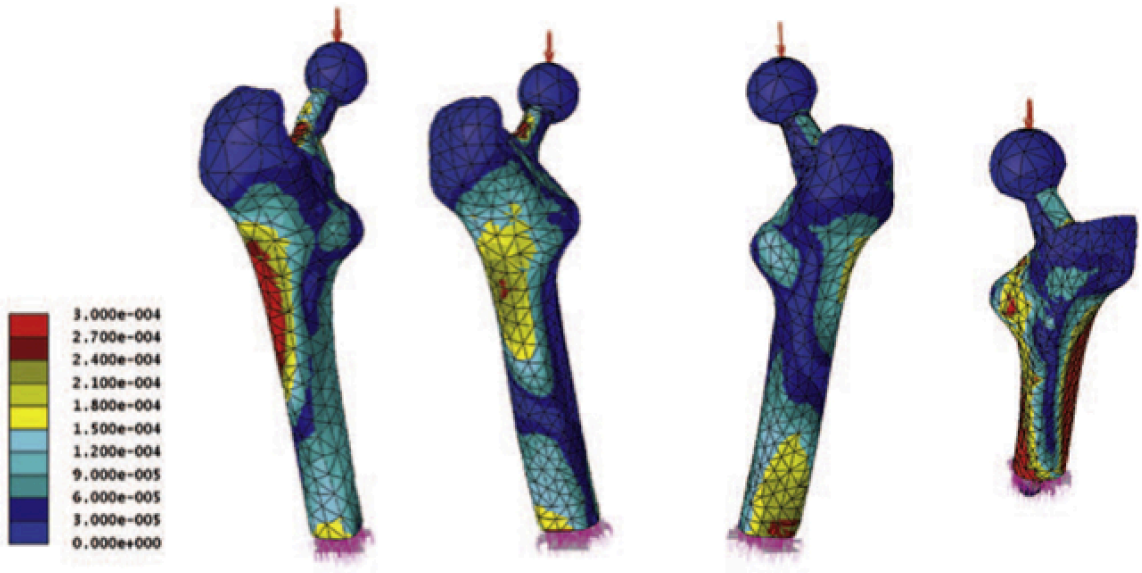

Figure 14: Finite Element Analysis of Femur Bones when Subjected to Different Loads. [76]

As the continuum-mechanical model describes the entire material in terms of a collection of different models, it is much more accurate than the heuristic model, which uses a single model. However, with the increased complexity, these models require higher computational abilities and, as a result, are difficult to simulate in real-time [57].

Hybrid soft tissue models attempt optimize results by combining the features of both models. The goal is to maintain the accuracy of continuum-mechanical models, namely in the event of contact with the soft tissue, while having the computational efficiency of a heuristic model. While hybrid models have tested, results from experimentation have not shown much promise [57].

2.4 Da Vinci Research Kit

Today, medical telerobotics continues to be a growing topic of interest, with many organizations looking to facilitate growth in the field. In particular, Intuitive Surgical Inc., the creators of the da Vinci Surgical System, aims to expand current technology by sharing resources to further develop the da Vinci Surgical System. Online, open-source research communities have free access to all software, documentation, and CAD models for the system [26][77]. Furthermore, a number of laboratories and institutions worldwide have been provided the da Vinci Research Kit (dVRK), a collection of parts and components from the original, first-generation da Vinci robot.

Each dVRK contains multiple manipulators, a stereo viewer, foot pedals, interface boards, and an accessory kit [26]. There are two manipulators, which mirror the master console, called the Master Tool Manipulators (MTMs), and two manipulators, the Patient Side Manipulators (PSMs), which mirror the slave consoles. Descriptions about each are provided below [78][79][80].

2.4.1 Master Tool Manipulator

The MTM is a joystick-like manipulator with 8 degrees of freedom. All DOFs are rotational with the exception of the end effector, which controls the opening and closing of the clasp tool. The first three DOFs control large movements, while the remaining four are used to mimic precise wrist motions. In addition, there are two passive, revolute joints used stabilize and limit the motion of the manipulator. Figure 15 below shows the

movement of the 7 rotational MTM joints separated into two parts: (a) showing the large movements from the first 3 DOFs and (b) showing the close-up joints required for the wrist rotation.

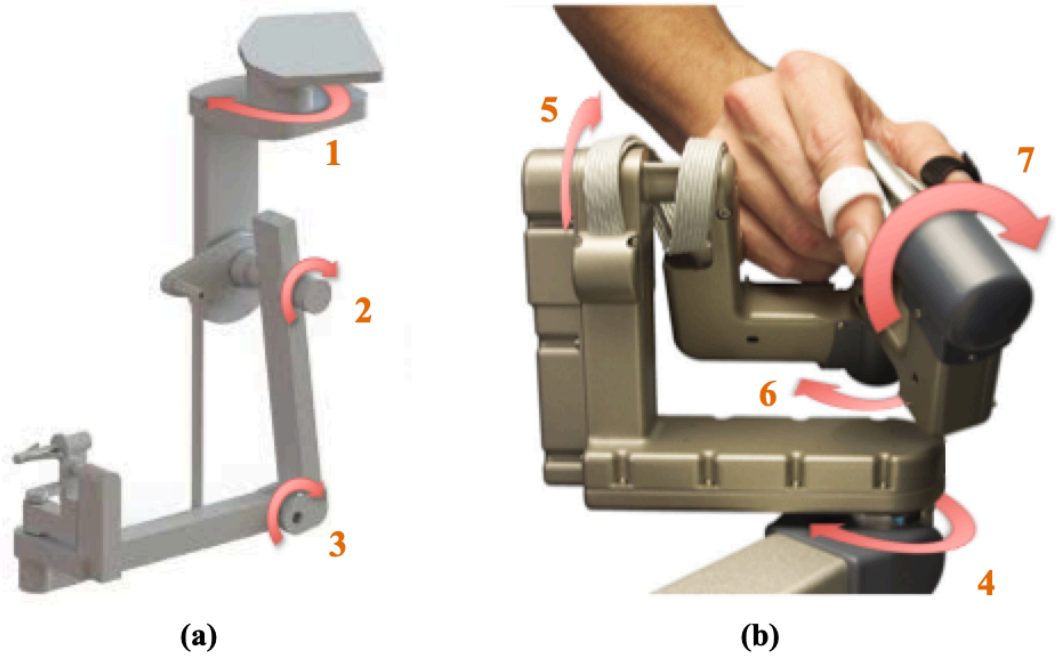

Figure 15: MTM Manipulated Joints for the (a) Full Body (b) Wrist. [78][81]

The design of the MTM is unique, as unlike standard manipulators, movement is not performed using a controller. Instead, MTMs use manual control, originating directly from the surgeon via finger grips located at the end effector. The direct manipulation allows for more precise and accurate movements, as desired by the operator. In particular, for the MTM, which controls the movements of the operating PSM, this control enhances hand-eye coordination and gives the surgeon the feeling of operating directly on the patient. These movements are then relayed to the PSM, which operates with a standard controller.

2.4.2 Patient Side Manipulator

The PSM is a 7-DOF manipulator, with three DOFs allocated to large movements, three for wrist movements, and the final joint for controlling the end effector tool. Not including the end effector, the manipulator is a RRPRRR, which indicates that all DOFs are revolute with the exception of the third large movement joint, which is prismatic. There are also six passive, revolute joints that are used to stabilize and restrict the movement of the manipulator. Figure 16 shows the labeled PSM joints for (a) the large full body movements and (b) the small wrist movements.

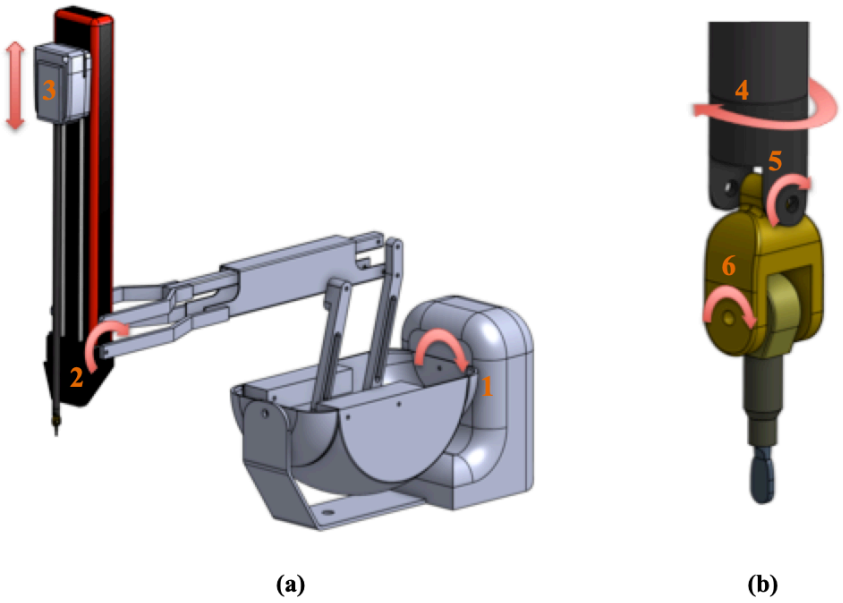

Figure 16: PSM Manipulated Joints for the (a) Full Body (b) Wrist.

Note that the MTM and the PSM have different designs and number of DOFs, despite one being used to control the other. The MTM is designed for the surgeon's ease of use, while the PSM is designed for functionality in an operating environment. These

manipulator designs make controlling the system is much more difficult than perceived and is one of the reasons why training to use the da Vinci system is so extensive.

When modeling or analyzing the MTM and PSM, the end effector joint is frequently excluded, as it is isolated and has no effect on other parts of the manipulators. Thus, models depicting the MTM and PSM generally show 7 and 6 DOFs for the manipulators respectively.

3. Chapter 3: Robotic Manipulator Motion

As the focus of this thesis is to explore the effects of different factors on telerobotic performance, it is important to understand how the manipulator moves and its state at a given time. In addition, with different surfaces will cause different reactions and also affect the manipulator's behaviour. This chapter defines and discusses robot kinematics and dynamics in greater detail.

There are two different manipulators setups used in the following experiments: one with 3-DOFs and one with 6-DOFs. The first setup aims to study the effects of time delay on robot-tissue interaction while the second aims to mimic the motions and performance of a more realistic surgical robot. Kinematics and dynamic equations of each are provided in the Appendix.

3.1 Kinematics

Kinematics is defined as the study of motion and describes how an object moves to follow its desired trajectory [82]. From a kinematics standpoint, fundamental properties that characterize the state of system, such as position, velocity, and acceleration are relevant, whereas the causes and consequences of motion are of no importance.

For manipulators, kinematics analysis explores the movement of a robot by examining its kinematics chain, which is the model that describes the relationship between the

manipulator joints and linkages [83]. Each joint, either prismatic or revolute, is assigned its own frame and moves from one state to the next via a series of translations and rotations across and about its axes [82]. Below, Figure 17 shows a basic RRR manipulator with its assigned kinematics frames and the manipulator motion as the joints move.

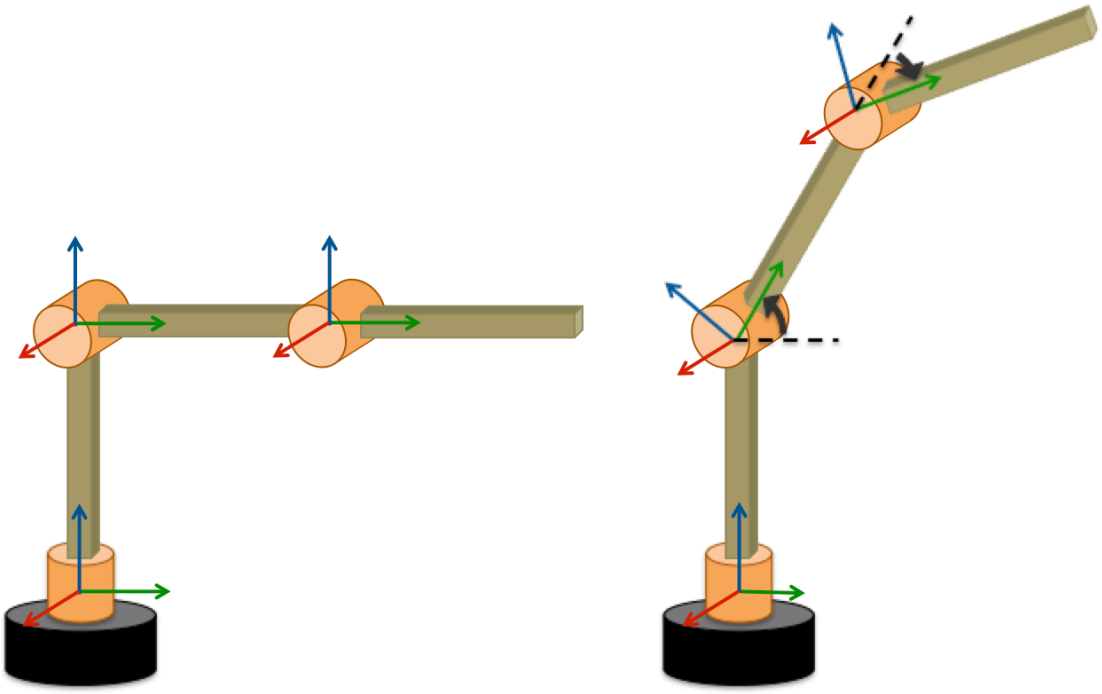

Figure 17: Movement of Kinematics Frames of a 3-Link RRR Manipulator.

With knowledge of its kinematics chain, motion planning for manipulators can be achieved in two ways: through forward or inverse kinematics [84][85]. In forward kinematics, the joint angles/positions are specified by the operator and are used alongside the linkage lengths to determine the end effector position. This method is useful for avoiding objects, as the exact trajectory of the manipulator body is controlled. On the

contrary, the inverse kinematics calculates joint angles/positions based on the end effector position. As most manipulator applications require the end effector to carry out a task, inverse kinematics is the more popular method of control. However, with inverse kinematics, the possibility of multiple arrangements resulting in the same end effector location must be considered. To avoid this, some applications may employ an optimization method, allowing them to achieve results in the most efficient manner.

3.2 Dynamics

While the kinematics deal strictly with the motion-based properties of a manipulator, dynamics look into the cause of motion and factors that affect movement [86]. In particular, internal forces and torques, which are applied to move the manipulator, and external forces, which result from contact with the manipulator, are investigated. The effect of these dynamics elements on the system behaviour must be well understood to carry out the designated objectives of the manipulator.

Dynamics equations are used to define the physical relationship between dynamics and kinematic elements. That is, the effects of applying internal forces and torques on the manipulator positions, velocities, and accelerations. These equations are often called the equations of motion, as they depict how a system moves, and the standard form for a manipulator is presented below in Equation (19) [85].

$$\tau = M(q)\ddot{q} + V(q, \dot{q}) + G(q) \tag{19}$$

Where:

- τ is the torque/force applied to the revolute/prismatic joints respectively
- q is the joint positions of manipulator
- $\dot{q}$ is the joint velocities of manipulator
- $\ddot{q}$ is the joint accelerations of manipulator
- $M(q)$ is the mass matrix, which depends on the manipulator position
- $V(q, \dot{q})$ is the joint centrifugal and coriolis matrix, which depends on the manipulator position and velocity
- $G(q)$ is the gravitational matrix, which depends on the manipulator position

If there is contact with the end effector, the resulting forces acting on the manipulator must also be considered in the dynamics equations. These external forces can be resolved into individual forces/torques that act on each joint, as shown in Equation (20) [85].

$$\tau_{ext} = J^T F_{ext} \tag{20}$$

Where:

- J is the manipulator Jacobian matrix
- F_{ext} is the external force acting at the manipulator end effector

The Jacobian matrix is the partial differentiation of the linkage positions, in the Cartesian plane, with respect to the joint position. The resultant matrix is always a 3-by-n, where n is the number of manipulator DOFS. Below, Equation (21) shows the Jacobian matrix,

while Equation (22) shows the applied external force, which is divided into its three Cartesian axes components.

$$J = \begin{bmatrix} \frac{\partial x}{\partial q_1} & \frac{\partial x}{\partial q_2} & \cdots & \frac{\partial x}{\partial q_n} \\ \frac{\partial y}{\partial q_1} & \frac{\partial y}{\partial q_2} & \cdots & \frac{\partial y}{\partial q_n} \\ \frac{\partial z}{\partial q_1} & \frac{\partial z}{\partial q_2} & \cdots & \frac{\partial z}{\partial q_n} \end{bmatrix} \tag{21}$$

$$F_{ext} = \begin{bmatrix} F_X \\ F_Y \\ F_Z \end{bmatrix} \tag{22}$$

Thus, the total equation of motion, including the effects of external forces, is as follows:

$$\tau + \tau_{ext} = M(q)\ddot{q} + V(q, \dot{q}) + G(q) \tag{23}$$

As with kinematics, there are also forward and inverse dynamics, which are used to control and carry out the desired movement of the manipulator. In forward dynamics, joint force/torque values are known, and the resultant position of the joints and end effector can be calculated. On the contrary, inverse kinematics takes an end effector position and calculates the joint forces/torques required to achieve the position. Both methods make use of the kinematics properties, chains, and equations to move the manipulator as desired.

There are many aspects to consider when formulating equations of motion, as manipulators are complex and have many DOFs. In addition, manipulator motion is both

rotational and linear, and singular joint movements will affect successive joints, since movement is not isolated. One method of developing the system's equations of motion is by using the Lagrangian approach.

3.2.1 Lagrangian Mechanics

The Lagrangian approach looks into dynamic analysis from an energy standpoint [87]. To obtain the equations of motion, the Lagrangian is implemented into the Euler-Lagrange's differential equation, shown in Equation (24) below [88][89]:

$$0 = \frac{d}{dt}\frac{\partial \mathcal{L}}{\partial \dot{q}_i} - \frac{\partial \mathcal{L}}{\partial q_i} \tag{24}$$

Where:

- q is the position
- $\dot{q}$ is the velocity
- $\frac{\partial \mathcal{L}}{\partial \boldsymbol{x}}$ is the partial derivative of the term, **x**
- $\frac{d}{dt}$ is the derivative with respect to time
- $\mathcal{L}$ is the Lagrangian, which is then defined as:

$$\mathcal{L} = T - V \tag{25}$$

Where:

- T is the kinetic energy
- V is the potential energy

The result from implementing Euler-Lagrange's equation is a series of equations, each corresponding to one of the system's DOFs. The equations of motion will be in the form of Equation (19), where the torque/forces applied to joints are initially set to 0.

4. Chapter 4: Experiment 1 – Different Surface Interactions

The first set of tests focus on investigating the effects of contact and external forces in a teleoperated, surgical setting. Two sets of simulations involving trajectories with different degrees of contact between the manipulator and environment are simulated under delays of 0ms, 200ms, 400ms, 600ms, and 800ms each. Results are recorded, discussed, and compared to the expected performance presented in Table 1. For these tests, a task is considered a failure if it shows no signs being completed during the simulation time or if oscillations are too large, as this behaviour is not acceptable for surgical applications.

For both tests, a 3-DOF RRR slave manipulator controller by an MPC is used. This MPC is linearized at the manipulator's starting position; that is when all states are 0. Table 5 contains the linkage properties for the manipulator, including the average density of steel, while Figure 18 shows the simulation setup [90].

Table 5: Properties and Magnitudes of RRR Manipulator for Experiment 1.

Property	**Magnitude**
Length (m)	0.1
Radius (m)	0.01
Density (kg/m^3)	7850

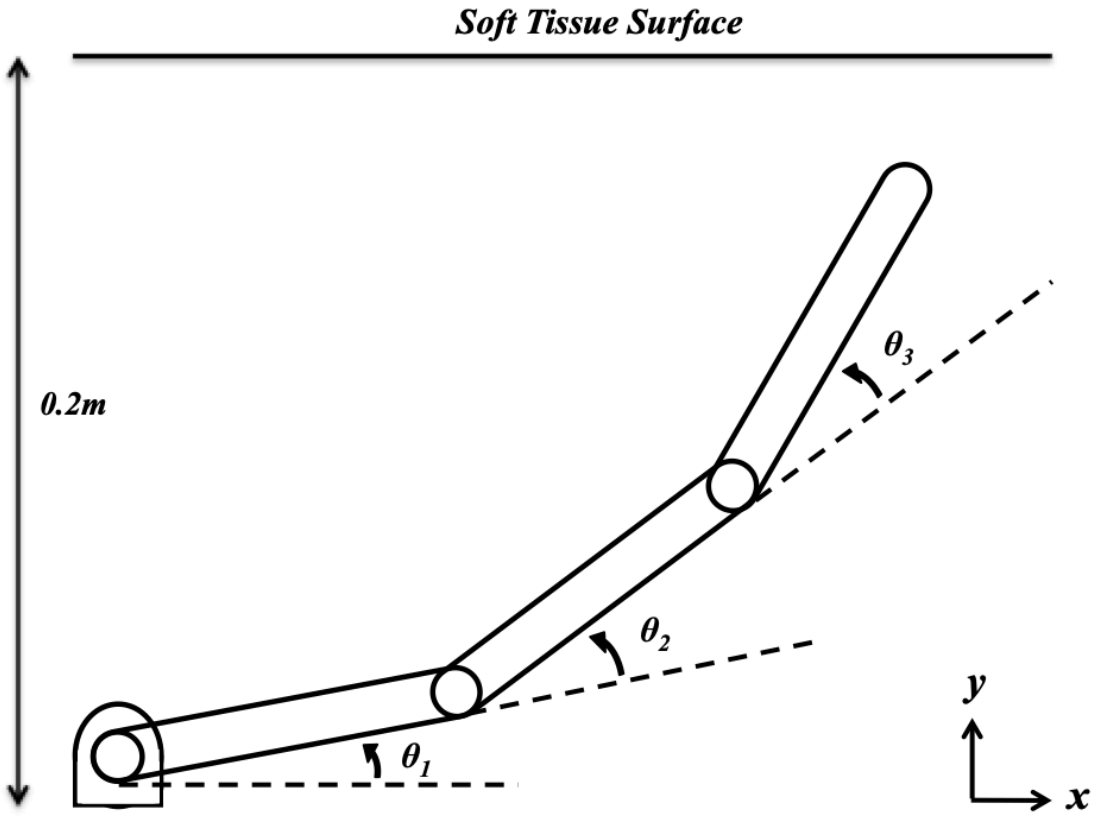

Figure 18: Simulation Setup for Experiment 1.

For the environment, a wall-like Hunt-Crossley model will represent the skin tissue. All essential parameters required for the experiment can be found in Table 2 and Table 4 from Sections 2.3.1 and 2.3.3 respectively.

As the effects of contact are investigated, the primary features to be observed include the position of the arm, the penetration depth of the manipulator into the tissue, and the measurement of forces, both normal and frictional, between the manipulator and wall.

4.1 Experiment 1, Scenario 1: Minimal, Sliding Contact

4.1.1 Setup

The first of the two experiments look into the effects of little to no contact on the performance of a manipulator when subjected to time delay. Figure 19 shows the simulation timeline, as described below, while Figure 20 provides two different viewpoints of the robotic arm's desired trajectory. At the start of the simulation, beginning 0.2m away from the wall, the arm moves towards the tissue and stops just as contact with the end effector is made. The end effector is then programmed to slide across the wall, while maintaining minimal contact between the surfaces. Initial contact occurs at 7 seconds and the total simulation time is 15 seconds.

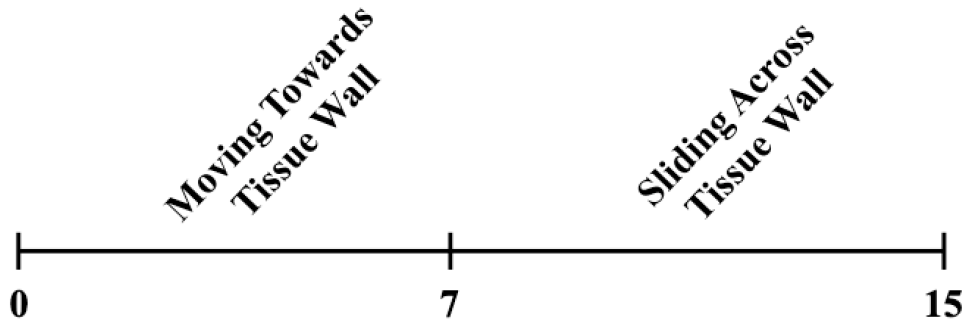

Figure 19: Timeline for Experiment 1, Scenario 1.

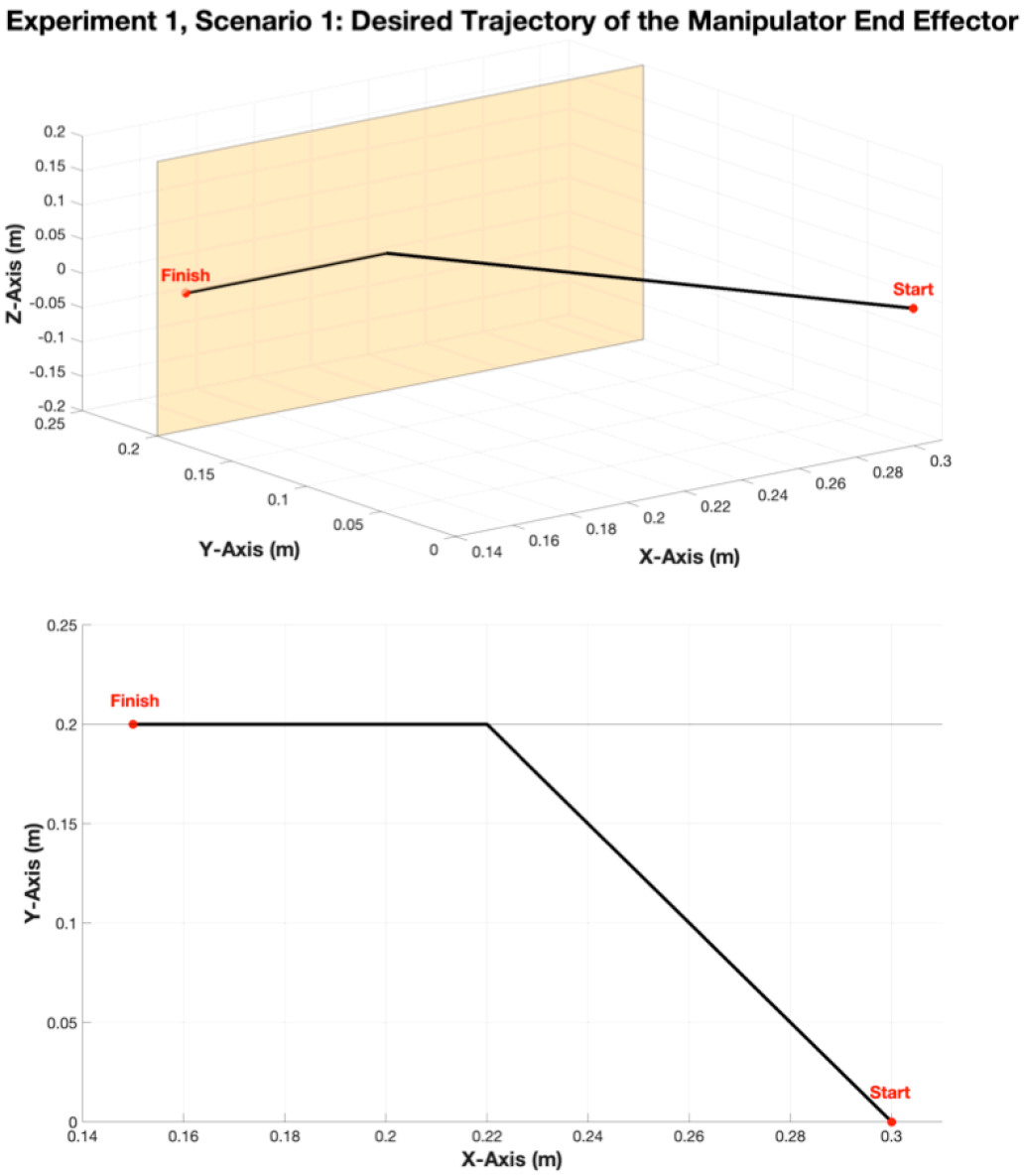

Figure 20: Desired Trajectory of Manipulator End Effector for Experiment 1, Scenario 1.

4.1.2 Results and Discussion

Positional results of the simulation, with the wall positioned at 0.2m, are presented in Figure 21 below. In addition, the desired trajectory is also included for analytical purposes.

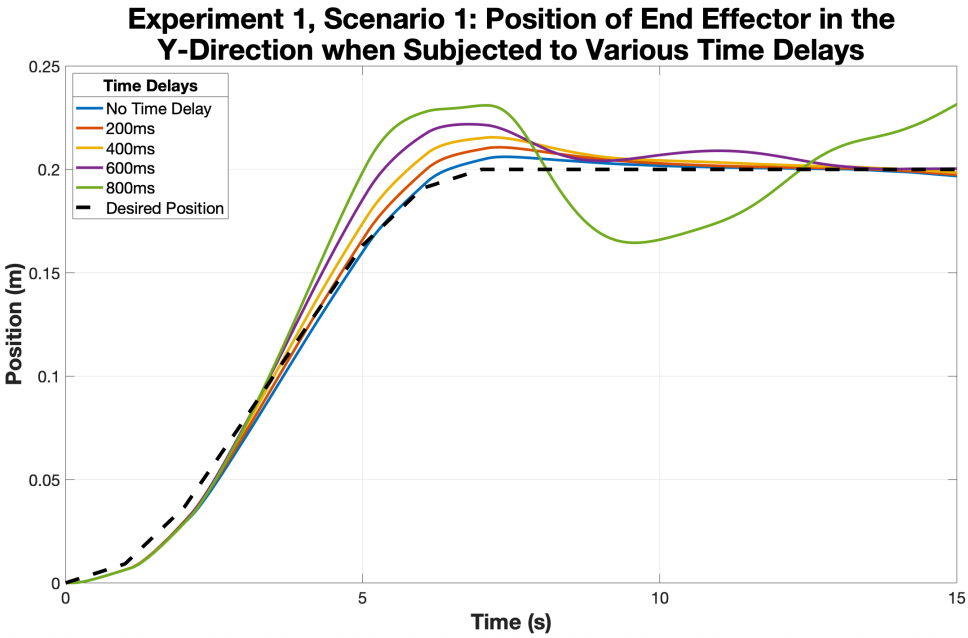

Figure 21: Position of Manipulator End Effector in the Y-Direction for Trials from Experiment 1, Scenario 1 that are Subjected to Various Time Delays.

All trials, with the exception of the simulation with a delay of 800ms, are successful to different degrees. Trials with greater time delays result in greater oscillations and an overall decrease in performance. These observations are shown quantitatively in Table 6 and Table 7 via increasing settling times and average positional errors, respectively, with the increasing delays.

Table 6: Settling Times (s) of RRR Manipulator for Successful Trials from Experiment 1, Scenario 1 that are Subjected to Various Time Delays.

	Time Delay			
	No Delay	200ms	400ms	600ms
Settling Time (s)	8.6348	9.4000	10.3962	12.4777

Table 7: Average Positional Errors (m) of RRR Manipulator for Successful Trials from Experiment 1, Scenario 1 that are Subjected to Various Time Delays.

		Time Delay			
		No Delay	200ms	400ms	600ms
Movement	Towards the Wall	0.0046	0.0048	0.0072	0.0117
	Sliding Across the Wall	0.0021	0.0038	0.0047	0.0062

When compared with the expected performance of telerobotics, these results accurately correspond to the behaviour presented in Table 1. Performance failures may be attributed to the linearization of the MPC model, which, as mentioned previously, is at the starting state of the system. Thus, as the manipulator moves further from the original point of linearization, predictions would become less precise, resulting in failure to accurately capture the entire system and carry out the desired motions.

All trials show contact and penetration into the wall model, despite the planned trajectory of the simulation. In particular, larger time delays result in deeper penetrations into the tissue. Looking closer into the details of these interactions, Figure 22 shows the penetration depth of the manipulator into the tissue model, while Figure 23 and Figure 24 show the normal and frictional forces from contact respectively. Only successful trials, those with delays from 0ms to 600ms are shown.

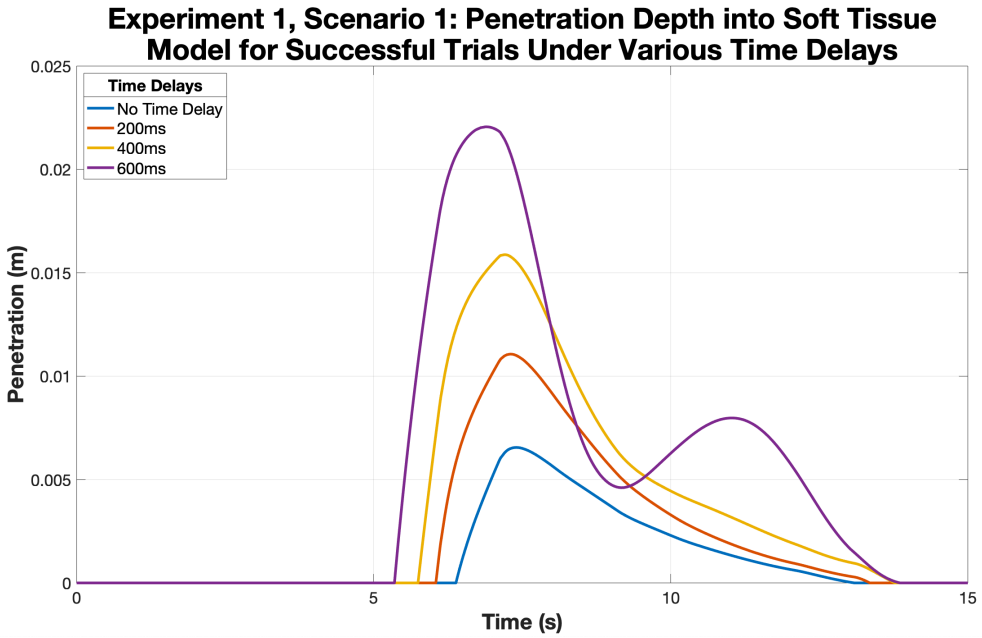

Figure 22: Penetration Depth of End Effector into Soft Tissue Model for Successful Trials from Experiment 1, Scenario 1 that are Subjected to Various Time Delays.

Figure 23: Measured Contact Force between the End Effector and Soft Tissue Model, in the Y-Direction, for Successful Trials from Experiment 1, Scenario 1 that are Subjected to Various Time Delays.

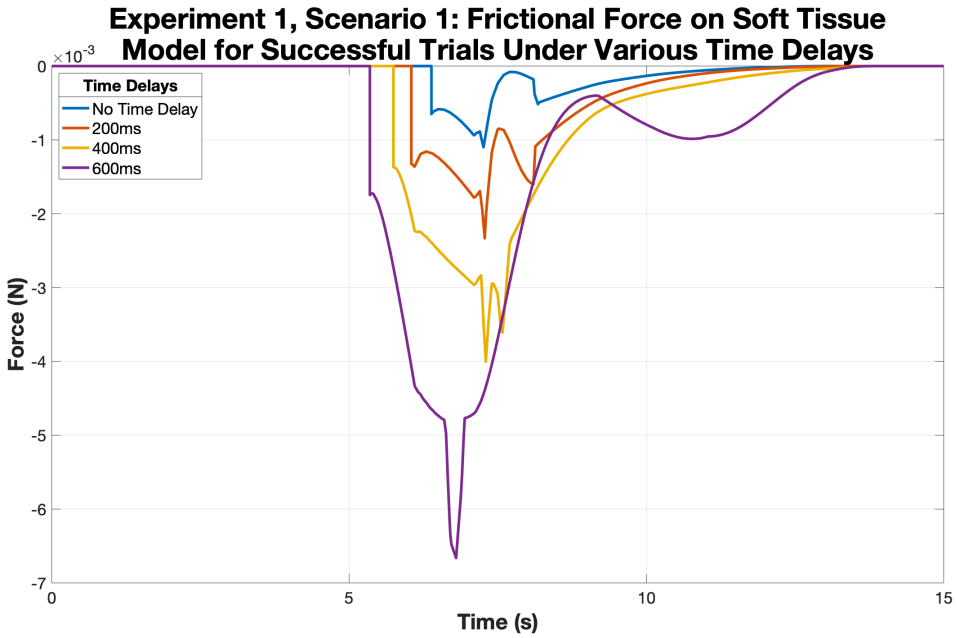

Figure 24: Measured Frictional Force between the End Effector and Soft Tissue Model, in the X-Direction, for Successful Trials from Experiment 1, Scenario 1 that are Subjected to Various Time Delays.

From Figure 22, it can be seen that tissue penetration depth and time delay are proportional, with larger delays resulting in greater penetrations and vice versa. Likewise, normal and frictional forces, shown in Figure 23 and Figure 24, are also proportional to time delay. Despite the planned motion of the manipulator, which is programmed to slide across the surface but not penetrate it, normal forces are greater than frictional ones.

4.2 Experiment 1, Scenario 2: Penetrative Contact

4.2.1 Setup

The second of the two scenarios looks into the performance effects of penetrative contact between a manipulator and tissue wall when subjected to time delay. Contrary to the previous scenario, where motion is along the tissue surface, the penetration is modeled by

perpendicular motion into the skin surface. Figure 25 provides the movement timeline, while Figure 26 shows the planned trajectory of the trials. Again, the manipulator's end effector begins 0.2m from the wall and moves towards it when the simulation begins. After contact with the surface, planned at a simulation time of 6 seconds, the manipulator compresses the tissue for a total of 2cm. Compression lasts a total of 7 seconds, until a simulation time of 13 seconds, then the manipulator is held in place until the end of the simulation. The total elapsed time is 15 seconds.

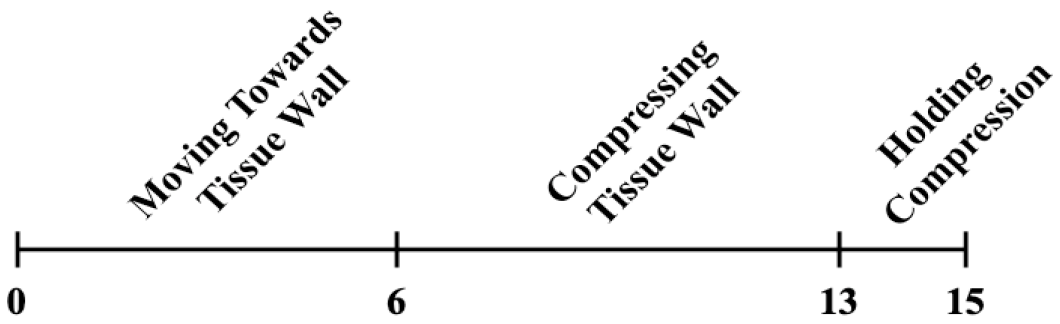

Figure 25: Timeline for Experiment 1, Scenario 2.

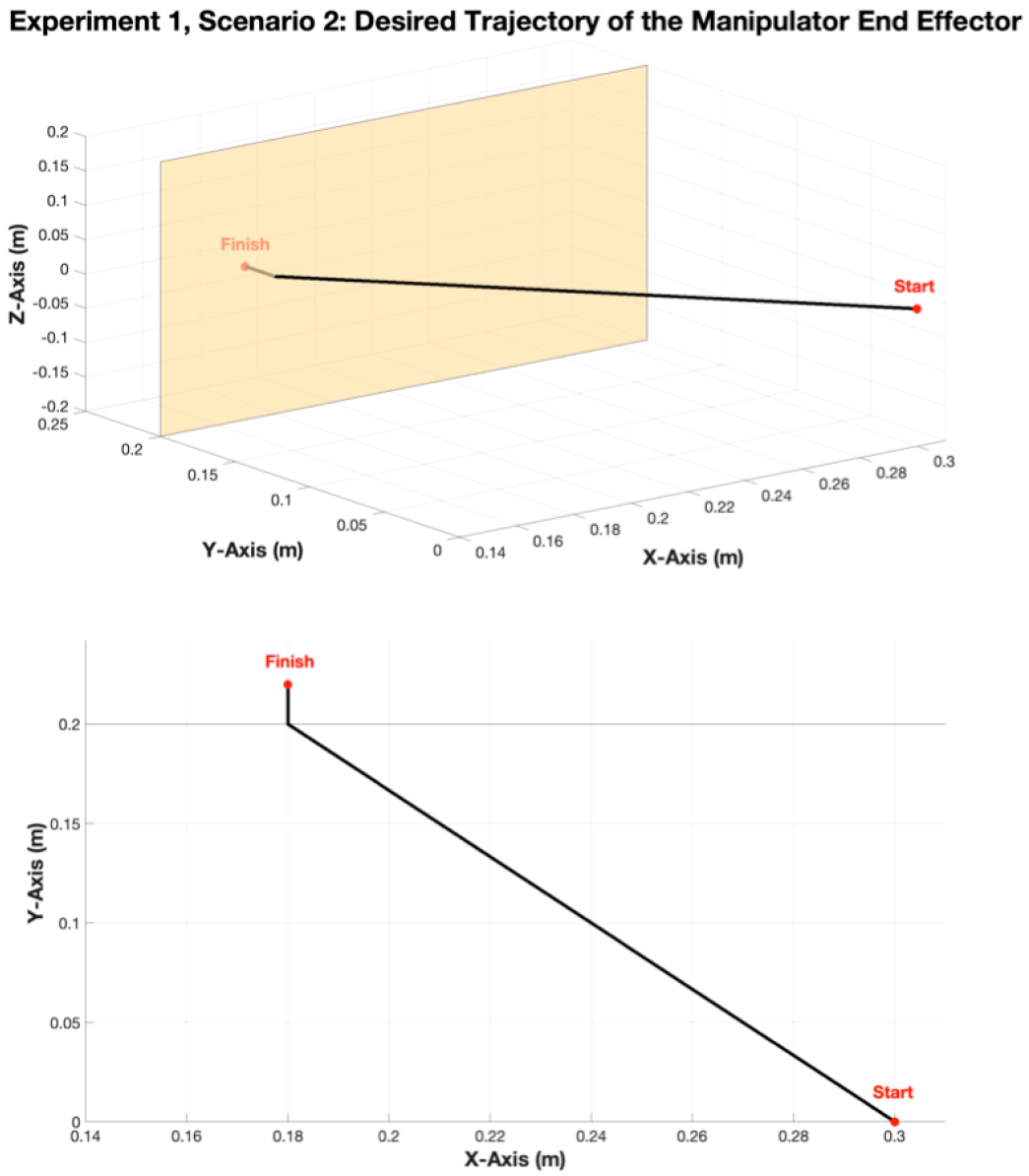

Figure 26: Desired Trajectory of Manipulator End Effector for Experiment 1, Scenario 2.

4.2.2 Results and Discussion

Positional results of the simulation, depicting the distance from the initial position to the wall, are presented in Figure 27. For comparison, the desired trajectory is also included.

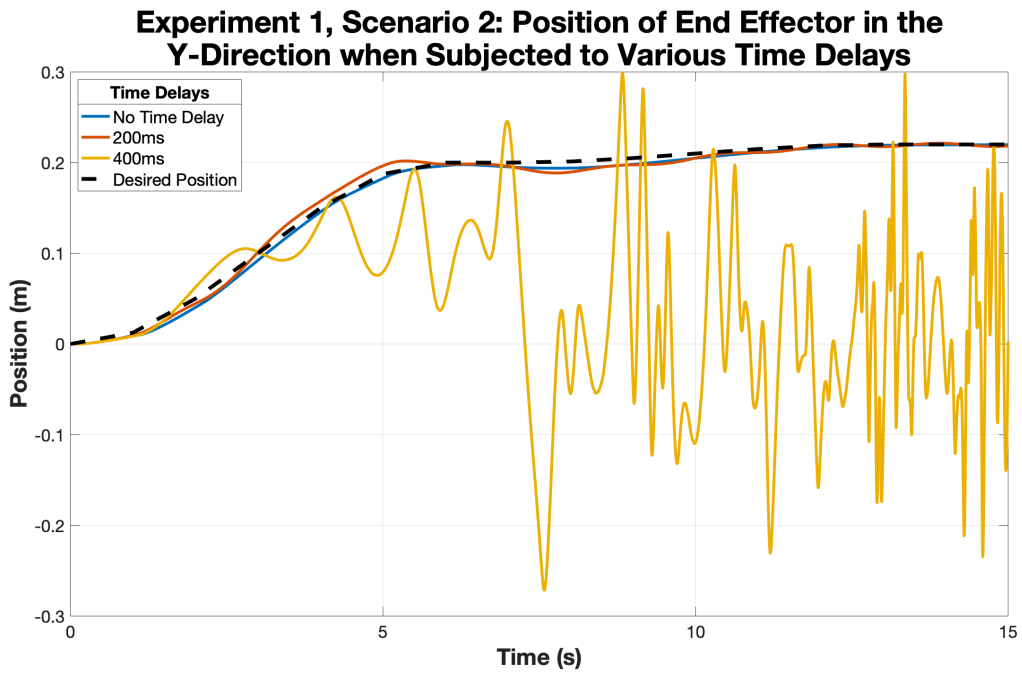

Figure 27: Position of Manipulator End Effector in the Y-Direction for Trials from Experiment 1, Scenario 2 that are Subjected to Various Time Delays.

Although trials with delays of 0ms, 200ms, 400ms, 600ms, and 800ms were all tested, only those with delays between 0-400ms are shown, as the remaining trials were too unstable. Even for the trial with a 400ms delay, there are large oscillations, which are a clear indication of task failure, even prior to contact with the tissue. This behaviour is contrary to the expected results, from Table 1, as the task failure first occurs for the trial with a 400ms delay, versus the expected 700ms+ delay.

Between the successful trials, the one with no delay and the one with a delay of 200ms, the undelayed trial appears to have fewer oscillations and be more stable. This can be seen via the average positional errors shown in Table 8. Though minimally in some cases, the no delay trial consistently has smaller errors than the 200ms delay trial.

Table 8: Average Positional Errors (m) of RRR Manipulator for Successful Trials from Experiment 1, Scenario 2 that are Subjected to Various Time Delays.

		Time Delay	
		No Delay	200ms
Movement	Towards the Wall	0.0049	0.0054
	Compression into the Wall	0.0045	0.0050
	Holding Against Wall	4.2907×10^{-4}	0.0013

Figure 28 shows the penetration depth of the manipulator into the tissue for the successful trials. The forces, normal and surface friction, from the contact between the manipulator and surface are measured and recorded in Figure 29 and Figure 30 respectively.

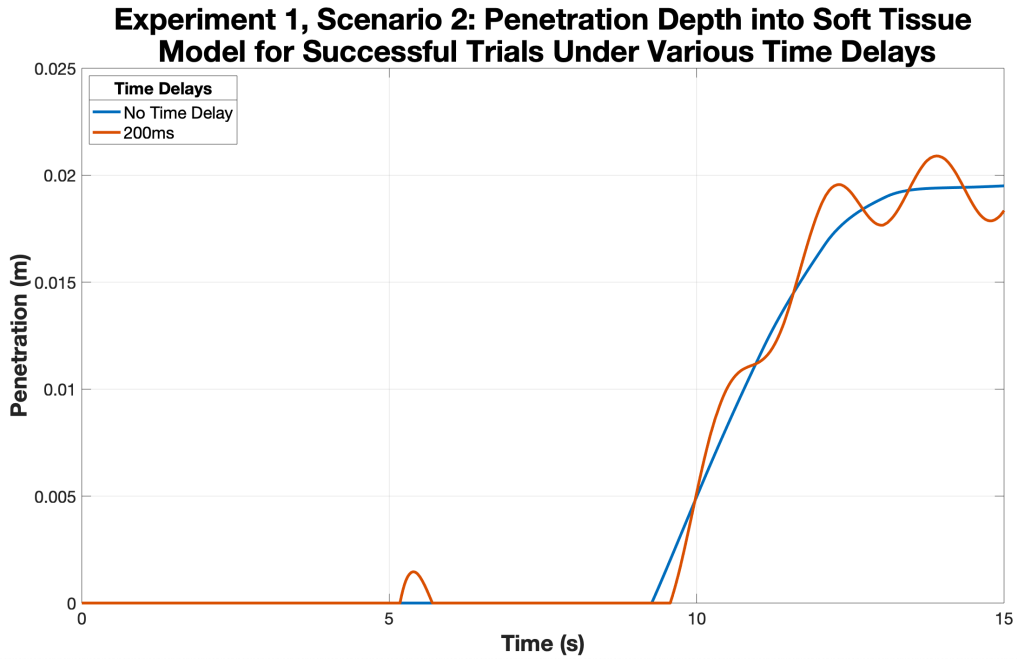

Figure 28: Penetration Depth of End Effector into Soft Tissue Model for Successful Trials from Experiment 1, Scenario 2 that are Subjected to Various Time Delays.

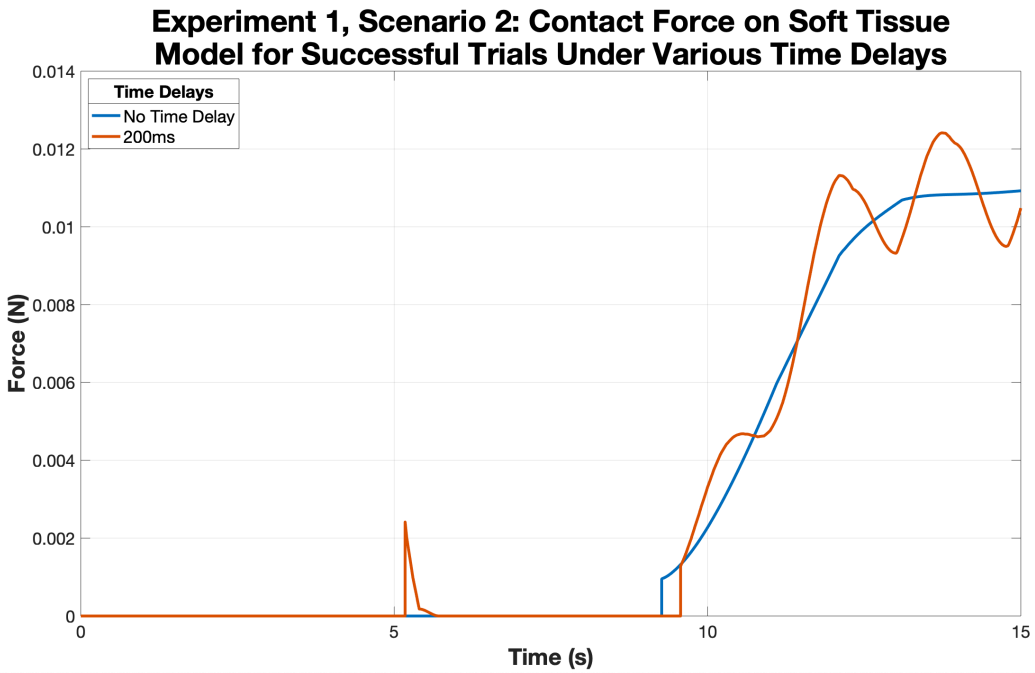

Figure 29: Measured Contact Force between the End Effector and Soft Tissue Model, in the Y-Direction, for Successful Trials from Experiment 1, Scenario 2 that are Subjected to Various Time Delays.

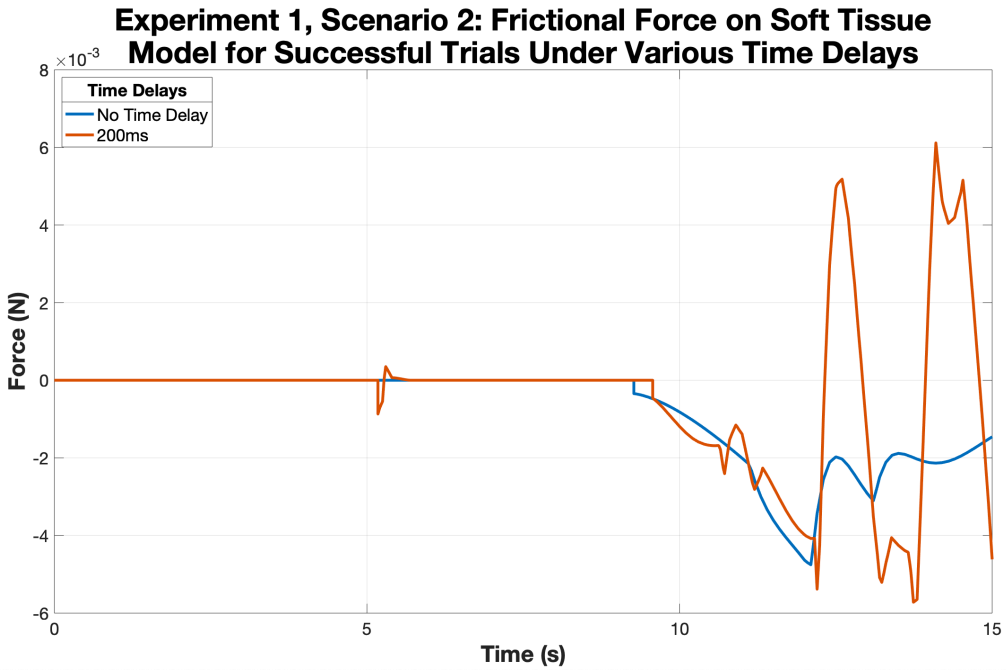

Figure 30: Measured Frictional Force between the End Effector and Soft Tissue Model, in the X-Direction, for Successful Trials from Experiment 1, Scenario 2 that are Subjected to Various Time Delays.

As expected, both figures depicting force measurements show that the larger forces correlate with deeper penetrations and vice versa. In addition, frictional forces are significantly lower than normal forces, given the designed trajectory of the manipulator.

4.3 Comparison

In both scenarios, it appears that the overall performance trend persists; where increasing time delay results in decreased performance and vice versa. However, external forces can affect performance, by increasing the rate in which the performance deteriorates, causing failure at shorter time delays.

From the positional plots, shown in Figure 21 and Figure 27, it can be seen that trials with longer delays react faster, generally reaching the tissue surface before the intended time of contact. In addition, they also have deeper penetrations into the tissue and larger overshoots. These negative behaviours reflect the expected trend and are likely due to the lack of signal, caused by the delays, which result in overcompensation by the controller.

From the normal and frictional force plots, presented in Figure 23, Figure 24, Figure 29, and Figure 30, various unique behaviours are observed. As expected, normal forces for Scenario 2 are greater than those in Scenario 1, while frictional forces are greater for Scenario 1 than Scenario 2. Given the planned trajectories of the scenarios, this outcome is as expected. However, in spite of the different trajectories of each scenario, the recorded normal forces are always greater than the frictional ones, thus, indicating that even minor contact will have a great effect on force transmitted into the tissue.

In addition, at the moment of initial contact with the surface, both scenarios show different reactions. In Scenario 1, where contact is not intentional, the normal and frictional forces show a sudden and sharp decrease in force upon contact with the tissue model. However, for trials with intentional penetration in Scenario 2, there is no repelling behaviour, indicating stable contact. As the environment is the same for both scenarios, it is believed that this behaviour stems from attempts to stabilize the system caused by unexpected forces.

In Scenario 1, there are moments where the penetration depth is shown to increase while force decreases, as shown in Figure 22 and Figure 23. Given the proportional relationship between the properties, as indicated in Equation (18), this behaviour is unexpected. It can be concluded that the decrease in force is caused by a decrease in manipulator's velocity. This reaction appears to be the result of contact resistance and the manipulator attempting to stabilize the system, while continuing to follow the planned position directives.

From both normal force plots, in Figure 23 and Figure 29, a force threshold, at approximately 0.013N can be noted. When measured forces are below this value, trials are successful, however, surpassing it results in trial failure. This occurs regardless of designated trajectory or time delay. Moving forward, it may be of interest to explore the force limitations of tissues and implement force control for improved performance.

5. Chapter 5: Experiment 2 – Position-Force Control

The second experiment focuses on the use of hybrid controllers to improve telerobotic performance in a surgical setting. Two sets of simulations involving different hybrid position-force controllers are simulated under delays of 0ms, 200ms, 400ms, 600ms, and 800ms each. Results are recorded, discussed, and compared to the expected performance presented in Table 1. For these scenarios, a trial is considered a failure if the planned motion is not carried out.

Both tests use a da Vinci PSM manipulator, as described in Section 2.4.2, paired with a hybrid controller. CAD models for the PSM, with accurate mass, inertial, and dimensional properties, are obtained via the open-source dVRK research community at the Johns Hopkins University [26]. In this experiment, the motion of the end effector joint will not be considered, thus focusing on controlling only the first six DOFs of the PSM. The surgical environment, skin tissue, will be represented using the Kelvin-Voigt model in the form of a wall, with parameters from Table 2 and Table 3.

The controllers, used in this experiment, are designed to switch between position and force law depending on the magnitude of the total forces, from normal and frictional forces, recorded at the end effector. A force threshold, which considers the physical limitations of the skin tissues, determines which law is applied: with positional law being applied when the force is below the threshold and the force law being applied when the threshold is equal or surpassed. This mechanism allows the controller to give more

weight to the factor that has a greater importance on the performance at the specified time in the simulation.

The force threshold is determined based on maximum pressure that the soft tissue can support. Using the yield strength and approximate surface area of the end effector tip, measured as $1.020\times10^{-7}m^2$, the maximum force can be calculated from Equation (14). This force, calculated as 2.193N, is rounded down to 2N to account for safety.

Of the six manipulated PSM joints, only one will be switching between laws: joint 2, as shown in Figure 16. Thus, the compliance vectors are as follows:

$$[1 \quad 1 \quad 1 \quad 1 \quad 1 \quad 1]^T \quad \text{for } F < 2N \tag{26}$$

$$[1 \quad 0 \quad 1 \quad 1 \quad 1 \quad 1]^T \quad \text{for } F \geq 2N \tag{27}$$

This joint was selected by considering the manipulator and environment layout. The center of the PSM's base sits 0.750m away from the tissue wall with the rotational axis of joint 2 lying parallel to it. This arrangement allows the rotational motion of the joint to move the end effector towards or away from the wall, regardless of the positions of the other joints. The setup showing the manipulator's starting position is shown in Figure 31.

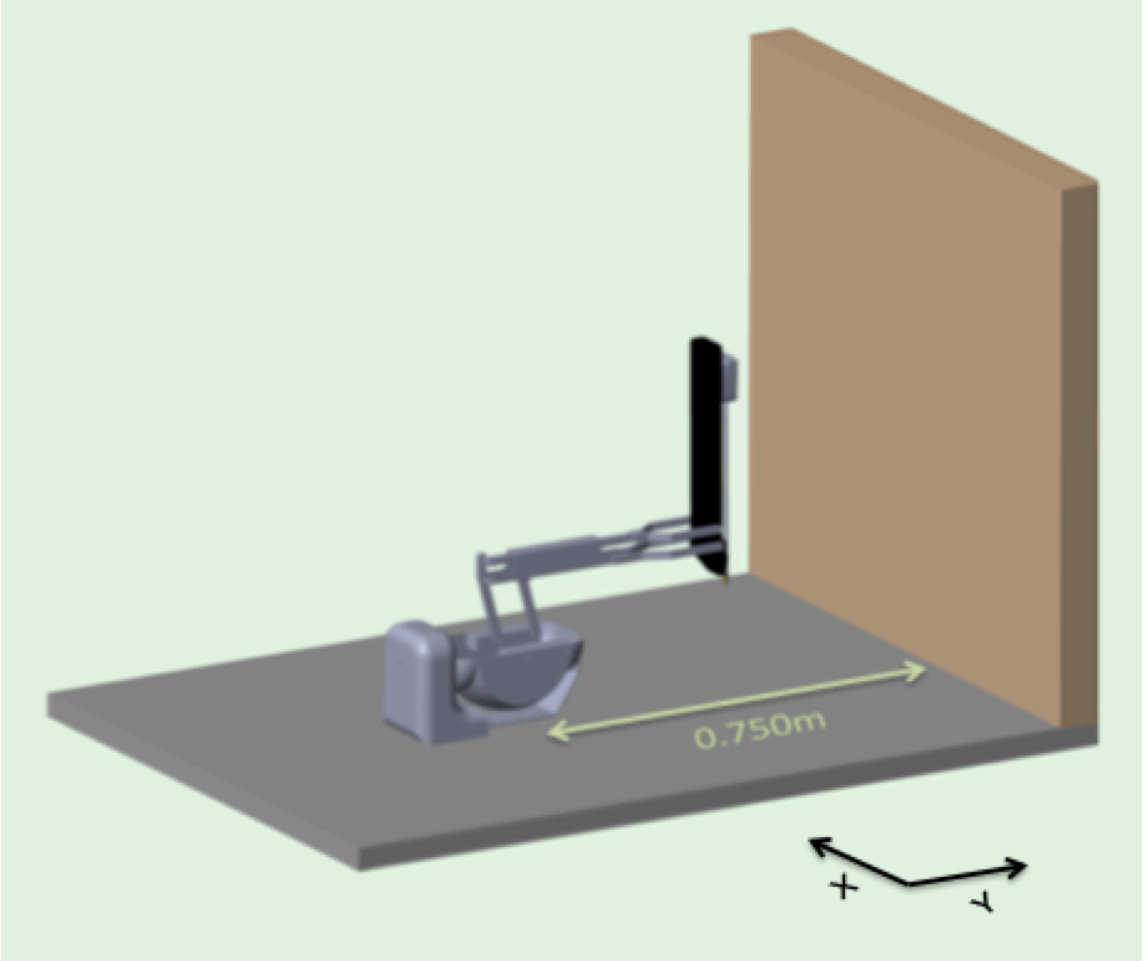

Figure 31: Simulation Setup for Experiment 2. Note that this diagram is not to scale; it is used to clarify the system arrangement.

In both experiments, the PSM model follows the same trajectory. From its starting position, where all states are zero, the tip of the manipulator is programmed to come in contact with the tissue model, and then slide down the wall while maintaining minimal contact. This entire simulation 10 seconds; with 3 seconds used to approach the wall and 3 seconds for sliding. There is a 2 second break between the two motions, to account for delay, and 1 second pauses at the start and end of the simulation. The original point of contact between the wall and end effector is 0.1m away from the ground, and the final

position has the end effector touching the ground. Figure 32 shows the end effector trajectory, from two different angles, while Figure 33 shows the movement timeline for the simulation.

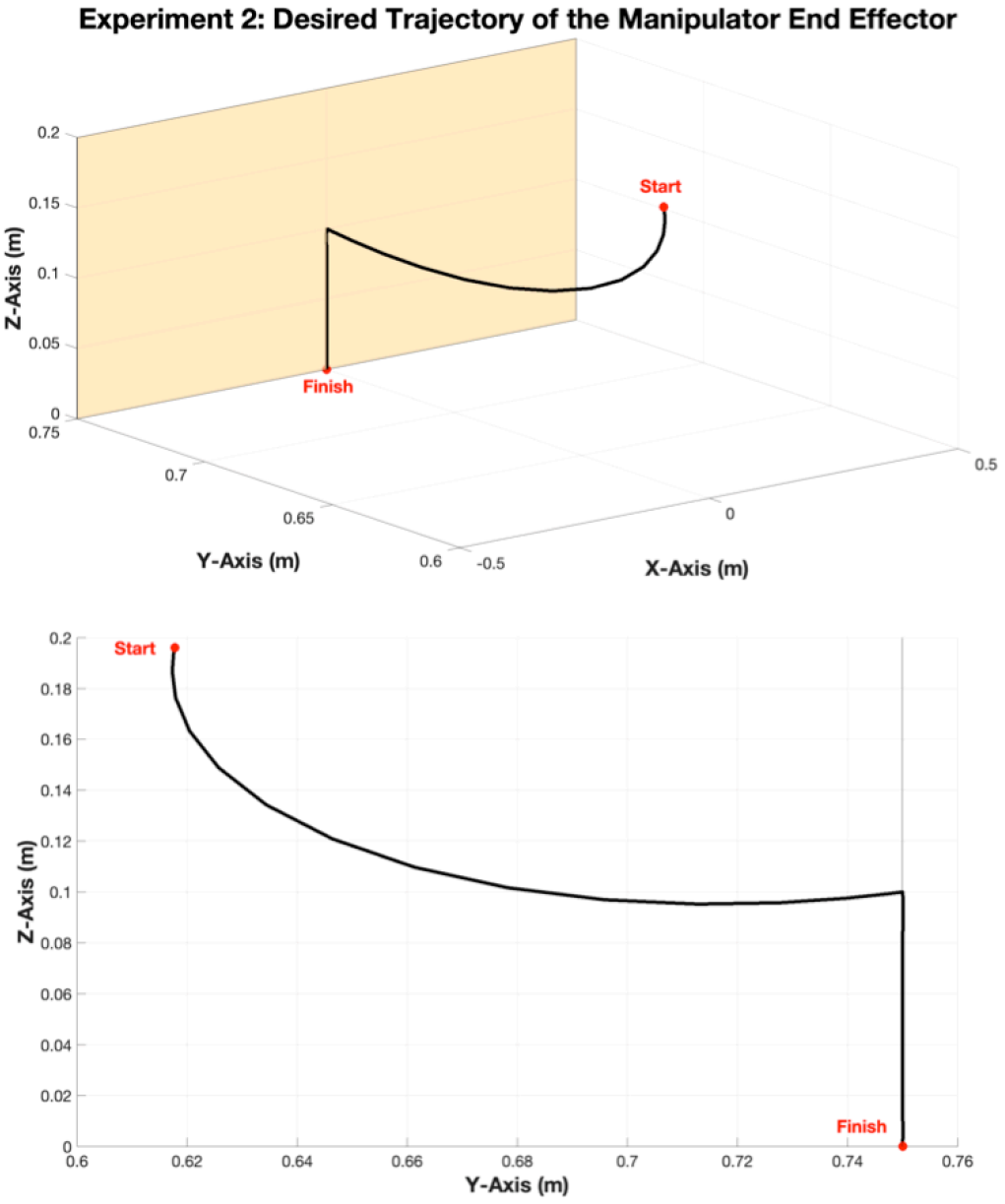

Figure 32: Desired Trajectory of Manipulator End Effector for Experiment 2.

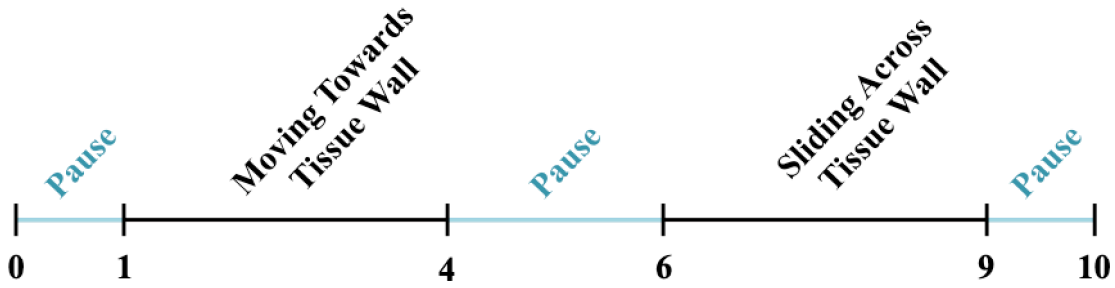

Figure 33: Timeline for Experiment 2.

The simulation only uses minimal contact between manipulator and wall as large forces are shown to be detrimental to performance resulting in difficulty in observing the effects of the hybrid controllers.

Important features to be observed include the position of the end effector in the y-direction, penetration depth into the tissue, as well as the total measured forces between the wall and manipulator. In addition, the performance of the two hybrid controllers will be compared to determine the advantages and disadvantages of each.

5.1 Experiment 2, Scenario 1: Hybrid PID Controller

5.1.1 Setup

The first of the two simulations employs PID controllers to control the manipulator. Each of the PSM joints are assigned a tuned controller (6 in total), which all work together to produce the best system performance. Factors such as operation speed, ability to follow the desired trajectory, and system stability are considered when tuning each PID.

5.1.2 Results and Discussion

Figure 34 shows the end effector trajectory of the PSM in the y-direction, with the wall located at 0.750, for the trials with different time delays, as well as the desired trajectory.

Figure 34: Position of Manipulator End Effector in the Y-Direction for Trials from Experiment 2, Scenario 1 that are Subjected to Various Time Delays.

From the figure, the trial with a delay of 800ms is shown to fail, while all other trials are successful. Unlike other successful trials, the manipulator's end effector in the 600ms delay trial does not reach its desired position by the end of the simulation time. However, it shows signs of stabilizing from its decreasing oscillations and expected to settle if the simulation time were to continue. On the contrary, the trial delayed by 800ms shows no signs of stabilization as oscillations increase rather than decrease; indicating larger errors and showing no clear settling time. These results agree the expected performance of telerobotics, as indicated in Table 1.

In addition, the effects of the time delays are reflected in the trial results. With each increasing delay, the manipulator reacts slower, as evidenced by the plots between the simulation times of 2-4 seconds. However, the correlation is not linear, as the delay between the 600ms to 800ms trials is much larger compared to the delay between the 0ms to 200ms delay trials. This behaviour shows the exponential decrease in performance associated with the constant time delay increases.

For the successful trials, all having contact with the tissue surface, the penetration depth into the tissue and measure forces are shown in Figure 35 and Figure 36 respectively. Note that the measured forces account for both normal and frictional forces, as the experiment considers the effect of the total force applied to the tissue.

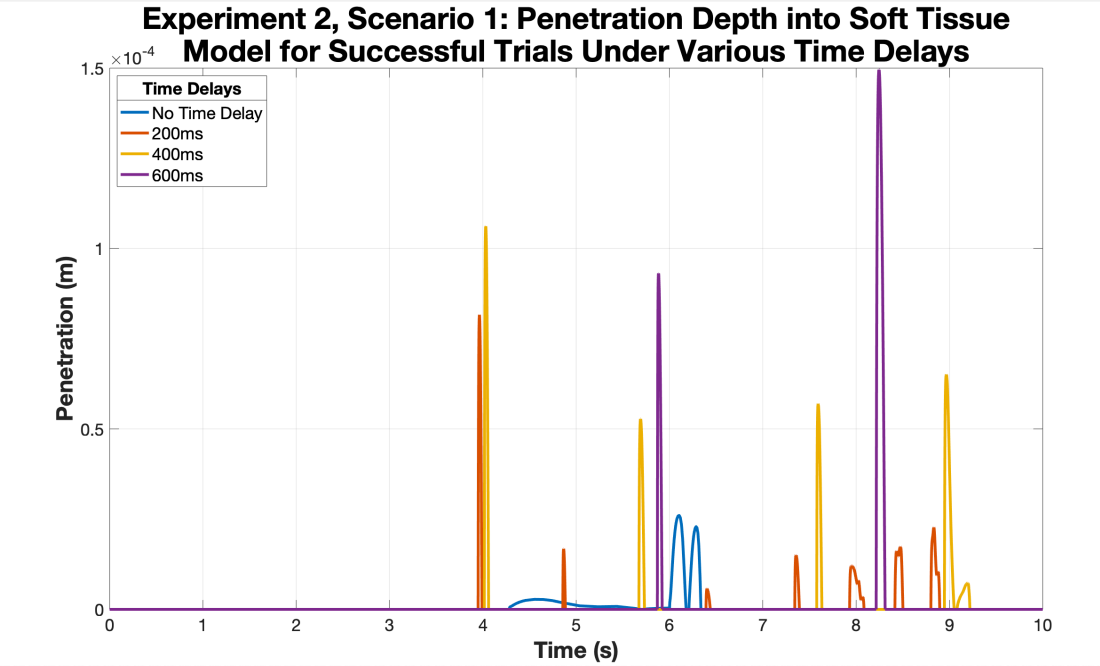

Figure 35: Penetration Depth of End Effector into Soft Tissue Model for Successful Trials from Experiment 2, Scenario 1 that are Subjected to Various Time Delays.

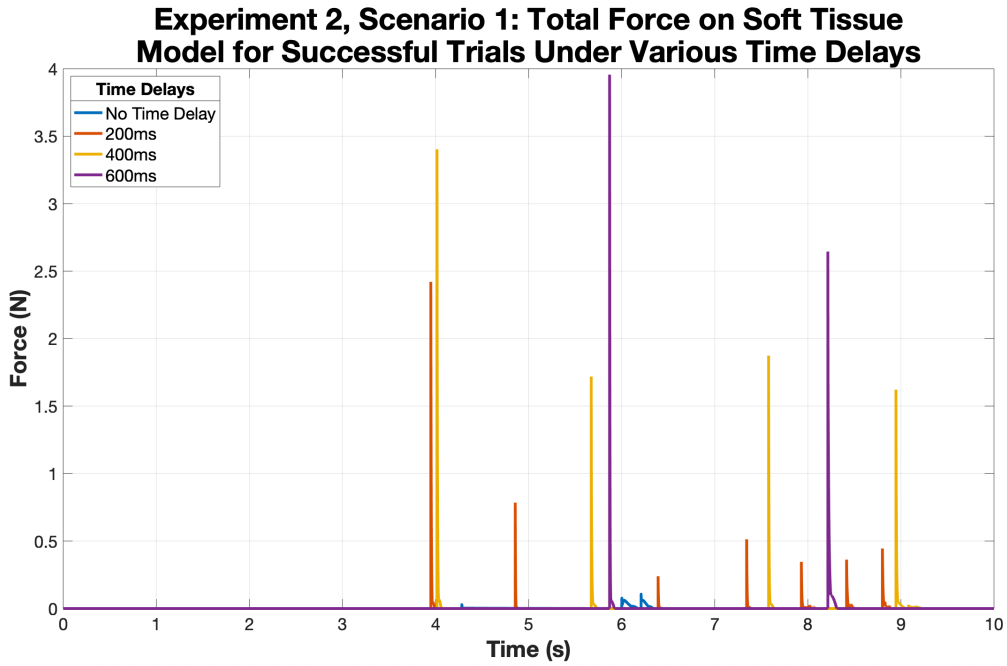

Figure 36: Measured Total Force between the End Effector and Soft Tissue Model for Successful Trials from Experiment 2, Scenario 1 that are Subjected to Various Time Delays.

As expected, penetrations and measured forces correspond to one another, both recording positive values at the same simulation time. However, the magnitudes of the factors are not always proportional, due to the differences in velocity, which is explained through Equation (16). This behaviour is most prominently seen in the 600ms delay simulation at times of 5-6 seconds and 8-9 seconds. The earlier point of contact has less penetration but greater measured forces, while the later point of contact has the opposite.

Overall, larger delays correspond to deeper penetrations and greater forces. This behaviour is expected, as the intended trajectory has no contact, indicating that there should be neither penetration nor measured forces. The greater magnitudes of these two factors meant there are more errors, which follows the time delay trend where longer time delays result in performance decline.

As mentioned previously, force control is activated when the forces applied by the manipulator to the tissue model exceed 2N, thus applying to successful trials with delays of 200ms to 600ms. From all three trials, the effects of the hybrid controller can be observed via the measured forces in Figure 36. After the initial force overshoot, the subsequent measured forces are shown to be significantly smaller. For the 200ms and 400ms delay trials, these successive forces are under 2N, while the 600ms trial shows a large force decrease, but still stays above 2N. This behaviour occurs in spite of penetration depth, as the 600ms delay trial shows an increase in penetration, contrary to the decrease in force from the data recorded at approximately 6-8.5 seconds. As the force reduction cannot be seen in the undelayed trial, where recorded forces do not surpass the 2N threshold, the reduction can be attributed to the force control aspect of the controller.

Comparison with a standard PID-controlled manipulator can used to provide a closer look into the effects of hybrid control. Figure 37 shows the positional comparison between these two controllers when under a time delay of 600ms. Until approximately the 6-second mark, both simulations are identical, but change shortly after. Looking to Figure 38, this corresponds to the time when force control is activated, as the 2N threshold is surpassed. From there, the hybrid controller shows superior performance, shown by the minimized oscillations. Furthermore, Figure 38 also shows a greater total force reduction for the hybrid controller when compared to the standard PID controller at approximately the 8-second mark. The diminished forces indicate safer contact with the tissue and improved overall performance.

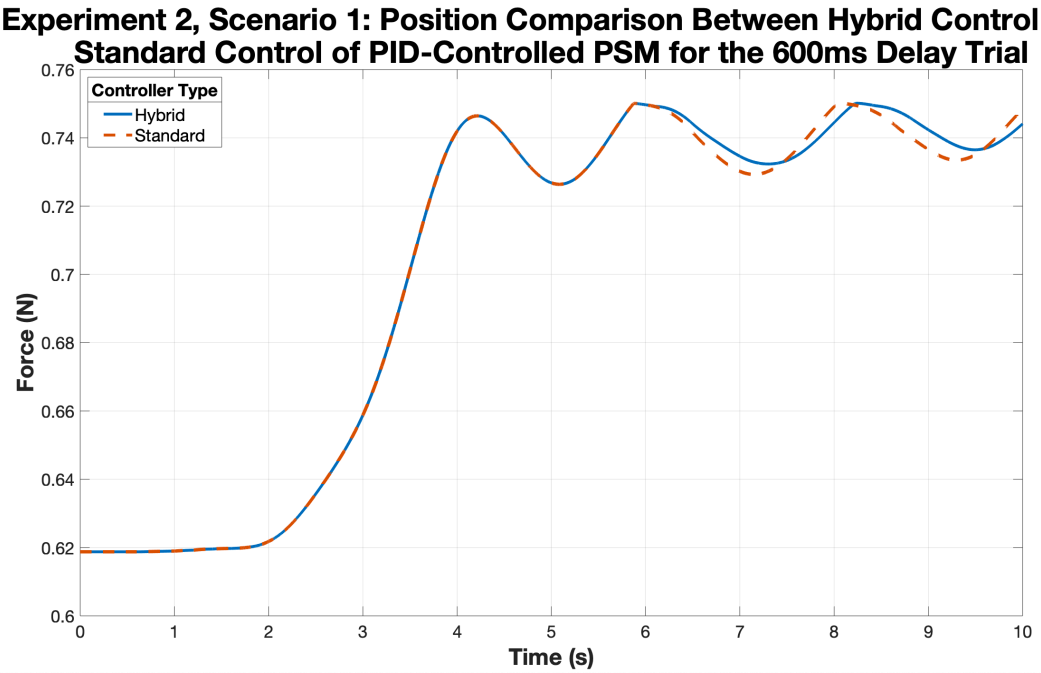

Figure 37: Position Comparison of Manipulator End Effector in the Y-Direction between the Hybrid PID-Controlled PSM and Standard PID-Controlled PSM.

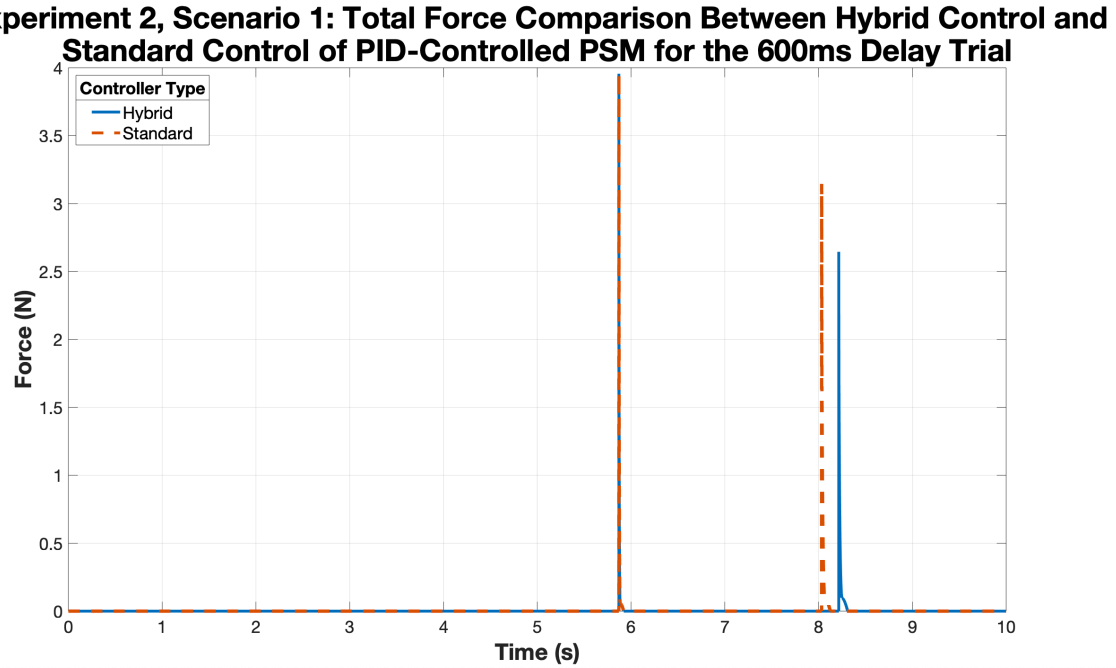

Figure 38: Total Force Comparison of Manipulator End Effector in the Y-Direction between the Hybrid PID-Controlled PSM and Standard PID-Controlled PSM.

5.2 Experiment 2, Scenario 2: Hybrid MPC Controller

5.2.1 Setup

The second scenario uses MPCs in the hybrid controller to manipulate the PSM. Only two controllers are employed, one for position and one for force control. The minimal controller setup is possible because MPCs use a system dynamics model to represent the manipulator. This model allows the controller to consider the effects of all joints on one another when generating controller output signals. In this scenario, the system dynamics of the MPC are linearized at the starting point, where all states are zero, of the manipulator.

5.2.2 Results and Discussion

Positional results of the MPC-controller manipulator are presented in Figure 39 below. The planned trajectory of PSM is also shown for reference.

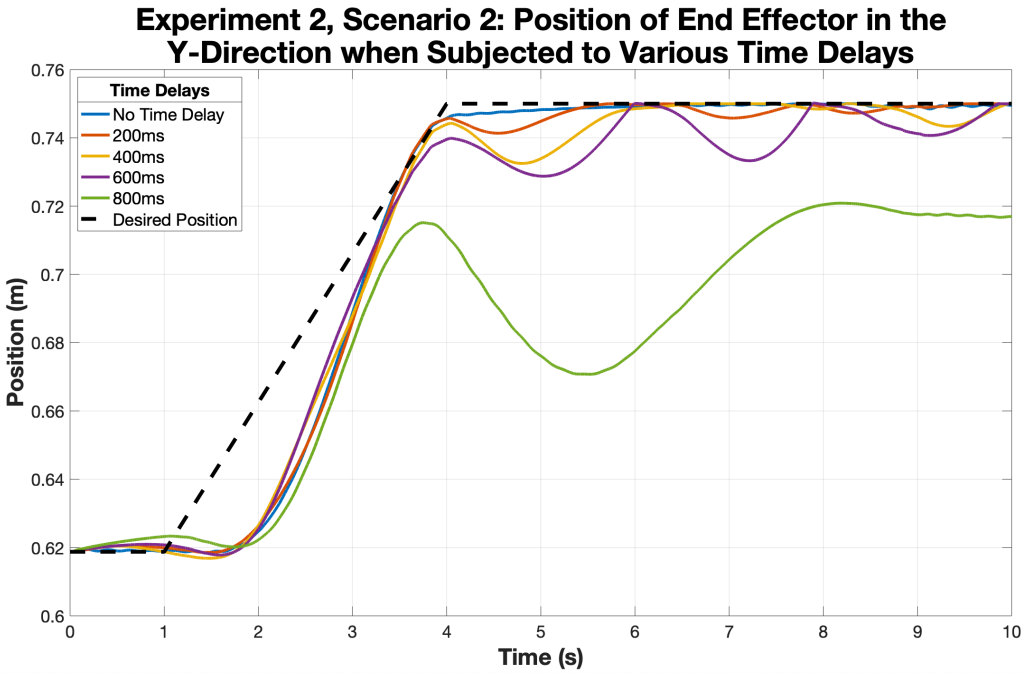

Figure 39: Position of Manipulator End Effector in the Y-Direction for Trials from Experiment 2, Scenario 2 that are Subjected to Various Time Delays.

Trials with delays of 0ms to 600ms show successful results, with all trials stabilizing and reaching the desired position at 0.750m prior to the end of the simulation. For the failed 800ms delay trial, the results show system stability, but settle at a distance far below the desired position, at 0.720m, without contact with the tissue wall model. Overall, these trials show that higher delays negatively affect performance, creating greater oscillations and longer settling times than the trials with lower delays.

Penetration depth and the recorded forces of the successful trials are presented in and Figure 40 and Figure 41 respectively. These figures provide more details about the simulation performances and allow easier comparison between trials.

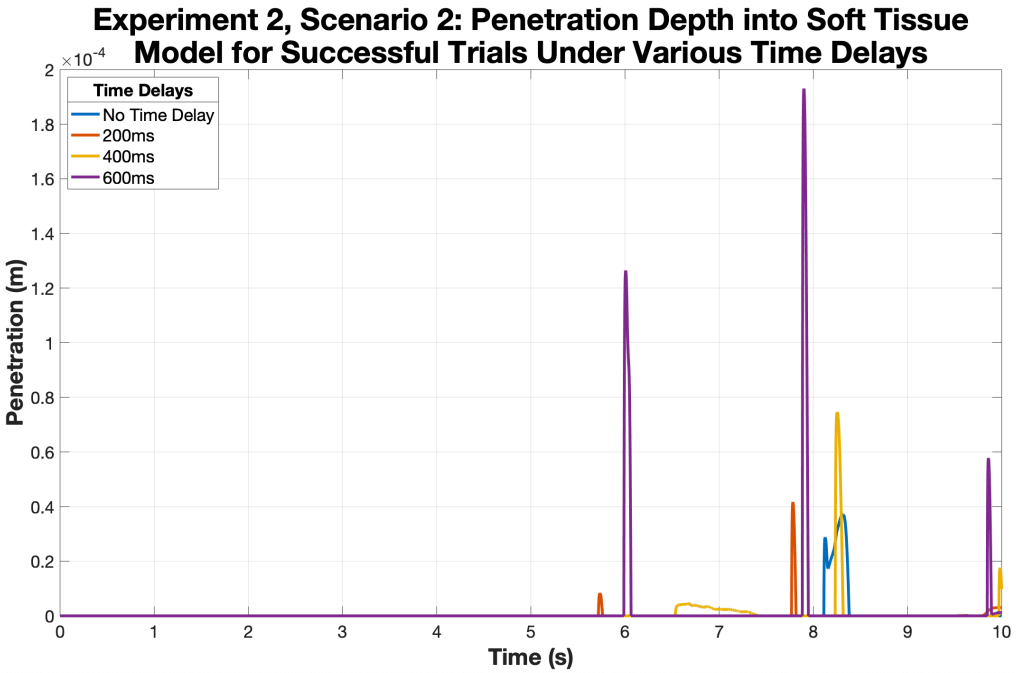

Figure 40: Penetration Depth of End Effector into Soft Tissue Model for Successful Trials from Experiment 2, Scenario 2 that are Subjected to Various Time Delays.

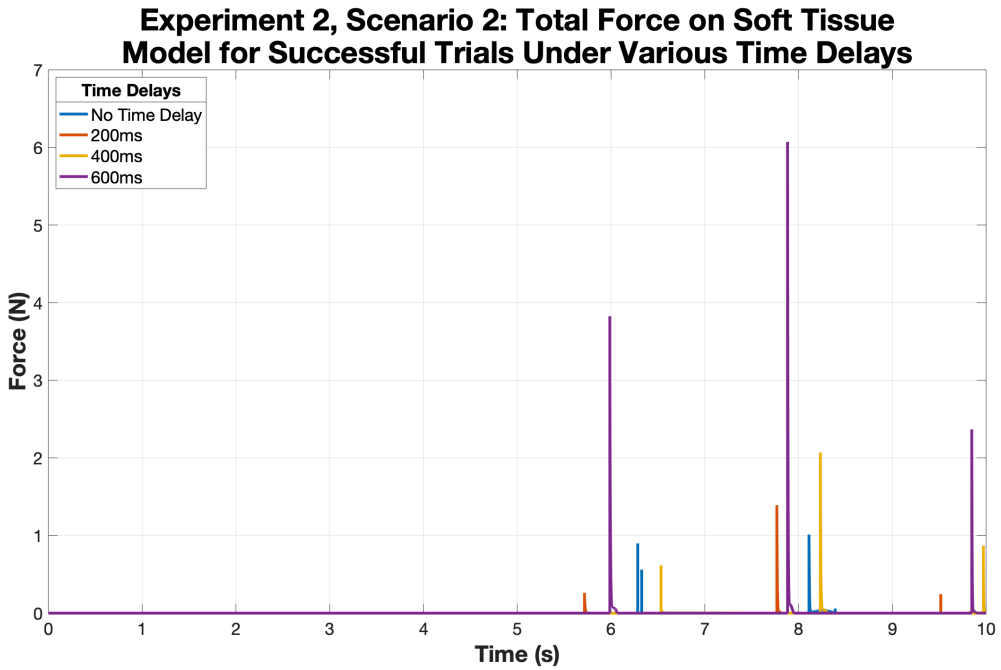

Figure 41: Measured Total Force between the End Effector and Soft Tissue Model, in the Y-Direction, for Successful Trials from Experiment 2, Scenario 2 that are Subjected to Various Time Delays.

The two figures show a proportional relationship, with the magnitudes of the penetrations and the measured forces corresponding to one another. Both factors also increase with increasing time delay, following the expected trend where larger delays result in decreased performance.

Contrary to the hybrid controller results in the first set of simulations, the hybrid MPC controller setup appears to have little to no effect on the performance, as there is no obvious change in measured forces in spite of the threshold force value. In particular, in the 600ms delay trial, the 2N threshold is surpassed twice, at approximately 6 seconds and 8 seconds into the simulation, but forces do not decrease, rather increase, from one point to the next.

For a closer look into the hybrid control effects, Figure 42 and Figure 43 provide comparisons between hybrid MPC and standard MPC for the planned simulation. Both figures show very little difference in both position and total, indicating ineffective force control. The failed MPC force control method may be due to the nature of the MPC, which uses the same cost function and similar space state models for both controllers. This results only minor changes in spite of the changed control law during the simulation.

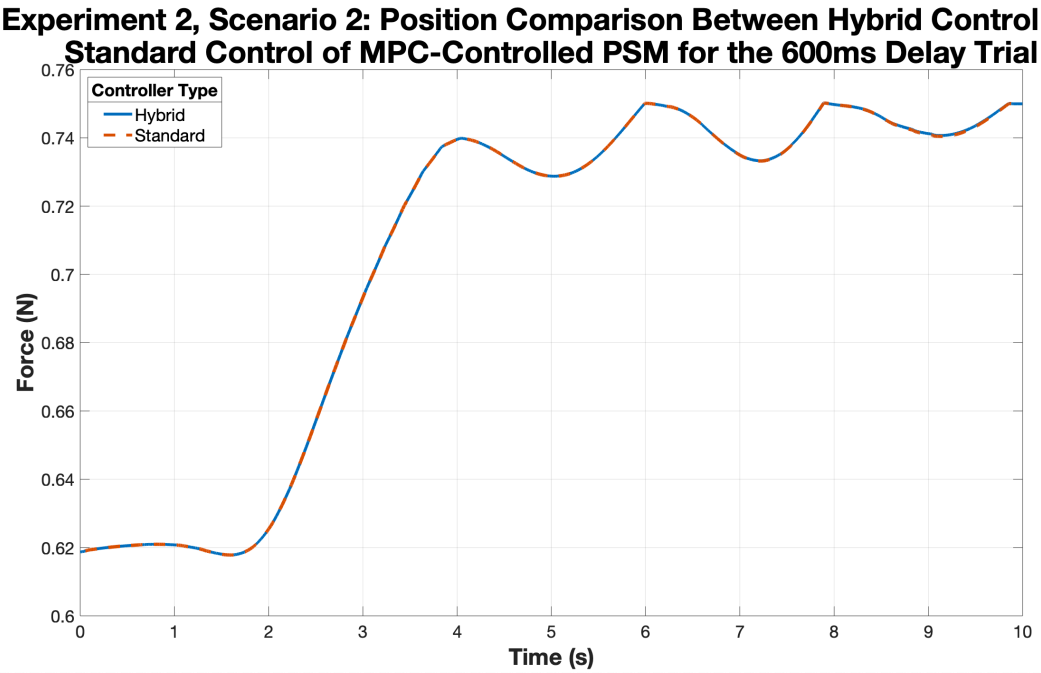

Figure 42: Position Comparison of Manipulator End Effector in the Y-Direction between the Hybrid MPC-Controlled PSM and Standard MPC-Controlled PSM.

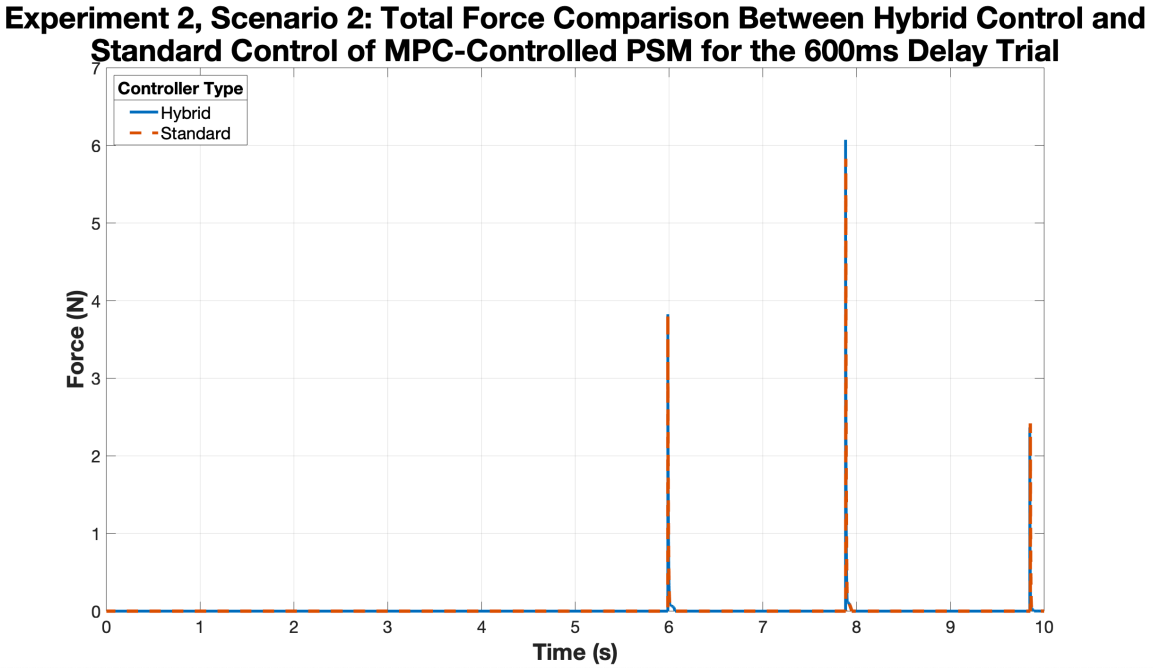

Figure 43: Total Force Comparison of Manipulator End Effector in the Y-Direction between the Hybrid MPC-Controlled PSM and Standard PID-Controlled PSM.

5.3 Comparison

From the two scenarios, both show results match the expected performance, but to different degrees. For comparison between the two controllers, Figure 44, Figure 45, Figure 46, and Figure 47 show the results of the PID and MPC trials for delays of 0ms, 200ms, 400ms, and 600ms respectively.

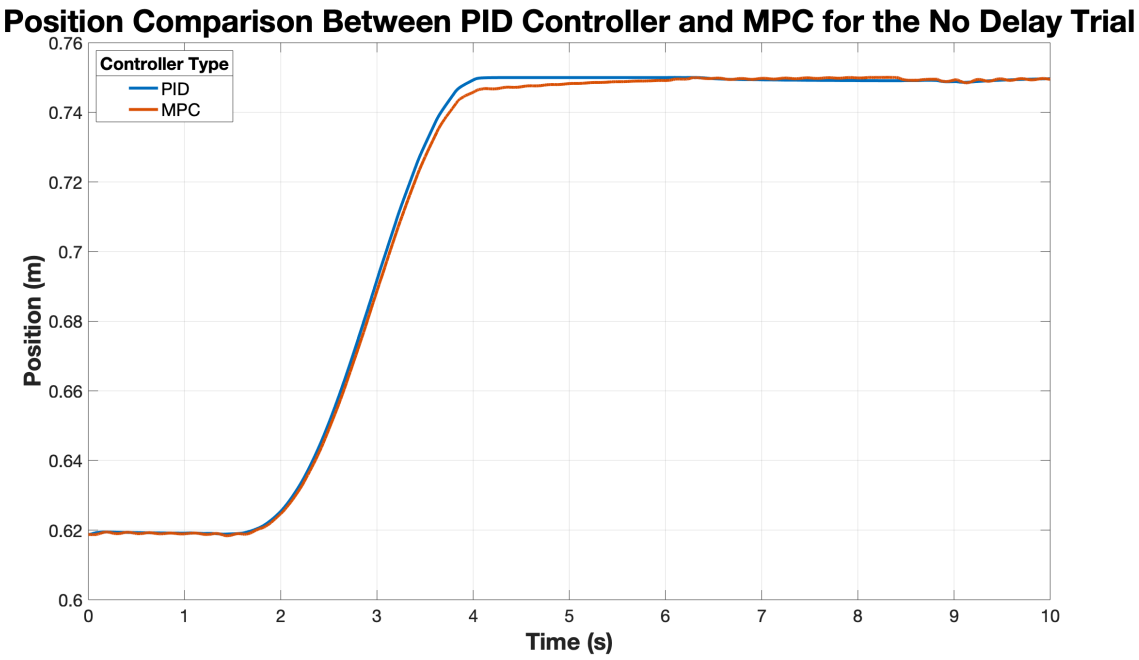

Figure 44: Position Comparison of Manipulator End Effector in the Y-Direction between the Hybrid PID and Hybrid MPC Simulations from Experiment 2 for the No Delay Trial.

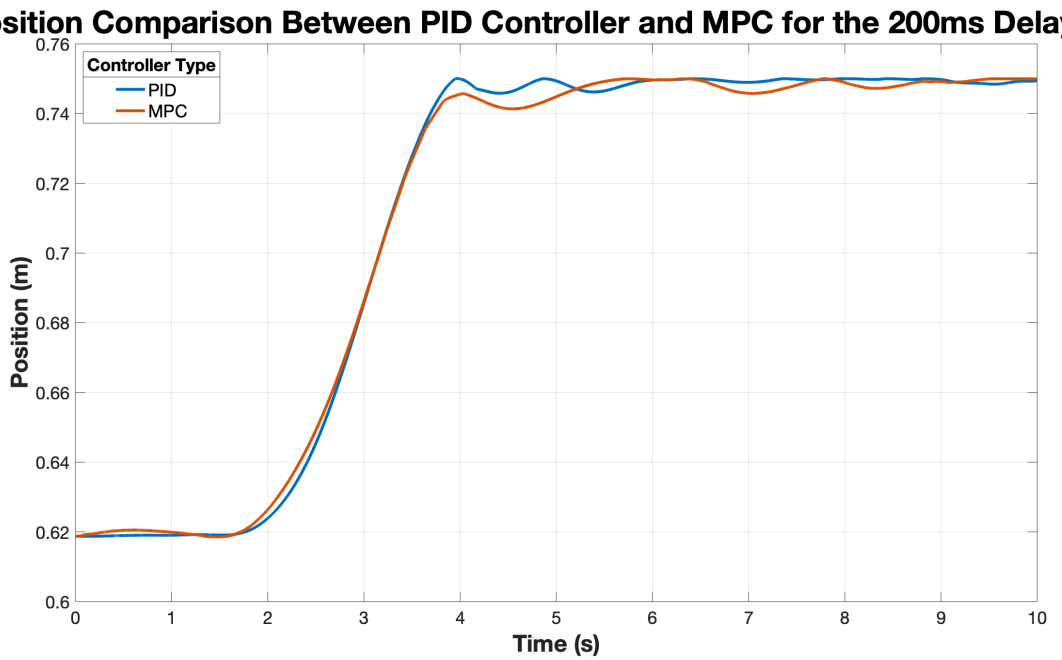

Figure 45: Position Comparison of Manipulator End Effector in the Y-Direction between the Hybrid PID and Hybrid MPC Simulations from Experiment 2 for the 200ms Delay Trial.

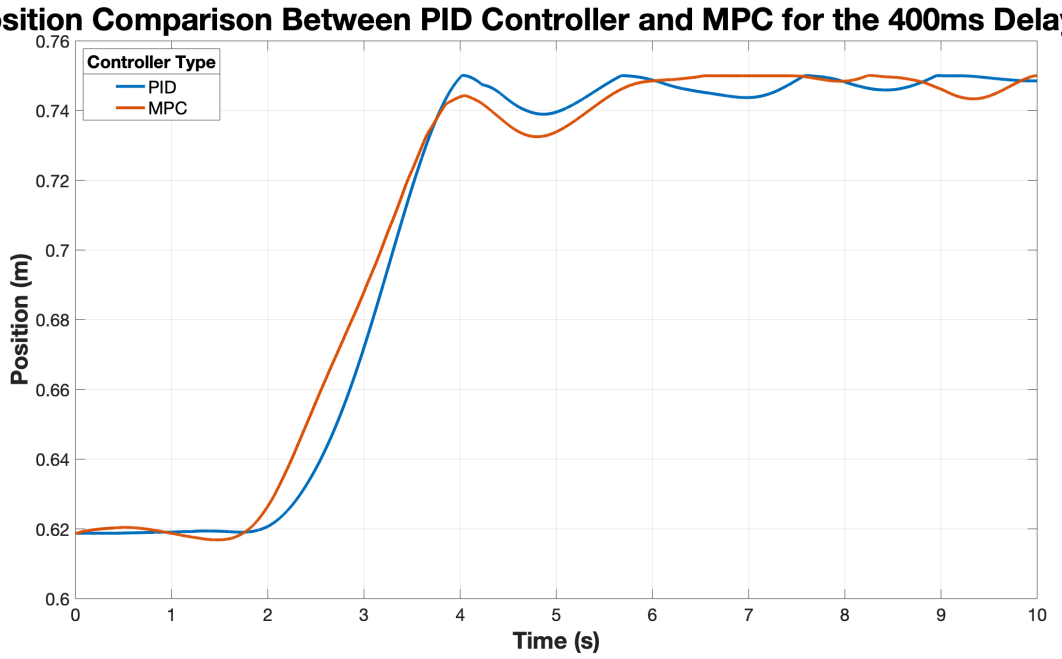

Figure 46: Position Comparison of Manipulator End Effector in the Y-Direction between the Hybrid PID and Hybrid MPC Simulations from Experiment 2 for the 400ms Delay Trial.

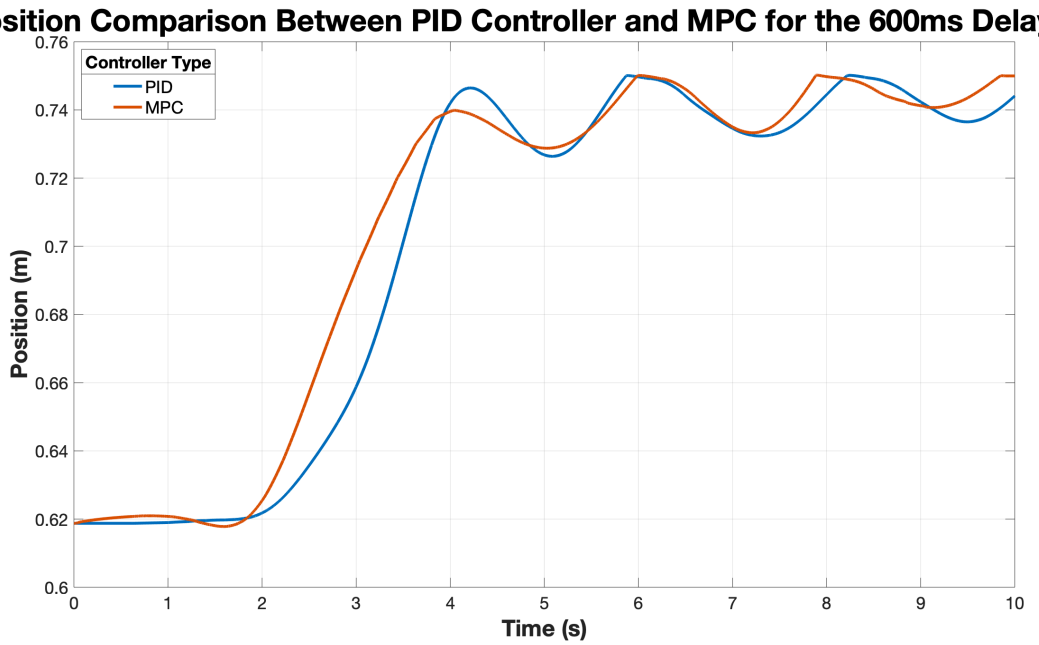

Figure 47: Position Comparison of Manipulator End Effector in the Y-Direction between the Hybrid PID and Hybrid MPC Simulations from Experiment 2 for the 600ms Delay Trial.

From all figures, the trajectories of both simulations show first attempted contact with the tissue surface at approximately 4 seconds, as intended. For the PID-controlled trials, represented by the blue plots, contact between surfaces is made, but delayed in proportion to the programmed time delay of the trial. Thus, the undelayed trial initiates contact at 4 seconds into the simulation and each subsequent delay trial makes contact later. On the contrary, the trials of the MPC-controlled PSM, represented by the orange plots, are not delayed, shown by the more aggressive initial movement, starting before the 2-second mark, and the initial peak at 4 seconds for all trials. However, the height of the peaks decreases with increasing delay and does not initially reach the 0.750m mark as intended. Overall, both controller setups are affected by the programmed time delays, but in different fashions: with one showing delayed results, and the other showing more cautious behaviours.

When comparing the scenarios side-by-side, both controllers appear to have similar performance with small delays. However, in the trials with larger delays of 400ms and 600ms, the MPC setup outperforms the PID setup. This behaviour is detailed in Table 9 and Table 10, which show the settling times and average positional errors, respectively, for the experiments using the hybrid PID-controlled PSM, in blue, and the hybrid MPC-controlled PSM, in orange. The quantitative results indicate that MPC has equal or superior performance for nearly all experiments, shown by the bold highlight. The exception, occurring in the error as the manipulator moves towards the wall for the undelayed trial, can be attributed to the MPC's previously mentioned cautious nature, causing the manipulator to slow down as it approaches the wall.

Table 9: Settling Times (s) of PSM for Successful Trials from Experiment 2 that are Subjected to Various Time Delays.

	Time Delay			
	No Delay	200ms	400ms	600ms
Settling Time (s)	4.0000	4.0000	5.2821	9.9732
	4.0000	4.0000	**5.0787**	**7.4141**

Table 10: Average Positional Errors (m) of PSM for Successful Trials from Experiment 2 that are Subjected to Various Time Delays.

		Time Delay			
		No Delay	200ms	400ms	600ms
Movement	Towards the Wall	**0.0187**	0.0209	0.0260	0.0317
		0.0195	**0.0196**	**0.0191**	**0.0183**
	Sliding Across the Wall	9.3367×10^{-4}	0.0023	0.0044	0.0099
		$\mathbf{4.7597\times10^{-4}}$	**0.0010**	**0.0034**	**0.0098**

The superior MPC performance may be caused by the controller setups; wherein only a single MPC controller is used to manipulate the PSM, versus the six required for the PID. In addition, MPCs have predictive properties, which may further enhance performance. The PID setup appears to be unable to surpass these factors.

Regardless of the programmed delay, both scenarios show lag when beginning the simulation, at best starting near the 2-second mark versus the intended 1-second into the simulation. This behaviour may be caused by the joint control limitations of the PSM being simulated in Matlab. In Matlab, all manipulator joints are considered active, allowing torques to be applied, without restriction, to all joints. Thus, the generated inverse kinematics of the simulated trajectory is based off this assumption. However, in the PSM, most joints are passive and cannot be manipulated directly. Therefore, from the generated torques, only six can be applied, one for each active joint, resulting in significantly less force applied to the manipulator and slowing the its movement. In addition, closed-loop mechanisms are not supported, thus the computed joint motions may be less accurate.

Both simulations also use linearized plant approximations to represent the PSM. These models fail to fully capture the complex movements of the PSM, resulting in increased errors. The usage of more accurate models would likely result in improved results, at the cost of significantly higher computational efforts and time.

From the simulations, the MPC-controlled trials show better overall performance, while the PID-controlled trials react more positively to the change in control laws in hybrid control. Moving forward, it may be of interest to explore the effects of combining controllers; such as using MPC for position control and using a PID for force control in a single hybrid controller.

6. Chapter 6: Experiment 3 – Corrective Predictive Control

In the third experiment, the application of predictive control is explored for telerobotic usage in a surgical setting. In particular, these predictive controller setups have corrective capabilities, which can adjust new predictions based on the error magnitude between the delayed output and old predictions. Two sets of simulations involving different predictive controller setups are simulated under delays of 0ms, 200ms, 400ms, 600ms, and 800ms each. Results are recorded, discussed, and compared to the expected performance presented in Table 1.

This experiment will use the same manipulator and environment setup as Experiment 2, from Section 5, but with different controllers and a different planned trajectory. The manipulator, the da Vinci PSM, will be located 0.750m away from the tissue wall, represented by the Kelvin-Voigt model. As with Experiment 2, only six of the PSM joints will be controlled. Figure 48 shows the simulation setup and Kelvin-Voigt parameters will, again, be taken from Table 2 and Table 3.

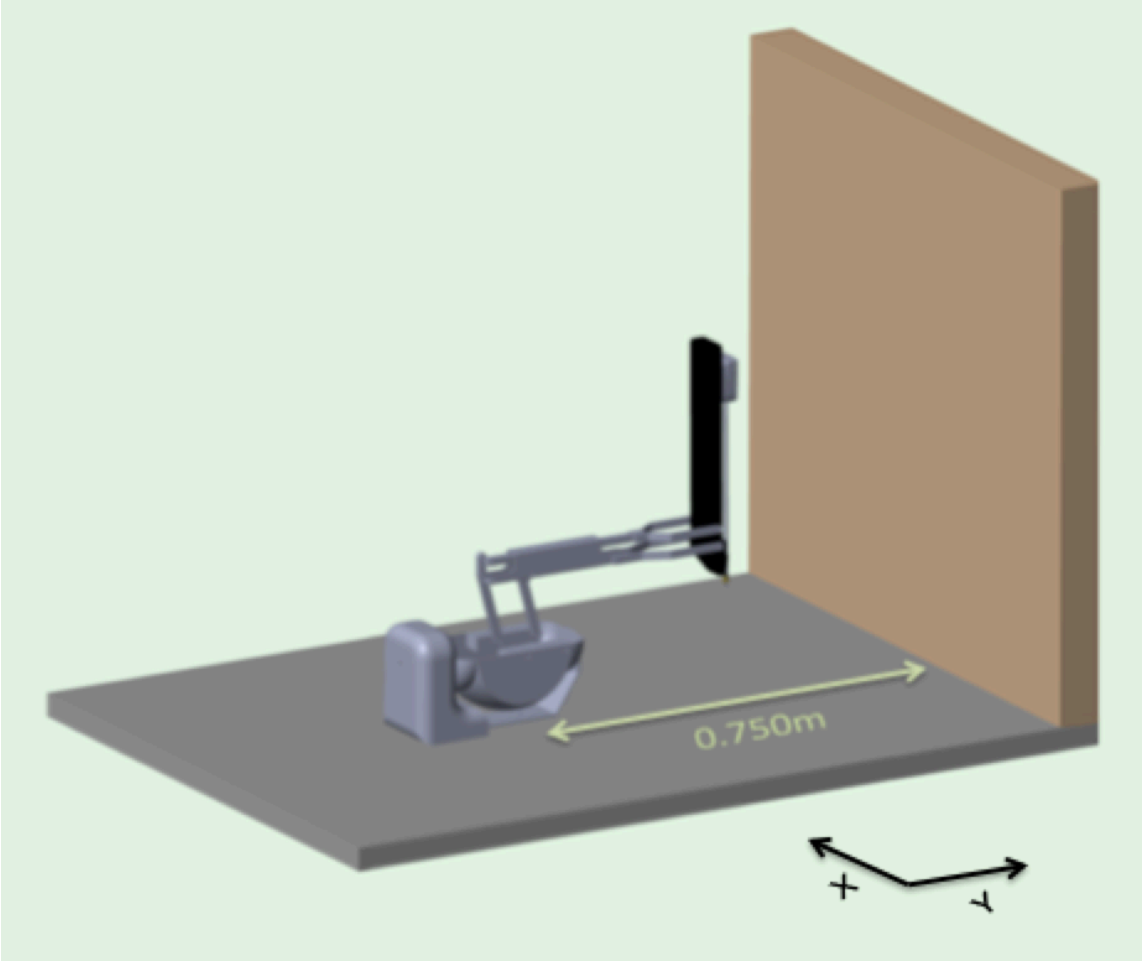

Figure 48: Simulation Setup for Experiment 3. Note that this diagram is not to scale; it is used to clarify the system arrangement.

Both simulations follow the same trajectory, shown from two perspectives in Figure 49. First, the PSM end effector will travel towards the tissue wall and make contact 3 seconds into the simulation. After a short 1 second pause, the manipulator slides, from 0.1m to 0m, down the wall, back up, then down again, with short 1 second breaks between each motion. Each sliding motion takes 3 seconds long, and after the final motion downwards, there is a 1 second pause before ending the simulation. In total, the elapsed simulation

time is 16 seconds. For further clarification, Figure 50 shows the movement timeline of the simulation.

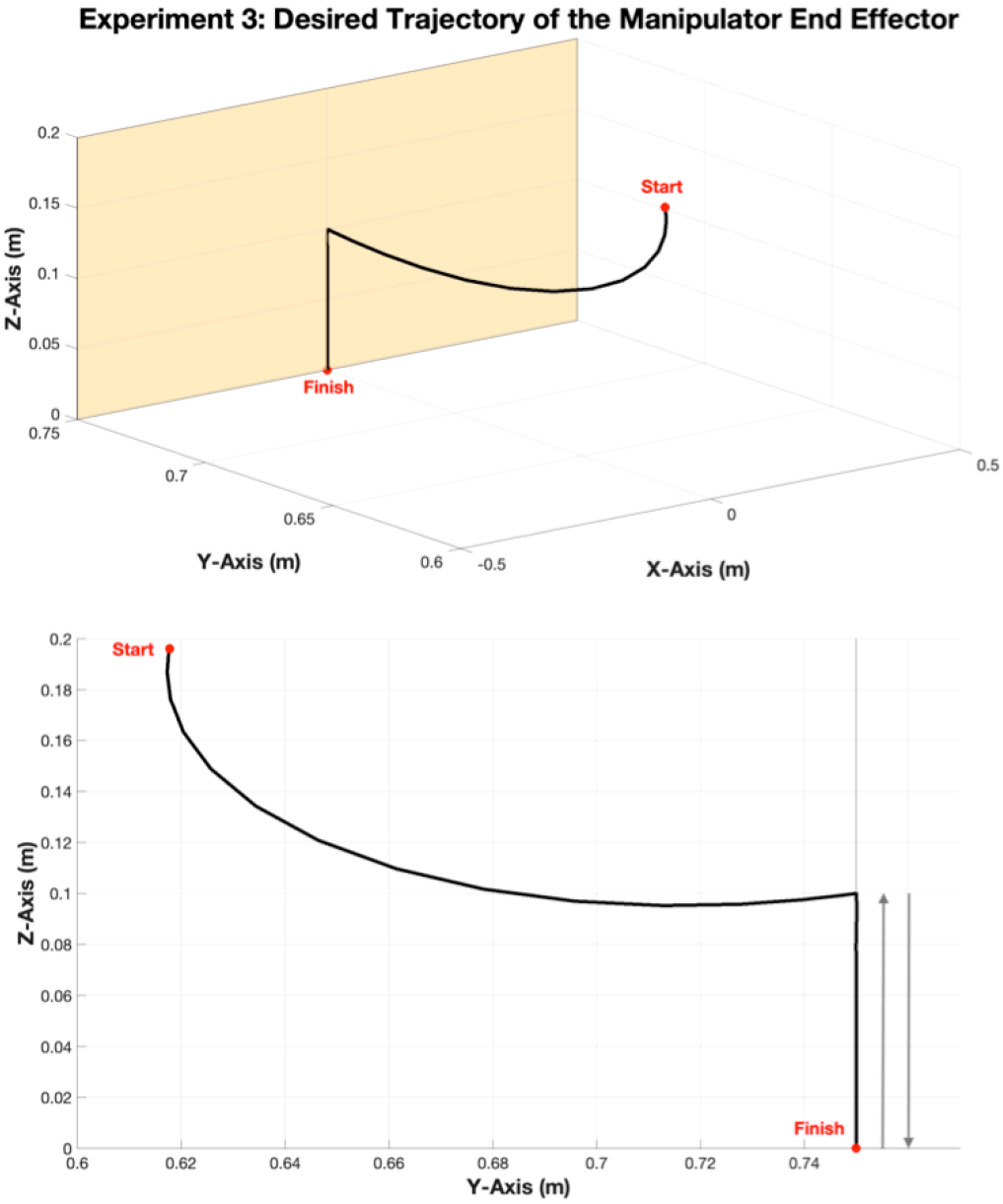

Figure 49: Desired Trajectory of Manipulator End Effector for Experiment 3.

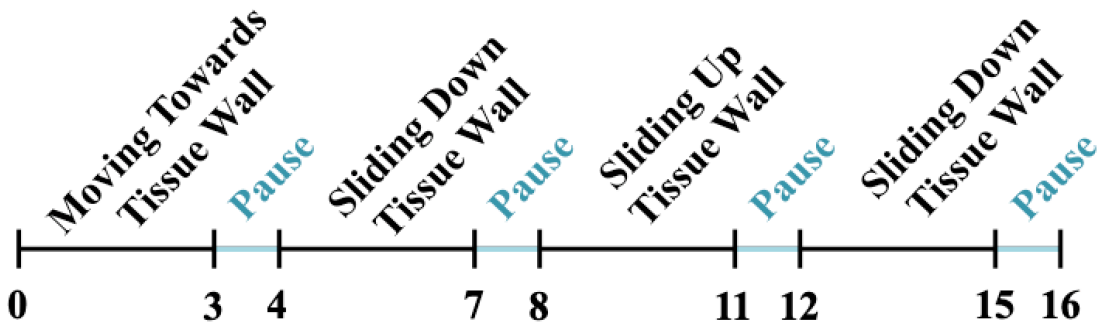

Figure 50: Timeline for Experiment 3.

For each simulation, the position of the end-effector, in the y-direction, as well as the positional error will be observed. In addition, penetration depth and the measured forces from contact will be analyzed. Finally, comparisons between the two simulations will also be carried out.

6.1 Experiment 3, Simulation 1: Smith Predictor and PID

6.1.1 Setup

The first of the two simulations uses a Smith Predictor with PID controllers for manipulator control. Each joint is manipulated by a PID for a total of 6 controllers used to move the PSM. These controllers are tuned by considering factors such as stability, performance in following the desired trajectory, settling time, and more. For the predictor, a non-linear model is used to predict manipulator motion and inverse kinematics are used to relay the actual joint positions from the position of the measured end effector back to the controller setup.

6.1.2 Results and Discussions

Below, Figure 51 shows the positional results of the simulation for the end effector, in the y-direction. Included is also the desired trajectory shown via the dotted black line.

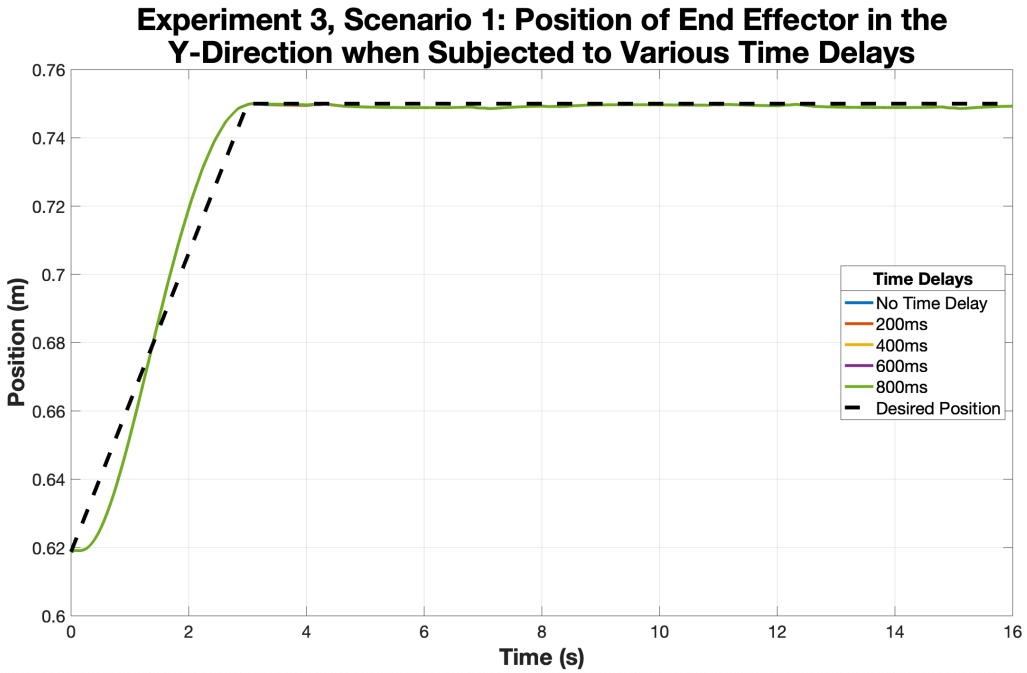

Figure 51: Position of Manipulator End Effector in the Y-Direction for Trials from Experiment 3, Scenario 1 that are Subjected to Various Time Delays.

All simulations appear to be very similar, with no visible differences between the trials. At the start of the simulation, the end effector shows a slight delay before beginning movement, but reaches the tissue wall at the intended contact time of approximately 3 seconds. The remainder of the simulation appears very stable and follows the desired trajectory accurately. Contrary to the expected performance presented in Table 1, all trials are successful, with no drop-off in performance despite the delays.

As little can be seen from the positional results in Figure 51, the error may provide more details on the manipulator performance. Figure 52 below shows the positional error for the duration of the entire simulation.

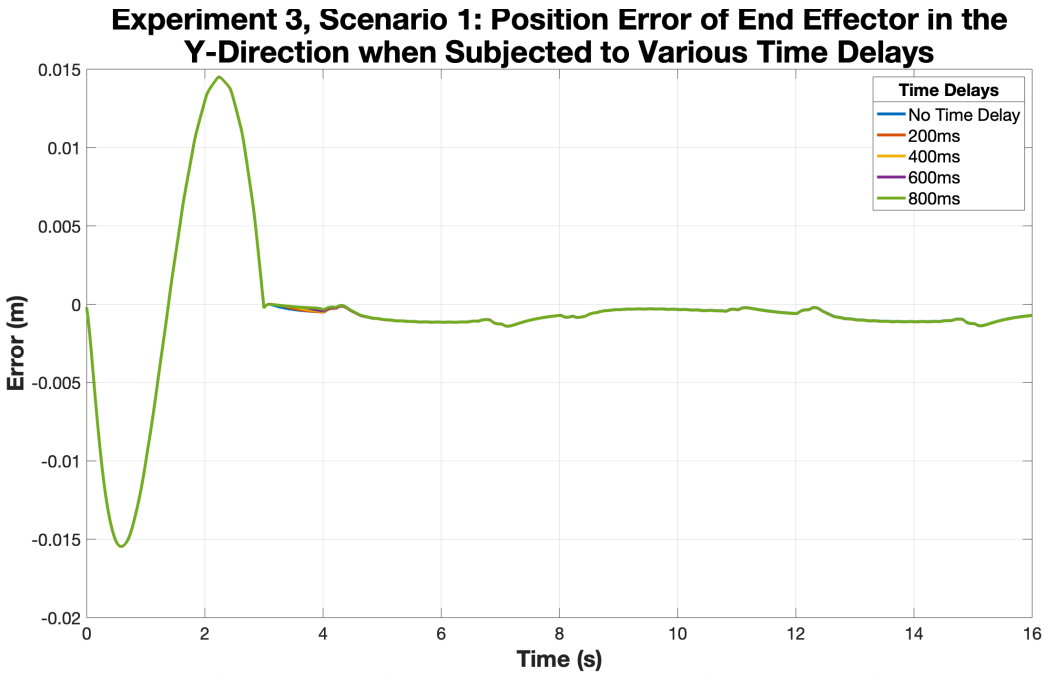

Figure 52: Position Error of Manipulator End Effector in the Y-Direction for Trials from Experiment 3, Scenario 1 that are Subjected to Various Time Delays.

With the exception of the region between simulation times of 0 to 3 seconds, the error is very minimal, appearing to be less than 1mm throughout. Looking back to Figure 51, the large error corresponds to the time when the manipulator is moving towards the tissue wall and appears to be the result of overcompensation.

In the simulation, the desired trajectory begins immediately with motion towards the wall. This motion is uniform, with proportionally increasing position and time, which corresponds with steady, uniform velocity. However, the original state of the manipulator

is stationary, thereby not having the desired uniform velocity to move following the desired trajectory. The overcompensation to move faster, making up for the slow start, allowing the end effector to reach the wall at the intended time of contact, 3 seconds into the simulation.

The error for all simulations appears very similar, with small differences in the region between 3 to 5 seconds. This area of interest, however, cannot be seen from the Figure 52. A closer look at this region is shown below in Figure 53.

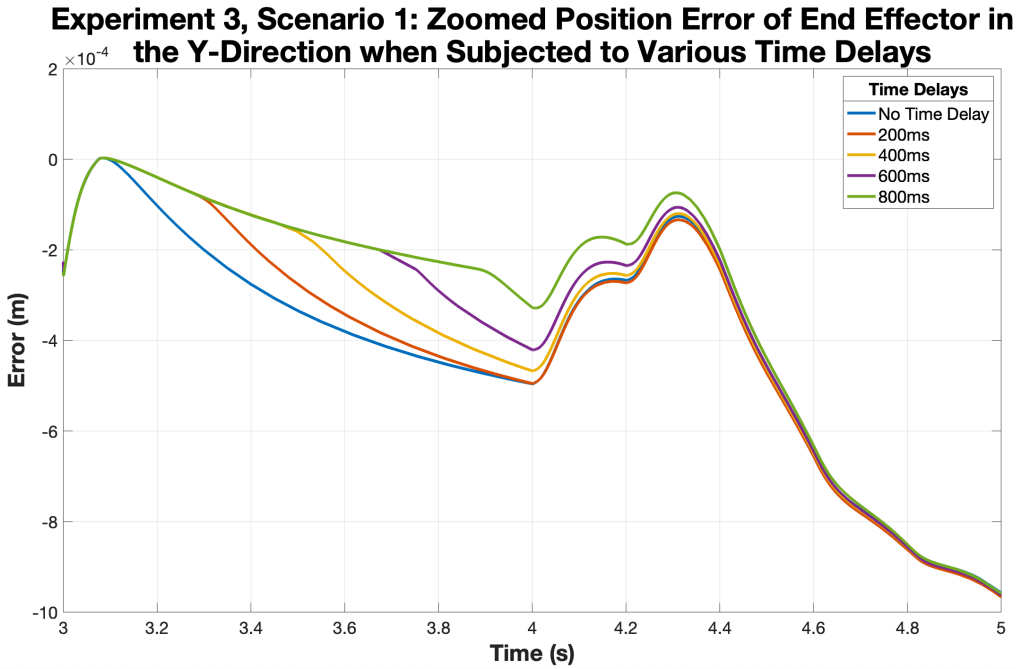

Figure 53: Region Between 3-5 Seconds for the Positional Error of Trials from Experiment 3, Scenario 1 that are Subjected to Various Time Delays.

From close up, it can be seen that trials with greater delay have better performance, with less deviation away from the desired 0 error mark, though minimally. The simulation result opposes the expected performance from Table 1, where tasks with short delays

have better performance than those with longer delays. This discrepancy may be due to the slower reaction of the delayed trials, stalling the reaction caused by contact with the tissue wall.

In the simulation, the setup uses a predictor to supplement delayed information. For shorter delays, the controller reacts much faster to correct any errors, thus following the predictor for less time. On the contrary, trials with longer delays would follow the predictor for longer periods of time before correction. From the point of contact, occurring at approximately 3.1s into the simulation time, the undelayed trial is shown to react immediately, pulling away from the wall and increasing error. The reactions of the subsequent trials are delayed in proportion to the corresponding time delays, each reacting 0.2s after the previous. Trials with longer delays benefit from the slow reaction as they continue to follow the predictions for a longer period of time, not reacting to the contact with the wall surface. This behaviour allows the end effector to stay closer to the wall, ultimately reducing the error and yielding better performance for larger delays.

As mentioned previously, there appears to be contact between the end effector and wall around the 3.1s mark. A closer look at this region, shown via Figure 54 and Figure 55 would provide more insight to the performance of the system.

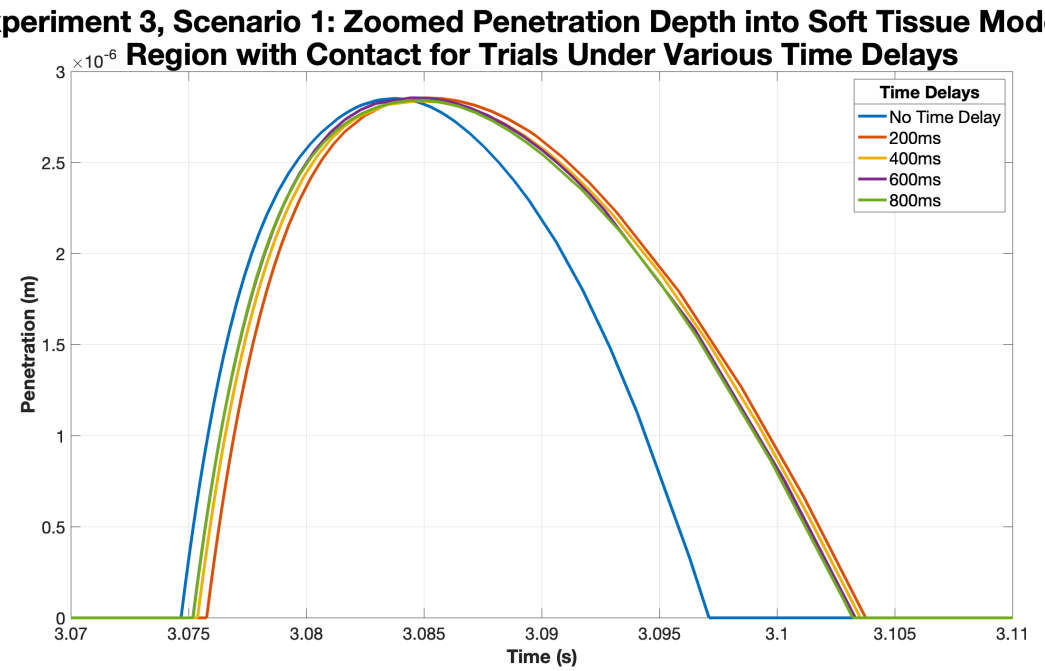

Figure 54: Region Between 3.07-3.11 Seconds for the Penetration Depth of Trials from Experiment 3, Scenario 1 that are Subjected to Various Time Delays.

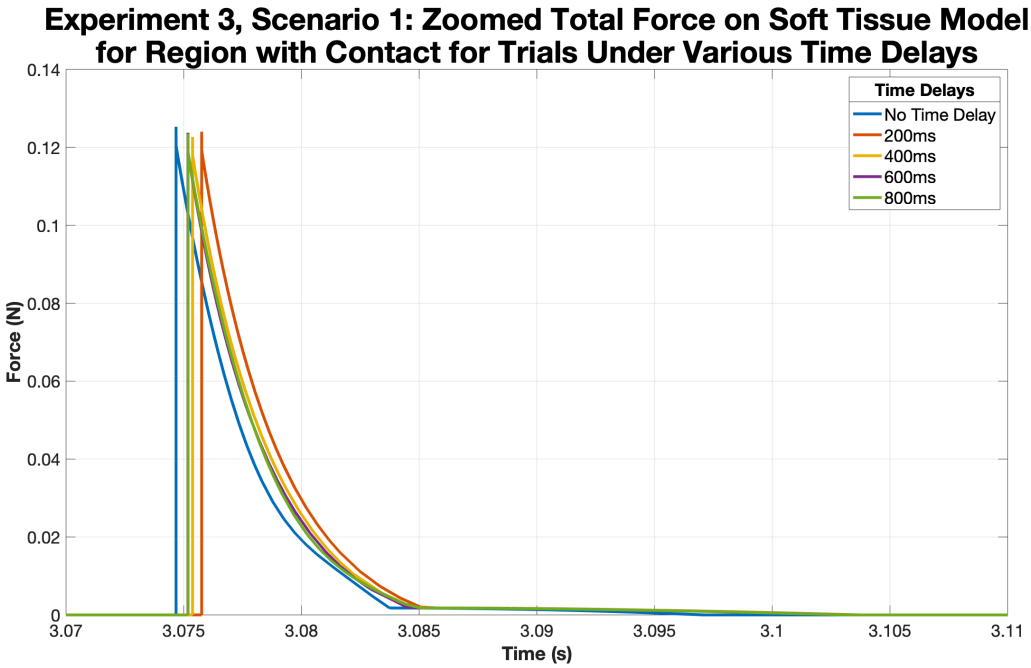

Figure 55: Region Between 3.07-3.11 Seconds for the Measured Contact Force of Trials from Experiment 3, Scenario 1 that are Subjected to Various Time Delays.

Figure 54 and Figure 55 show the region where contact is made, between simulation times of 3.07s to 3.11s. Both figures show similar magnitudes for penetration and forces in spite of different delays. None of the penetrations are very deep, measuring in the thousandths of millimeters, while the total recorded force is just above 0.12N. From all trials, a significant difference in penetration between the undelayed trial and the trials that are delayed can be noted.

Compared to the delayed trials, the trial with no delay reacts faster and penetrates the tissue for a shorter amount of time. The faster reaction can be attributed to the lack of delay while the shorter penetration may be due to the immediate response of the manipulator to contact with the surface.

Between the delayed trials, it appears that trials with shorter delays penetrate the tissue for shorter amounts of time, though minimally. On the contrary, trials with larger delays penetrate the tissue earlier than those with short delays. As penetration is not intended, this behaviour is the result of the manipulator overcorrecting for the error when moving towards to wall. When taking into account the delayed error at this time, it be noted that the error is larger for the longer delays when compared to shorter ones: that is, the error 0.8s prior to penetration is larger than the error 0.2s before it. The larger error may induce greater corrective motion, resulting in quicker penetration into the tissue surface for longer delays.

Of all the trials, the undelayed has the best performance, followed by trials with longer delays. This behaviour is contrary to expected results from Table 1, where larger delays have poor performance, specifically those with delays above 700ms. However, all trials in this scenario, which incorporate the Smith predictor and PID controller setup, are shown to be very successful.

6.2 Experiment 3, Simulation 2: Adaptive MPC Setup

6.2.1 Setup

The second of the two scenarios employs a single, adaptive MPC for manipulator control. In this scenario, the MPC uses a symbolic space state plant model to predict future motion of the PSM. With the symbolic notation, the model is linearized at every time step, allowing it to maintain as much of the system's complexity as possible for signal generation.

6.2.2 Results and Discussions

The positional results of the PSM controlled by the adaptive MPC are shown in Figure 56. The planned end effector trajectory is also plotted for comparison purposes.

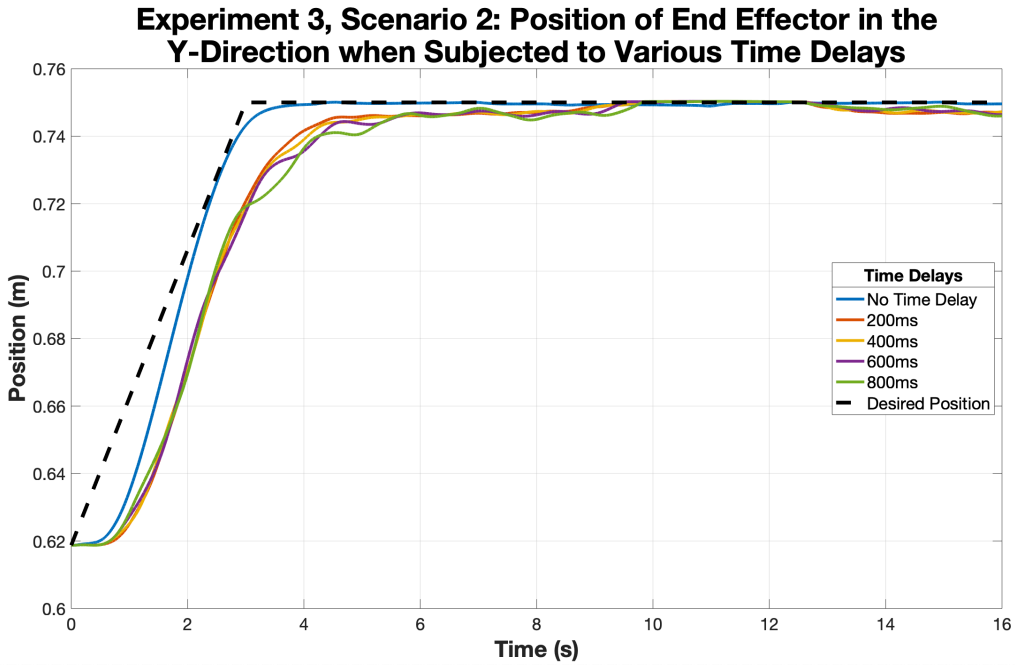

Figure 56: Position of Manipulator End Effector in the Y-Direction for Trials from Experiment 3, Scenario 2 that are Subjected to Various Time Delays.

From in Figure 56, all trials are shown to be successful, but to varying degrees. There is a visible difference between the performance of the undelayed trial and the delayed trials, with the undelay trial performing significantly better. With no delay, the manipulator appears to follow the desired trajectory quite accurately, reaching the tissue wall close to the desired time of 3 seconds and maintaining steady state after.

In comparison, the delayed trials appear more cautious, stabilizing at around the 4-second mark, but only making contact at approximately the 9-second mark. This does not match the desired trajectory, which has expected contact occurring 3 seconds into the simulation. Longer delays also correlate with a decrease in performance, with greater oscillations and longer settling times, reflecting manipulator instability. In particular, this behaviour can be seen between simulation times of 3 to 6 seconds for the delayed trials.

To gain a better understanding of the how the performance results compare with one another, Figure 57 below shows the positional error, when compared to the desired trajectory, for all trials.

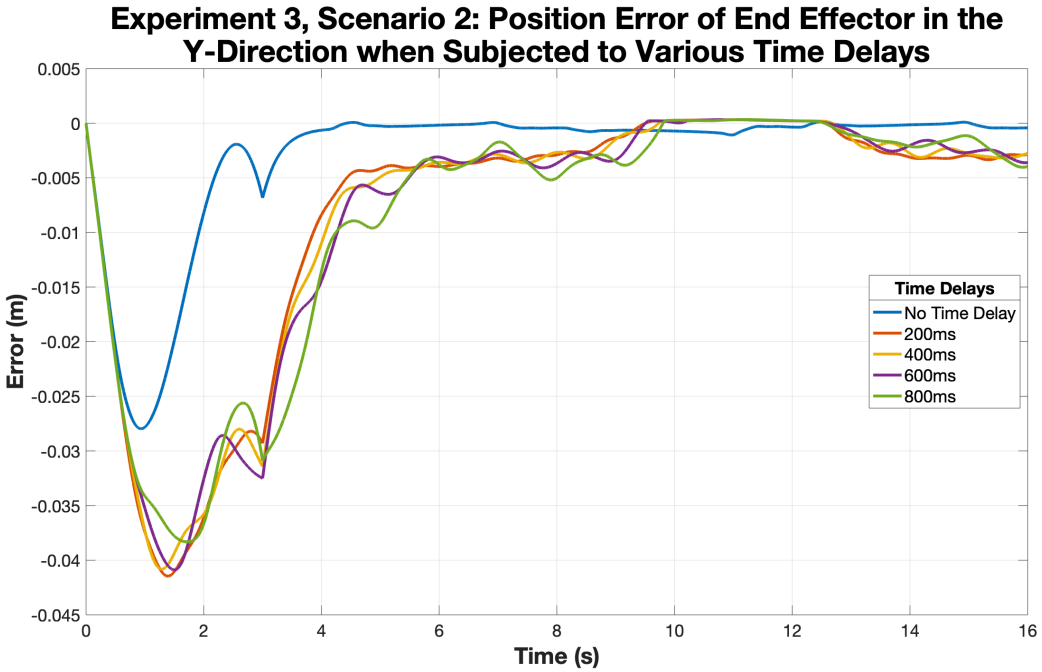

Figure 57: Position Error of Manipulator End Effector in the Y-Direction for Trials from Experiment 3, Scenario 2 that are Subjected to Various Time Delays.

The error plot can be separated into two sections: between 0-4 seconds, when the manipulator approaches the wall and between 4-16 seconds, when it reaches the wall. Though contact is planned for the 3-second mark, the delays push this intended time back by approximately 1 second. The largest errors are shown to occur at the beginning of the simulation, before stabilizing in the latter part.

The large error at the start of the simulation can be attributed to the desired trajectory, which does not take into account the state of the manipulator at the beginning of the

situation. Initially, the manipulator is stationary, while the desired trajectory demands uniform velocity from the start of the simulation. Thus the error comes from the manipulator speeding up to match the desired position.

Once the manipulator has approached the wall, approximately 4 seconds into the simulation, errors are significantly minimized. A closer look at this region can be seen in Figure 58 below.

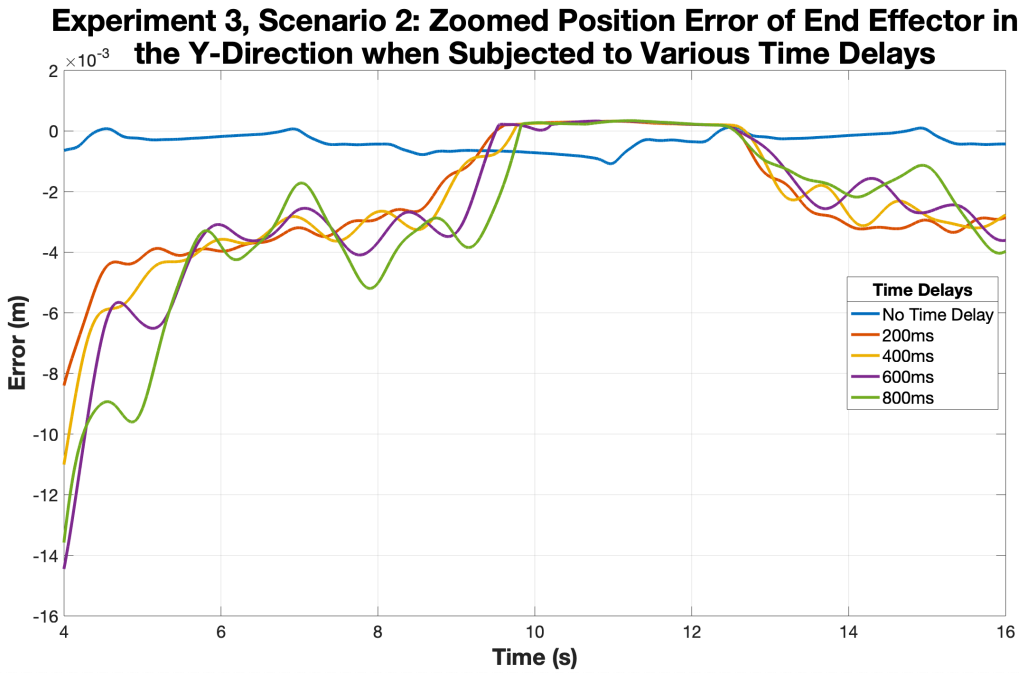

Figure 58: Region Between 4-16 Seconds for the Positional Error of Trials from Experiment 3, Scenario 2 that are Subjected to Various Time Delays.

In this region, the undelayed trial shows stable performance, with maximum error at approximately 1mm. There appears to be no penetration or direct contact with the wall, but end effector remains very close throughout the remainder of the simulation.

For the delayed trials, there is deviation in when the manipulator stabilizes, with trials with shorter delays stabilizing faster compared to those with long delays. For comparison, the 200ms delay trial reaches stability shortly after 4 seconds, whereas the 800ms delay trial stabilizes closer to the 6-second mark. Once stabilized, the error in these trials is quite small, not surpassing 6mm.

From up close, it can be seen that larger delays have larger oscillations and errors, matching the previous comment that the manipulator has decreased performance with increasing time delay. This behaviour is shown in most parts of the stabilized region, with the exception of apparent contact, from approximately 9-13 seconds into the simulation time. For a closer look into this contact region, Figure 59 and Figure 60 provide a close-up look at the penetration and measured force results from this area.

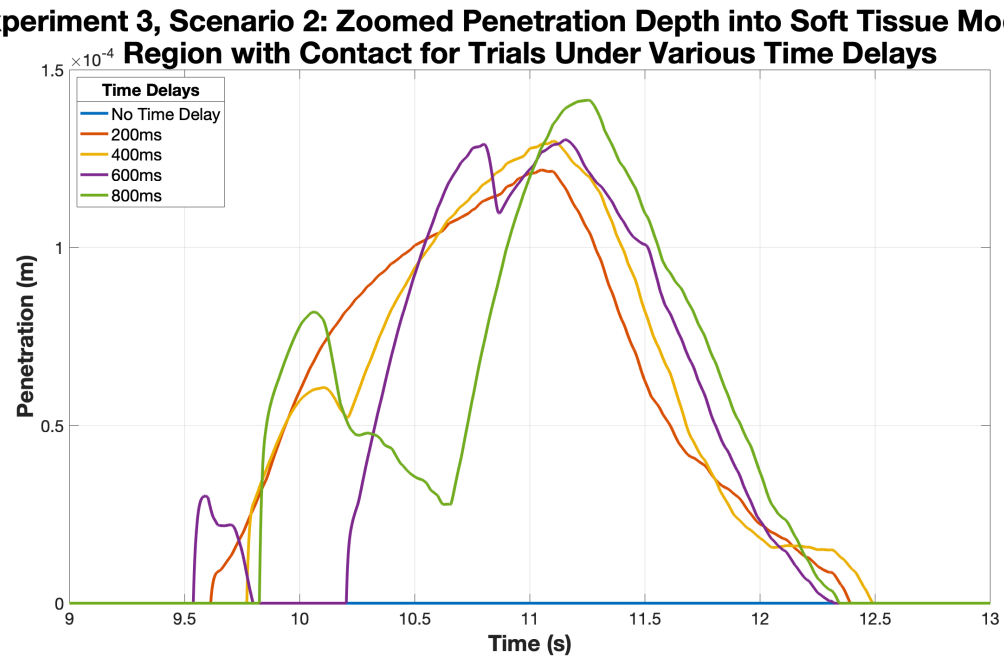

Figure 59: Region Between 9-13 Seconds for the Penetration Depth of Trials from Experiment 3, Scenario 2 that are Subjected to Various Time Delays.

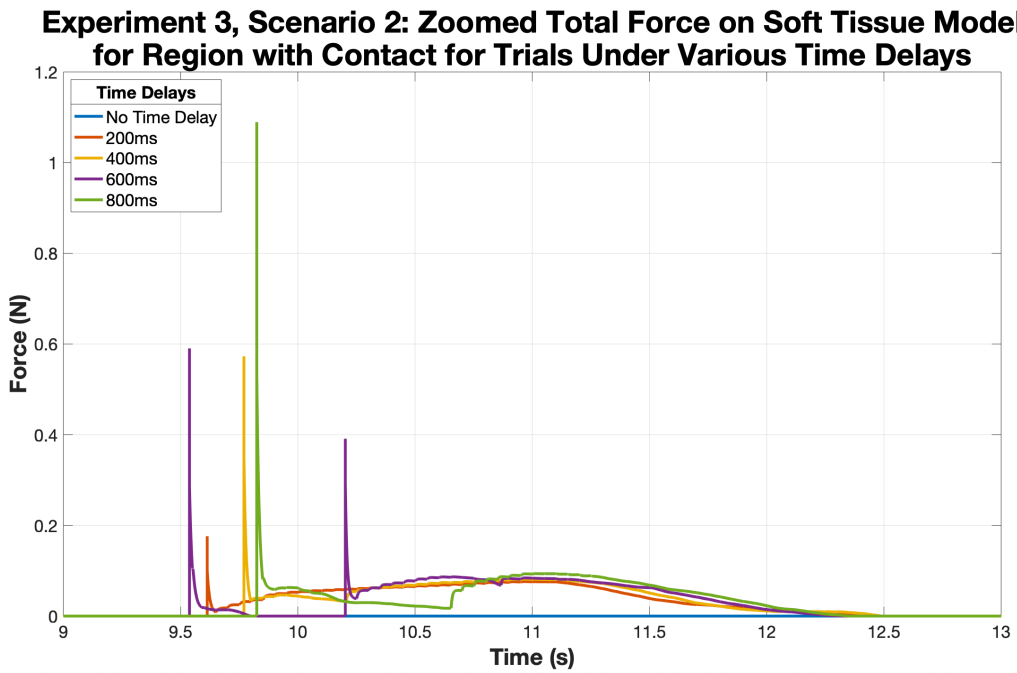

Figure 60: Region Between 9-13 Seconds for the Measured Contact Force of Trials from Experiment 3, Scenario 2 that are Subjected to Various Time Delays.

Figure 59 show a proportional relationship between time delay and penetration depth delay, with larger delays yielding deeper penetrations. Likewise, longer time delays correlate to greater measured forces, while shorter delays result in smaller forces, as seen in Figure 60.

Interestingly, despite the relationship between penetration and forces, established in Equation (16), deeper penetrations do not necessarily correspond to larger forces. In particular, this behaviour can be seen in both the 600ms delay and 800ms delay trials. For the 600ms delay trial, penetration occurs twice, once at approximately 9.5 seconds and once at about 10.25 seconds. While the first occurrence has less penetration than the second, it records greater forces, as shown in Figure 59 and Figure 60. Similarly, for the

800ms delay trial, the contact made at about 9.75 seconds has less penetration but greater forces than the interaction at approximately 10.75 seconds. From Equation (16), it can be concluded that a significant decrease in velocity can result in decreased forces despite increased penetration. This behaviour may be the result of the adaptive control attempting to minimize force, thus reducing the velocity of the manipulator.

Results do not follow the expected performance from Table 1, but the general behavioural trend is maintained. Small delays produce better results, while large delays have negative effects on performance. However, the minimal errors and the success of the 800ms delay trial indicate superior performance than expected.

6.3 Comparison

Both scenarios show satisfactory performance for all time delays, with Scenario 1, involving the Smith predictor and PID setup, showing superior performance to Scenario 2, which implements the adaptive MPC. In Scenario 1, the desired trajectory is followed more accurately and the manipulator shows more stability throughout the simulation. On the contrary, Scenario 2 shows more cautious movements, approaching the tissue wall much slower and with oscillating behaviour, showing more instability. The settling times and average positional errors, presented in Table 11 and Table 12 respectively, also support this finding.

Table 11: Settling Times (s) of PSM for Successful Trials from Experiment 3 that are Subjected to Various Time Delays.

	Time Delay				
	No Delay	200ms	400ms	600ms	800ms
Settling Time (s)	**3.0000**	**3.0000**	**3.0000**	**3.0000**	**3.0000**
	3.0153	4.2309	4.3470	4.5077	5.2742

Table 12: Average Positional Errors (m) of PSM for Successful Trials from Experiment 3 that are Subjected to Various Time Delays.

		Time Delay				
		No Delay	200ms	400ms	600ms	800ms
Movement	Towards the Wall	**0.0096**	**0.0096**	**0.0096**	**0.0096**	**0.0096**
		0.0138	0.0393	0.0399	0.0296	0.0287
	Sliding Down the Wall	9.0710×10^{-4}	$\mathbf{9.1458\times10^{-4}}$	$\mathbf{9.0816\times10^{-4}}$	$\mathbf{9.0590\times10^{-4}}$	$\mathbf{8.9610\times10^{-4}}$
		$\mathbf{1.9722\times10^{-4}}$	0.0043	0.0046	0.0055	0.0062
	Sliding Up the Wall	$\mathbf{4.3127\times10^{-4}}$	$\mathbf{4.3990\times10^{-4}}$	$\mathbf{4.3583\times10^{-4}}$	$\mathbf{4.3791\times10^{-4}}$	$\mathbf{4.3678\times10^{-4}}$
		7.1059×10^{-4}	0.0010	0.0012	0.0015	0.0020
	Sliding Down the Wall	9.1092×10^{-4}	$\mathbf{9.2311\times10^{-4}}$	$\mathbf{9.1932\times10^{-4}}$	$\mathbf{9.2211\times10^{-4}}$	$\mathbf{9.2121\times10^{-4}}$
		$\mathbf{1.5862\times10^{-4}}$	0.0020	0.0017	0.0014	0.0012

The qualitative results, from Table 11 and Table 12 are heavily in favour of the Smith Predictor and PID setup, shown in blue, over the adaptive MPC, shown in orange. There are small exceptions, from the no delay trial as it slides down the wall, however, these errors are so small, within tenths of millimeters, that they can be considered negligible.

In spite of its worse performance, adaptive MPC also shows interesting behaviour with its ability to improve performance via force reduction. As large forces are shown to be dangerous and detrimental to many applications, controlling this property can significantly benefit performance.

The performance differences can be due to a variety of reasons, one of which may be the predictive plant model used in each setup. The Smith predictor and PID setup uses a non-linear model, whereas the adaptive MPC uses one that is linearized at each given time step. For the MPC, which generates a control signal based on predictions over the course of a prediction horizon, results may not be ideal. Predictions close to current step will be accurate, but over the course of the horizon, predictions would become less reliable. As optimization factors all these predictions into account when generating a signal, the output may not be the best selection due to the prediction errors from the linearized model.

Overall, predictive technology shows very promising results for telerobotic applications, showing excellent performance that exceeds expectations. Both scenarios consist of successful predictive models, with the Smith predictor and PID setup showing superior performance over the adaptive MPC setup. However, the scenario is very idealistic and does not consider the effects of external disturbances or forces. Under more realistic circumstances, the performance Smith predictor and PID controller setup, which only makes predictions of the current time step, is expected to decline. On the contrary, the adaptive MPC setup, which has shown the ability to accommodate unexpected disturbances, is expected to perform better. Moving forward, it may be of interest to explore the effects of applying disturbances or forces to these controller setups to test these hypotheses.

7. Chapter 7: Conclusions

This thesis explores the performance of different manipulator and controller setups in a telerobotic, surgical setting via simulation. These experiments were subjected to various time delays and the manipulators were programmed to come in contact with a soft tissue model to mimic patient-robot interactions. The objective of these simulations was to gain a better understanding of the effects of time delay and disturbances on telerobotic performance as well as investigate possible methods on improving performance when in a surgical environment.

From the conducted experiments, it was observed that there are force limitations for successful task completion. That is, it appears a manipulator can complete a given task as long as the externally applied forces are below a certain threshold. However, when the force threshold is surpassed, tasks will fail. Factors such as model or controller setup can affect threshold limitations, with more complex and advanced components resulting higher threshold values and more tolerance to larger forces.

In particular, hybrid position-force controllers are designed to handle larger forces, with different types having different effects on system performance. From the simulations conducted in this thesis, it was found that the hybrid PID controller shows the ability to adapt to excessive forces despite having only mediocre performance in terms of position control. On the contrary, the hybrid model predictive controller (MPC) produces more stable positional results, but show minimal corrective capabilities to external forces.

Further elaborating on improving performance with different controller setups, the experiments involving corrective, predictive control showed very promising results. Both setups, the Smith predictor and PID setup and the adaptive MPC setup, are able to surpass standard expected performance, not failing under any of the tested time delay lengths. In particular, the simulations of Smith predictor and PID setup show excellent performance and appear to be very minimally affected by the effects of time delay. On the contrary, the adaptive MPC setup's performance is inferior, but mirrors the desired ability of a hybrid position-force controller, wherein forces are minimized after contact.

The results from the experiments also display the MPC's inflexibility, which restricts the motion of the manipulator. In the case of the hybrid MPC, the controller does not show a significant ability to reduce forces, while the adaptive MPC is slow to react and settles later than the desired time. These behaviours can be heavily attributed to the prediction horizon, which causes control signals to be selected based on both current and future predictions. As a result, the controller is much more cautious to optimize for future movement as well. For the specific simulations in this thesis, the MPC behaviour negatively affects performance, however it will likely be quite effective for more intensive tasks with greater disturbances.

The overall thesis results show that while time delay and external disturbances restrict a manipulator's ability to carry out a task, the effects of these factors can be significantly reduced with different controller setups. However, each controller setup has unique advantages and disadvantages that have to be considered depending on the application of

the manipulator. Further exploration into the usage of controller setups in different settings would be beneficial to improving system performance and overcoming the current limitations of telerobotics.

References

[1] S. Avgousti *et al.*, "Medical Telerobotic Systems: Current Status and Future Trends," *BioMed Eng OnLine*, vol. 15, no. 1, p. 96, Dec. 2016, doi: 10.1186/s12938-016-0217-7.

[2] A. Buia, F. Stockhausen, and E. Hanisch, "Laparoscopic Surgery: A Qualified Systematic Review," *WJM*, vol. 5, no. 4, p. 238, 2015, doi: 10.5662/wjm.v5.i4.238.

[3] C. Ho *et al.*, *Robot-Assisted Surgery Compared with Open Surgery and Laparoscopic Surgery: Clinical Effectiveness and Economic Analyses*. Ottawa (ON): Canadian Agency for Drugs and Technologies in Health, 2011.

[4] J. Arata *et al.*, "A Remote Surgery Experiment between Japan and Thailand over Internet Using a Low Latency CODEC System," in *Proceedings 2007 IEEE International Conference on Robotics and Automation*, Rome, Italy, Apr. 2007, pp. 953–959. doi: 10.1109/ROBOT.2007.363108.

[5] Stefan H.E.M. Clermonts, "The Evolution of Minimally Invasive Techniques in Restoration of Colonic Continuity," in *Laparoscopic Surgery*, Laurents P.S. Stassen, Ed. Rijeka: IntechOpen, 2017, p. Ch. 1. doi: 10.5772/66720.

[6] L. van den Bedem, R. Hendrix, N. Rosielle, M. Steinbuch, and H. Nijmeijer, "Design of a Minimally Invasive Surgical Teleoperated Master-Slave System with Haptic Feedback," in *2009 International Conference on Mechatronics and Automation*, Changchun, China, Aug. 2009, pp. 60–65. doi: 10.1109/ICMA.2009.5246502.

[7] M. J. H. Lum *et al.*, "Teleoperation of a Surgical Robot Via Airborne Wireless Radio and Transatlantic Internet Links," in *Field and Service Robotics: Results of the 6th International Conference*, C. Laugier and R. Siegwart, Eds. Berlin, Heidelberg: Springer Berlin Heidelberg, 2008, pp. 305–314. doi: 10.1007/978-3-540-75404-6_29.

[8] "Raven II - ROBOTS: Your Guide to the World of Robotics," *IEEE*. https://robots.ieee.org/robots/ravensurgical/ (accessed Jul. 21, 2020).

[9] B. Hannaford *et al.*, "Raven-II: An Open Platform for Surgical Robotics Research," *IEEE Transactions on Biomedical Engineering*, vol. 60, no. 4, pp. 954–959, Apr. 2013, doi: 10.1109/TBME.2012.2228858.

[10] S. E. Butner and M. Ghodoussi, “Transforming a Surgical Robot for Human Telesurgery,” *IEEE Transactions on Robotics and Automation*, vol. 19, no. 5, pp. 818–824, Oct. 2003, doi: 10.1109/TRA.2003.817214.

[11] F. Pugin, P. Bucher, and P. Morel, “History of Robotic Surgery: From AESOP® and ZEUS® to da Vinci®,” *Journal of Visceral Surgery*, vol. 148, no. 5, Supplement, pp. e3–e8, Oct. 2011, doi: 10.1016/j.jviscsurg.2011.04.007.

[12] A. Mendivil, R. Holloway, and J. Boggess, “Emergence of Robotic Assisted Surgery in Gynecologic Oncology: American Perspective,” *Gynecologic Oncology*, vol. 114, pp. S24-31, Aug. 2009, doi: 10.1016/j.ygyno.2009.02.002.

[13] L. Mettler, M. Ibrahim, and W. Jonat, “One Year of Experience Working with the Aid of a Robotic Assistant (the Voice-Controlled Optic Holder AESOP) in Gynaecological Endoscopic Surgery,” *Human Reproduction (Oxford, England)*, vol. 13, pp. 2748–50, Nov. 1998, doi: 10.1093/humrep/13.10.2748.

[14] M. Hoeckelmann, I. J. Rudas, P. Fiorini, F. Kirchner, and T. Haidegger, “Current Capabilities and Development Potential in Surgical Robotics,” *International Journal of Advanced Robotic Systems*, vol. 12, no. 5, p. 61, Jan. 2015, doi: 10.5772/60133.

[15] W. R. Chitwood Jr *et al.*, “Robotic Surgical Training in an Academic Institution,” *Ann Surg*, vol. 234, no. 4, pp. 475–486, Oct. 2001, doi: 10.1097/00000658-200110000-00007.

[16] A. N. Sridhar, T. P. Briggs, J. D. Kelly, and S. Nathan, “Training in Robotic Surgery-an Overview,” *Curr Urol Rep*, vol. 18, no. 8, pp. 58–58, Aug. 2017, doi: 10.1007/s11934-017-0710-y.

[17] P. Farajiparvar, H. Ying, and A. Pandya, “A Brief Survey of Telerobotic Time Delay Mitigation,” *Frontiers in Robotics and AI*, vol. 7, p. 198, 2020, doi: 10.3389/frobt.2020.578805.

[18] M. J. H. Lum, J. Rosen, T. S. Lendvay, M. N. Sinanan, and B. Hannaford, “Effect of Time Delay on Telesurgical Performance,” in *2009 IEEE International Conference on Robotics and Automation*, May 2009, pp. 4246–4252. doi: 10.1109/ROBOT.2009.5152725.

[19] J. A. Vazquez-Santacruz, M. Velasco-Villa, R. de J. Portillo-Velez, L. F. Marin-Urias, and M. Vigueras-Zuniga, "Autonomous Navigation for Multiple Mobile Robots under Time Delay in Communication," *Journal of Intelligent & Robotic Systems*, vol. 86, no. 3–4, pp. 583–597, Jun. 2017, doi: 10.1007/s10846-016-0444-y.

[20] L. Stark *et al.*, "Telerobotics: Problems and Research Needs," *IEEE Transactions on Aerospace and Electronic Systems*, vol. 24, no. 5, pp. 542–551, 1988, doi: 10.1109/7.9682.

[21] N. A. Tanner and G. Niemeyer, "Improving Perception in Time Delayed Teleoperation," in *Proceedings of the 2005 IEEE International Conference on Robotics and Automation*, Apr. 2005, pp. 354–359. doi: 10.1109/ROBOT.2005.1570144.

[22] J.-Q. Huang, F. L. Lewis, and K. Liu, "A Neural Net Predictive Control for Telerobots with Time Delay," *Journal of Intelligent and Robotic Systems*, vol. 29, no. 1, pp. 1–25, Sep. 2000, doi: 10.1023/A:1008158209668.

[23] V. Chai and D.-S. Necsulescu, "Time Delay Investigation in Telerobotic Surgery," Jan. 2021, p. 8. doi: 10.5220/0010515600002994.

[24] V. Chai, D.-S. Necsulescu, and J. Sasiadek, "Hybrid Control for Remote Surgery Subject to Time Delay," Międzyzdroje, Poland, Aug. 2021, p. 6. doi: 10.1109/MMAR49549.2021.9528461.

[25] V. Chai, D.-S. Necsulescu, and J. Sasiadek, "Implementation of Predictive Control for Remote Surgery Subject to Time Delay," Międzyzdroje, Poland, Aug. 2022, p. 6. doi: 10.1109/MMAR55195.2022.9874321.

[26] P. Kazanzides, Z. Chen, A. Deguet, G. S. Fischer, R. H. Taylor, and S. P. DiMaio, "An Open-Source Research Kit for the da Vinci Surgical System," in *IEEE Intl. Conf. on Robotics and Auto. (ICRA)*, Hong Kong, China, Jun. 2014, pp. 6434–6439.

[27] M. Velasco-Villa, R. Castro-Linares, F. Rosales-Hernández, B. del Muro-Cuéllar, and M. A. Hernández-Pérez, "Discrete-Time Synchronization Strategy for Input Time-Delay Mobile Robots," *Journal of the Franklin Institute*, vol. 350, no. 10, pp. 2911–2935, Dec. 2013, doi: 10.1016/j.jfranklin.2013.05.029.

[28] M. Fabrizio *et al.*, “Effect of Time Delay on Surgical Performance During Telesurgical Manipulation,” *Journal of Endourology / Endourological Society*, vol. 14, pp. 133–8, Mar. 2000, doi: 10.1089/end.2000.14.133.

[29] M. Anvari *et al.*, “The Impact of Latency on Surgical Precision and Task Completion during Robotic-Assisted Remote Telepresence Surgery,” *Computer Aided Surgery*, vol. 10, no. 2, pp. 93–99, Jan. 2005, doi: 10.3109/10929080500228654.

[30] M. Lum *et al.*, “Teleoperation in Surgical Robotics - Network Latency Effects on Surgical Performance,” *Conference proceedings: Annual International Conference of the IEEE Engineering in Medicine and Biology Society. IEEE Engineering in Medicine and Biology Society*, vol. 2009, pp. 6860–3, Sep. 2009, doi: 10.1109/IEMBS.2009.5333120.

[31] C. Korte, S. Nair, V. Nistor, T. Low, C. Doarn, and G. Schaffner, “Determining the Threshold of Time-Delay for Teleoperation Accuracy and Efficiency in Relation to Telesurgery,” *Telemedicine Journal and E-Health: The Official Journal of the American Telemedicine Association*, vol. 20, Oct. 2014, doi: 10.1089/tmj.2013.0367.

[32] D. Hristu, D. A. Kontarinis, and R. D. Howe, “A Comparison of Delay and Bandwidth Limitations in Teleoperation,” *IFAC Proceedings Volumes*, vol. 29, no. 1, pp. 5709–5714, Jun. 1996, doi: 10.1016/S1474-6670(17)58593-6.

[33] M. Uebel, M. Ali, and I. Minis, “The Effect of Bandwidth on Telerobotic System Performance,” *IEEE Transactions on Systems, Man, and Cybernetics*, vol. 24, no. 2, pp. 342–348, Feb. 1994, doi: 10.1109/21.281433.

[34] R. Orosco *et al.*, “Compensatory Motion Scaling for Time-Delayed Robotic Surgery,” *Surgical Endoscopy*, Jun. 2020, doi: 10.1007/s00464-020-07681-7.

[35] M. Perez *et al.*, “Impact of Delay on Telesurgical Performance: Study on the Robotic Simulator dV-Trainer,” *International Journal of Computer Assisted Radiology and Surgery*, vol. 11, Oct. 2015, doi: 10.1007/s11548-015-1306-y.

[36] S. Xu, M. Perez, K. Yang, C. Perrenot, J. Felblinger, and J. Hubert, “Determination of the Latency Effects on Surgical Performance and the Acceptable Latency Levels in Telesurgery Using the dV-Trainer (R) Simulator,” *Surgical Endoscopy*, vol. 28, Mar. 2014, doi: 10.1007/s00464-014-3504-z.

[37] J. Ladoiye, D. Necsulescu, and J. Sasiadek, *Force Control of Surgical Robot with Time Delay using Model Predictive Control*. 2018, p. 210. doi: 10.5220/0006908602020210.

[38] P. V. G. K. Rao, M. V. Subramanyam, and K. Satyaprasad, "Study on PID Controller Design and Performance Based on Tuning Techniques," in *2014 International Conference on Control, Instrumentation, Communication and Computational Technologies (ICCICCT)*, 2014, pp. 1411–1417. doi: 10.1109/ICCICCT.2014.6993183.

[39] K. J. Åström and R. Murray, "Chapter 11 PID Control," in *Feedback Systems: An Introduction for Scientists and Engineers*, 2008, pp. 293–314.

[40] K. Nouman, Z. Asim, and K. Qasim, "Comprehensive Study on Performance of PID Controller and its Applications," in *2018 2nd IEEE Advanced Information Management,Communicates,Electronic and Automation Control Conference (IMCEC)*, 2018, pp. 1574–1579. doi: 10.1109/IMCEC.2018.8469267.

[41] R. Paz, "The Design of the PID Controller," *Klipsch School of Electrical and Computer Engineering*, p. 23, Jan. 2001.

[42] R. Borase, D. Maghade, S. Sondkar, and S. Pawar, "A Review of PID Control, Tuning Methods and Applications," *International Journal of Dynamics and Control*, Jul. 2020, doi: 10.1007/s40435-020-00665-4.

[43] K. Ang, G. Chong, and Y. Li, "PID Control System Analysis, Design, and Technology," *Control Systems Technology, IEEE Transactions on*, vol. 13, pp. 559–576, Aug. 2005, doi: 10.1109/TCST.2005.847331.

[44] L. Wang, *Model Predictive Control System Design and Implementation Using MATLAB®*. London: Springer London, 2009. doi: 10.1007/978-1-84882-331-0.

[45] D. Simon, "Model Predictive Control in Flight Control Design - Stability and Reference Tracking," 2014. doi: 10.3384/lic.diva-103742.

[46] Y. Kim and H. Bang, "Introduction to Kalman Filter and Its Applications," *Introduction and Implementations of the Kalman Filter*, Nov. 2018, doi: 10.5772/intechopen.80600.

[47] Felix Govaers, *Introduction and Implementations of the Kalman Filter*. IntechOpen, 2019.

[48] A. Bemporad, N. L. Ricker, and M. Morari, "Model Predictive Control Toolbox™," *The Mathworks Inc.*, no. 7.3, p. 994.

[49] A. C. Smith and K. Hashtrudi-Zaad, "Smith Predictor Type Control Architectures for Time Delayed Teleoperation," *The International Journal of Robotics Research*, vol. 25, no. 8, pp. 797–818, Aug. 2006, doi: 10.1177/0278364906068393.

[50] S. Sang and P. Nie, "Modified Smith Predictor Based on H2 and Predictive PI Control Strategy," *Mathematical Problems in Engineering*, vol. 2021, p. 7228637, Aug. 2021, doi: 10.1155/2021/7228637.

[51] N. Abe and K. Yamanaka, "Smith Predictor Control and Internal Model Control - A Tutorial," in *SICE 2003 Annual Conference (IEEE Cat. No.03TH8734)*, 2003, vol. 2, pp. 1383-1387 Vol.2.

[52] C. C. Hang, "Smith Predictor and its Modifications," *Control Systems, Robotics, and Automation*, vol. 2, p. 6.

[53] J. Pliego-Jiménez and M. A. Arteaga-Pérez, "Adaptive Position/Force Control for Robot Manipulators in Contact with a Rigid Surface with Uncertain Parameters," *European Journal of Control*, vol. 22, pp. 1–12, Mar. 2015, doi: 10.1016/j.ejcon.2015.01.003.

[54] M. H. Raibert and J. J. Craig, "Hybrid Position/Force Control of Manipulators," *Journal of Dynamic Systems, Measurement, and Control*, vol. 103, no. 2, pp. 126–133, Jun. 1981, doi: 10.1115/1.3139652.

[55] W. D. Fisher and M. S. Mujtaba, "Hybrid Position/Force Control: A Correct Formulation," *The International Journal of Robotics Research*, vol. 11, no. 4, pp. 299–311, 1992, doi: 10.1177/027836499201100403.

[56] A. N. Natali, E. Carniel, P. Pavan, P. Dario, and I. Izzo, "Hyperelastic Models for the Analysis of Soft Tissue Mechanics: Definition of Constitutive Parameters," in *The First IEEE/RAS-EMBS International Conference on Biomedical Robotics and Biomechatronics*, 2006, pp. 188–191. doi: 10.1109/BIOROB.2006.1639082.

[57] S. Misra, K. T. Ramesh, and A. M. Okamura, “Modeling of Tool-Tissue Interactions for Computer-Based Surgical Simulation: A Literature Review,” *Presence: Teleoperators and Virtual Environments*, vol. 17, no. 5, pp. 463–491, Oct. 2008, doi: 10.1162/pres.17.5.463.

[58] J. Bergström, “5 - Elasticity/Hyperelasticity,” in *Mechanics of Solid Polymers*, J. Bergström, Ed. William Andrew Publishing, 2015, pp. 209–307. doi: 10.1016/B978-0-323-31150-2.00005-4.

[59] M. Amabili, Ed., “Hyperelasticity of Soft Biological and Rubber Materials,” in *Nonlinear Mechanics of Shells and Plates in Composite, Soft and Biological Materials*, Cambridge: Cambridge University Press, 2018, pp. 151–224. doi: 10.1017/9781316422892.007.

[60] T. E. Gould, M. Jesunathadas, S. Nazarenko, and S. G. Piland, “Chapter 6 - Mouth Protection in Sports,” in *Materials in Sports Equipment (Second Edition)*, A. Subic, Ed. Woodhead Publishing, 2019, pp. 199–231. doi: 10.1016/B978-0-08-102582-6.00006-X.

[61] S. Abramowitch and D. Easley, “Chapter Four - Introduction to Classical Mechanics,” in *Biomechanics of the Female Pelvic Floor*, L. Hoyte and M. Damaser, Eds. Academic Press, 2016, pp. 89–107. doi: https://doi.org/10.1016/B978-0-12-803228-2.00004-0.

[62] N. Famaey and J. V. Sloten, “Soft Tissue Modelling for Applications in Virtual Surgery and Surgical Robotics,” *Computer Methods in Biomechanics and Biomedical Engineering*, vol. 11, no. 4, pp. 351–366, Aug. 2008, doi: 10.1080/10255840802020412.

[63] J. Urban, “An Induction to the Theory of Stochastic Systems,” Institute of Physical Biology Department of Bioengineering Nove Hrady, 2010.

[64] N. K. Veijgen, “Skin Friction: A Novel Approach to Measuring In Vivo Human Skin,” PhD Thesis, University of Twente, Netherlands, 2013. doi: 10.3990/1.9789036534918.

[65] X. Liang and S. A. Boppart, “Biomechanical Properties of In Vivo Human Skin from Dynamic Optical Coherence Elastography,” *IEEE Transactions on Bio-Medical*

Engineering, vol. 57, no. 4, pp. 953–959, Apr. 2010, doi: 10.1109/TBME.2009.2033464.

[66] A. Ní Annaidh, M. Ottenio, K. Bruyère-Garnier, M. Destrade, and M. Gilchrist, "Mechanical Properties of Excised Human Skin," in *IFMBE Proceedings*, vol. 31, 2010, pp. 1000–1003. doi: 10.1007/978-3-642-14515-5_255.

[67] P. Moreira, C. Liu, N. Zemiti, and P. Poignet, "Force Control for Robotic-Assisted Surgery Based on Viscoelastic Tissue Model," *BIO Web of Conferences*, vol. 1, p. 00066, 2011, doi: 10.1051/bioconf/20110100066.

[68] A. Pappalardo, A. Albakri, C. Liu, L. Bascetta, E. De Momi, and P. Poignet, "Hunt–Crossley Model based Force Control for Minimally Invasive Robotic Surgery," *Biomedical Signal Processing and Control*, vol. 29, pp. 31–43, Aug. 2016, doi: 10.1016/j.bspc.2016.05.003.

[69] Á. Takács *et al.*, "Review of Tool–Tissue Interaction Models for Robotic Surgery Applications," in *SAMI 2014 - IEEE 12th International Symposium on Applied Machine Intelligence and Informatics, Proceedings*, 2014, pp. 339–344. doi: 10.1109/SAMI.2014.6822435.

[70] T. Yamamoto, B. Vágvölgyi, K. Balaji, L. Whitcomb, and A. Okamura, "Tissue Property Estimation and Graphical Display for Teleoperated Robot-Assisted Surgery," *2009 IEEE International Conference on Robotics and Automation*, pp. 4239–4245, 2009.

[71] F. Irgens, "Work and Energy," in *Continuum Mechanics*, Springer Berlin Heidelberg, 2008, pp. 183–198. doi: 10.1007/978-3-540-74298-2.

[72] M. H. Sadd, "Chapter 1 - Introduction," in *Continuum Mechanics Modeling of Material Behavior*, M. H. Sadd, Ed. Academic Press, 2019, pp. 1–10. doi: 10.1016/B978-0-12-811474-2.00001-0.

[73] S. E. Bechtel and R. L. Lowe, "Chapter 1 - What is a Continuum?," in *Fundamentals of Continuum Mechanics*, S. E. Bechtel and R. L. Lowe, Eds. Boston: Academic Press, 2015, pp. 3–4. doi: 10.1016/B978-0-12-394600-3.00001-0.

[74] N. Kida and Y. Morishita, "Continuum Mechanical Modeling of Developing Epithelial Tissues with Anisotropic Surface Growth," *Finite Elements in Analysis*

and Design, vol. 144, pp. 49–60, 2018, doi: https://doi.org/10.1016/j.finel.2018.03.001.

[75] M. Moatamedi, *Finite Element Analysis*, First edition. Boca Raton, FL : CRC Press, 2018.

[76] Y. Katz, O. Lubovsky, and Z. Yosibash, "Patient-Specific Finite Element Analysis of Femurs with Cemented Hip Implants," *Clinical Biomechanics*, vol. 58, pp. 74–89, 2018, doi: https://doi.org/10.1016/j.clinbiomech.2018.06.012.

[77] Z. Chen, A. Deguet, R. Taylor, and P. Kazanzides, "Software Architecture of the Da Vinci Research Kit," *2017 First IEEE International Conference on Robotic Computing (IRC)*, pp. 180–187, 2017.

[78] Y. Wang, R. Gondokaryono, A. Munawar, and G. S. Fischer, "A Convex Optimization-Based Dynamic Model Identification Package for the da Vinci Research Kit," *IEEE Robotics and Automation Letters*, vol. 4, no. 4, pp. 3657–3664, 2019, doi: 10.1109/LRA.2019.2927947.

[79] R. Gondokaryono, "Cooperative Object Manipulation with Force Tracking on the da Vinci Research Kit," Worcester Polytechnic Institute, 2018.

[80] G. A. Fontanelli, F. Ficuciello, L. Villani, and B. Siciliano, "Modelling and Identification of the da Vinci Research Kit Robotic Arms," in *2017 IEEE/RSJ International Conference on Intelligent Robots and Systems (IROS)*, 2017, pp. 1464–1469. doi: 10.1109/IROS.2017.8205948.

[81] C. Freschi, V. Ferrari, F. M. A. Melfi, M. Ferrari, F. Mosca, and A. Cuschieri, "Technical Review of the da Vinci Surgical Telemanipulator," *The International Journal of Medical Robotics and Computer Assisted Surgery*, vol. 9, 2013.

[82] M. T. Mason, Ed., "Kinematics," in *Mechanics of Robotic Manipulation*, The MIT Press, 2001, p. 0. doi: 10.7551/mitpress/4527.003.0003.

[83] J. Edward. Shigley and J. Joseph. Uicker, *Theory of machines and mechanisms*, 2nd ed. New York: McGraw-Hill, 1995.

[84] Serdar Kucuk, “Robot Kinematics: Forward and Inverse Kinematics,” in *Industrial Robotics*, Zafer Bingul ED1 - Sam Cubero, Ed. Rijeka: IntechOpen, 2006, p. Ch. 4. doi: 10.5772/5015.

[85] J. J. Craig, *Introduction to Robotics: Mechanics and Control*. Pearson/Prentice Hall, 2005. [Online]. Available: https://books.google.ca/books?id=MqMeAQAAIAAJ

[86] M. T. Mason, Ed., “Dynamics,” in *Mechanics of Robotic Manipulation*, The MIT Press, 2001, p. 0. doi: 10.7551/mitpress/4527.003.0009.

[87] D. Cline, “Chapter 6: Lagrangian Dynamics,” in *Variational Principles on Classical Mechanics*, University of Rochester, 2021.

[88] J. Vanier and C. Tomescu, *Universe Dynamics: The Least Action Principle and Lagrange’s Equations*. CRC Press, 2019. [Online]. Available: https://books.google.ca/books?id=DnWCDwAAQBAJ

[89] P. Hamill, *A Student’s Guide to Lagrangians and Hamiltonians*. Cambridge University Press, 2014. [Online]. Available: https://books.google.ca/books?id=ebTCAQAAQBAJ

[90] Atlas Steels Technical Department, “Stainless Steel Grade Datasheets,” *Atlas Technical Handbook of Stainless Steels*, Aug. 2013.

Appendix

Robotic Manipulator Motion for RRR Manipulator Used in Experiment 1

Variables and abbreviations used in the kinematics and dynamics of this manipulator are listed below:

- $l_1 = l_2 = l_3 = l = 0.1m$
- $m = 0.246615kg$
- $c_{123} = cos(\theta_1 + \theta_2 + \theta_3)$
- $c_{1+12+123} = cos(\theta_1) + cos(\theta_1 + \theta_2) + cos(\theta_1 + \theta_2 + \theta_3)$

Kinematics of Experiment 1 Manipulator

$$x = l_1\, cos(\theta_1) + l_2\, cos(\theta_1 + \theta_2) + l_3\, cos(\theta_1 + \theta_2 + \theta_3)$$
$$y = l_1 sin\,(\theta_1) + l_2 sin\,(\theta_1 + \theta_2) + l_3 sin(\theta_1 + \theta_2 + \theta_3)$$

Dynamics of Experiment 1 Manipulator

$$\begin{bmatrix} A_1 & B_1 & C_1 \\ D_1 & E_1 & F_1 \\ G_1 & H_1 & I_1 \end{bmatrix}\begin{bmatrix} \ddot{\theta}_1 \\ \ddot{\theta}_2 \\ \ddot{\theta}_3 \end{bmatrix} + \begin{bmatrix} A_2 & B_2 & C_2 \\ D_2 & E_2 & F_2 \\ G_2 & H_2 & I_2 \end{bmatrix}\begin{bmatrix} \dot{\theta}_1{}^2 \\ \dot{\theta}_2{}^2 \\ \dot{\theta}_3{}^2 \end{bmatrix} + \begin{bmatrix} A_3 & B_3 & C_3 \\ D_3 & E_3 & F_3 \\ G_3 & H_3 & I_3 \end{bmatrix}\begin{bmatrix} \dot{\theta}_1\dot{\theta}_2 \\ \dot{\theta}_1\dot{\theta}_3 \\ \dot{\theta}_2\dot{\theta}_3 \end{bmatrix} = \begin{bmatrix} \tau_1 \\ \tau_2 \\ \tau_3 \end{bmatrix}$$

$A_1 = 0.5ml^2[(c_{1+12} - s_{1+12})^2 + (c_{1+12+123} - s_{1+12+123})^2] + ms_1{}^2$
$B_1 = D_1 = 0.5ml^2[(c_{12} - s_{12})(c_{1+12} - s_{1+12})$
$\quad -(c_{12+123} - s_{12+123})\,(c_{1+12+123} - s_{1+12+123})] - ms_1s_2$
$C_1 = G_1 = 0.5ml^2(c_{123} - s_{123})(c_{1+12+123} - s_{1+12+123})$
$E_1 = 0.5ml^2[(c_{12} - s_{12})^2 + (c_{12+123} - s_{12+123})^2] + ms_2{}^2$
$F_1 = H_1 = 0.5ml^2(c_{123} - s_{123})(c_{12+123} - s_{12+123})$
$I_1 = 0.5ml^2(c_{123} - s_{123})^2$

$A_2 = 0.5ml^2[(c_{1+12} + s_{1+12})(c_{1+12} - s_{1+12})$
$\quad +(c_{1+12+123} + s_{1+12+123})\,(c_{1+12+123} - s_{1+12+123})] - mc_1s_1$
$B_2 = 0.5ml^2[(c_{12} + s_{12})(c_{12} - s_{12}) + (c_{12+123} + s_{12+123})(c_{12+123} - s_{12+123})]$
$C_2 = F_2 = I_2 = 0.5ml^2(c_{123} + s_{123})(c_{123} - s_{123})$
$D_2 = 0.5ml^2[(c_{12} + s_{12})(c_{1+12} - s_{1+12}) + (c_{12+123} + s_{12+123})(c_{12+123} - s_{12+123})]$
$E_2 = 0.5ml^2[(c_{12} + s_{12})(c_{12} - s_{12}) + (c_{12+123} + s_{12+123})(c_{12+123} - s_{12+123})] - mc_2s_2$
$G_2 = 0.5ml^2(c_{123} + s_{123})(c_{1+12+123} - s_{1+12+123})$
$H_2 = 0.5ml^2(c_{123} + s_{123})(c_{12+123} - s_{12+123})$

$$A_3 = 0.5ml^2[(c_{12} + s_{12})(c_{1+12} - s_{1+12}) + (c_{12} - s_{12})(c_{1+12} + s_{1+12}) + (c_{12+123} + s_{12+123})(c_{1+12+123} - s_{1+12+123}) + (c_{12+123} - s_{12+123})(c_{1+12+123} + s_{1+12+123})] - mc_1s_2$$

$$B_3 = 0.5ml^2[(c_{123} + s_{123})(c_{1+12+123} - s_{1+12+123}) + (c_{123} - s_{123})(c_{1+12+123} + s_{1+12+123})]$$

$$C_3 = F_3 = 0.5ml^2[(c_{123} + s_{123})(c_{12+123} - s_{12+123}) + (c_{123} - s_{123})(c_{12+123} + s_{12+123})]$$

$$D_3 = 0.5ml^2[(c_{12} + s_{12})(c_{12} - s_{12}) + (c_{12} + s_{12})(c_{1+12} - s_{1+12}) + (c_{12+123} + s_{12+123})(c_{12+123} - s_{12+123}) + (c_{12+123} + s_{12+123})(c_{1+12+123} - s_{1+12+123})] - mc_2s_1$$

$$E_3 = 0.5ml^2[(c_{123} - s_{123})(c_{12+123} + s_{12+123}) + (c_{123} + s_{123})(c_{1+12+123} - s_{1+12+123})]$$

$$G = 0.5ml^2[(c_{123} + s_{123})(c_{12+123} - s_{12+123}) + (c_{123} + s_{123})(c_{1+12+123} - s_{1+12+123})]$$

$$H_3 = 0.5ml^2[(c_{123} + s_{123})(c_{123} - s_{123}) + (c_{123} + s_{123})(c_{1+12+123} - s_{1+12+123})]$$

$$I_3 = 0.5ml^2[(c_{123} + s_{123})(c_{123} - s_{123}) + (c_{123} + s_{123})(c_{12+123} - s_{12+123})]$$

Robotic Manipulator Motion for PSM Used in Experiment 2 and Experiment 3

Variables and abbreviations used in the kinematics and dynamics of this manipulator are listed below:

- $l_1 = 0.04009m$
- $l_2 = 0.14454m$
- $l_3 = 0.4162m$
- $l_4 = 0.00091m$
- $l_5 = 0.516m$
- $l_6 = 0.04009m$
- $l_7 = -0.28726m$
- $c_1 = cos(\theta_1)$

Kinematics of Experiment 2 and 3 Manipulator

$$x = l_3c_1 - l_1c_1 - l_2c_1s_2 - l_7c_2s_1 - q_3c_2s_1 + l_6s_1s_2 + l_5s_1s_2 + l_2c_2s_1s_2 + l_4(c_1c_6 - c_2c_4c_5s_1s_6 + c_2s_1s_4s_5s_6 + c_4s_1s_2s_5s_6 + c_5s_1s_2s_4s_6)$$

$$y = l_3s_1 - l_1s_1 - l_2s_1s_2 + l_7c_1c_2 + q_3c_1c_2 - l_6c_1s_2 - l_5c_1s_2 - l_2c_1c_2s_2 + l_4(c_6s_1 + c_1c_2c_4c_5s_6 - c_1c_2s_4s_5s_6 - c_1c_4s_2s_5s_6 - c_1c_5s_2s_4s_6)$$

$$z = 0.5l_2[1 + cos(2q_2)] + 0.5l_4[cos(q_2 + q_4 + q_5 - q_6) - cos(q_2 + q_4 + q_5 + q_6)] + l_6c_2 + l_5c_2 + l_7s_2 + q_3s_2$$

Dynamics of Experiment 2 and 3 Manipulator

$$\begin{bmatrix}\tau_1\\ \tau_2\\ \tau_3\\ \tau_4\\ \tau_5\\ \tau_6\end{bmatrix}\begin{bmatrix}Aa_1 & Ab_1 & Ac_1 & Ad_1 & Ae_1 & Af_1\\ Ba_1 & Bb_1 & Bc_1 & Bd_1 & Be_1 & Bf_1\\ Ca_1 & Cb_1 & Cc_1 & Cd_1 & Ce_1 & Cf_1\\ Da_1 & Db_1 & Dc_1 & Dd_1 & De_1 & Df_1\\ Ea_1 & Eb_1 & Ec_1 & Ed_1 & Ee_1 & Ef_1\\ Fa_1 & Fb_1 & Fc_1 & Fd_1 & Fe_1 & Ff_1\end{bmatrix}\begin{bmatrix}\ddot{\theta}_1\\ \ddot{\theta}_2\\ \ddot{\theta}_3\\ \ddot{\theta}_4\\ \ddot{\theta}_5\\ \ddot{\theta}_6\end{bmatrix}+\begin{bmatrix}Aa_2 & Ab_2 & Ac_2 & Ad_2 & Ae_2 & Af_2\\ Ba_2 & Bb_2 & Bc_2 & Bd_2 & Be_2 & Bf_2\\ Ca_2 & Cb_2 & Cc_2 & Cd_2 & Ce_2 & Cf_2\\ Da_2 & Db_2 & Dc_2 & Dd_2 & De_2 & Df_2\\ Ea_2 & Eb_2 & Ec_2 & Ed_2 & Ee_2 & Ef_2\\ Fa_2 & Fb_2 & Fc_2 & Fd_2 & Fe_2 & Ff_2\end{bmatrix}\begin{bmatrix}\dot{\theta}_1\\ \dot{\theta}_1\\ \dot{\theta}_1\\ \dot{\theta}_1\\ \dot{\theta}_1\\ \dot{\theta}_1\end{bmatrix}+\begin{bmatrix}A\\ B\\ C\\ D\\ E\\ F\end{bmatrix}=\begin{bmatrix}\tau_1\\ \tau_2\\ \tau_3\\ \tau_4\\ \tau_5\\ \tau_6\end{bmatrix}$$

$$\begin{aligned}Aa_1 = {} & 2.9645\times10^{-7}\,sin(2\theta_2+2\theta_4+2\theta_5+2\theta_6)-1.2902\times10^{-6}\,cos(2\theta_2+2\theta_4+2\theta_5-\theta_6)\\ & -1.3125\times10^{-7}\,cos(2\theta_2+2\theta_4+2\theta_5-2\theta_6)-1.3125\times10^{-7}\,cos(2\theta_2+2\theta_4+2\theta_5+2\theta_6)\\ & -8.3976\times10^{-7}\,sin(2\theta_2+2\theta_4+2\theta_5-\theta_6)-2.9645\times10^{-7}\,sin(2\theta_2+2\theta_4+2\theta_5-2\theta_6)\\ & -0.56122\theta_3-8.399\times10^{-6}\,cos(\theta_4+\theta_5+\theta_6)+1.3731\times10^{-6}\,sin(\theta_4+\theta_5+\theta_6)\\ & -1.157\times10^{-6}\,cos(\theta_4-\theta_2+\theta_5+\theta_6)+4.6558\times10^{-6}\,cos(2\theta_2+\theta_4+\theta_5+\theta_6)\\ & +7.5304\times10^{-7}\,sin(\theta_4-\theta_2+\theta_5+\theta_6)-7.124\times10^{-6}\,sin(2\theta_2+\theta_4+\theta_5+\theta_6)\\ & +3.004\times10^{-6}\,cos(\theta_2-\theta_4)-1.6948\times10^{-5}\,cos(2\theta_2+\theta_4)\\ & +3.0122\times10^{-6}\,cos(\theta_2-\theta_6)+1.157\times10^{-6}\,cos(3\theta_2+\theta_4+\theta_5+\theta_6)\\ & +7.4661\times10^{-6}\,sin(2\theta_2+\theta_4)-4.6278\times10^{-6}\,sin(\theta_2-\theta_6)\\ & -7.5304\times10^{-7}\,sin(3\theta_2+\theta_4+\theta_5+\theta_6)-3.004\times10^{-6}\,cos(3\theta_2+\theta_4)\\ & +1.2902\times10^{-6}\,cos(2\theta_2+2\theta_4+2\theta_5+\theta_6)-2.7897\,cos(2\theta_2)-0.14882\,cos(4\theta_2)\\ & +2.625\times10^{-7}\,cos(2\theta_6)-8.3976\times10^{-7}\,sin(2\theta_2+2\theta_4+2\theta_5+\theta_6)\\ & +0.3998\,sin(2\theta_2)+0.0028829\,sin(4\theta_2)-5.9289\times10^{-7}\,sin(2\theta_6)\\ & -0.87438\,cos(3\theta_2)+0.065777\,sin(3\theta_2)-3.0122\times10^{-6}\,cos(\theta_2+\theta_6)\\ & +1.2753\times10^{-5}\,cos(\theta_4+\theta_5)-4.6278\times10^{-6}\,sin(\theta_2+\theta_6)\\ & +2.1169\times10^{-5}\,sin(\theta_4+\theta_5)+3.2774\times10^{-6}\,cos(\theta_4-\theta_2+\theta_5)\\ & -2.4228\times10^{-5}\,cos(2\theta_2+\theta_4+\theta_5)+4.6558\times10^{-6}\,cos(\theta_4+\theta_5-\theta_6)\\ & +2.3083\times10^{-6}\,sin(\theta_4-\theta_2+\theta_5)-4.8778\times10^{-6}\,sin(2\theta_2+\theta_4+\theta_5)\\ & +7.124\times10^{-6}\,sin(\theta_4+\theta_5-\theta_6)+1.157\times10^{-6}\,cos(\theta_2-\theta_4-\theta_5+\theta_6)\\ & -8.399\times10^{-6}\,cos(2\theta_2+\theta_4+\theta_5-\theta_6)+0.86942\,cos(\theta_2)+1.6948\times10^{-5}\,cos(\theta_4)\\ & +2.2372\times10^{-5}\,cos(\theta_6)-3.2774\times10^{-6}\,cos(3\theta_2+\theta_4+\theta_5)\\ & -7.5304\times10^{-7}\,sin(\theta_2-\theta_4-\theta_5+\theta_6)-1.3731\times10^{-6}\,sin(2\theta_2+\theta_4+\theta_5-\theta_6)\\ & -7.6764\times10^{-7}\,cos(2\theta_2+2\theta_4)+0.01466\,sin(\theta_2)+7.4661\times10^{-6}\,sin(\theta_4)\\ & -1.4561\times10^{-5}\,sin(\theta_6)-2.3083\times10^{-6}\,sin(3\theta_2+\theta_4+\theta_5)\\ & -1.157\times10^{-6}\,cos(3\theta_2+\theta_4+\theta_5-\theta_6)-7.2573\times10^{-7}\,cos(2\theta_2+2\theta_4+2\theta_5)\\ & -7.5304\times10^{-7}\,sin(3\theta_2+\theta_4+\theta_5-\theta_6)+1.001\times10^{-5}\theta_3\,sin(2\theta_2+\theta_4+\theta_5+\theta_6)\\ & -2.5991\times10^{-5}\theta_3\,sin(2\theta_2+\theta_4)-0.56122\theta_3\,cos(2\theta_2)-1.3717\theta_3\,sin(2\theta_2)\\ & -0.22581\theta_3\,sin(3\theta_2)+1.9972\times10^{-5}\theta_3\,cos(\theta_4+\theta_5)-2.8356\times10^{-5}\theta_3\,sin(\theta_4+\theta_5)\\ & +1.9972\times10^{-5}\theta_3\,cos(2\theta_2+\theta_4+\theta_5)+6.5153\times10^{-6}\theta_3\,cos(\theta_4+\theta_5-\theta_6)\\ & -2.8356\times10^{-5}\theta_3\,sin(2\theta_2+\theta_4+\theta_5)-1.001\times10^{-5}\theta_3\,sin(\theta_4+\theta_5-\theta_6)\\ & +6.5153\times10^{-6}\theta_3\,cos(2\theta_2+\theta_4+\theta_5-\theta_6)+0.97685{\theta_3}^2\,cos(2\theta_2)\\ & -1.001\times10^{-5}\theta_3\,sin(2\theta_2+\theta_4+\theta_5-\theta_6)-0.22581\theta_3\,sin(\theta_2)\end{aligned}$$

$$-2.5991\times10^{-5}\theta_3 sin(\theta_4)+0.97685{\theta_3}^2+6.5153\times10^{-6}\theta_3 cos(\theta_4+\theta_5+\theta_6)$$
$$+1.001\times10^{-5}\theta_3 sin(\theta_4+\theta_5+\theta_6)+6.5153\times10^{-6}\theta_3 cos(2\theta_2+\theta_4+\theta_5+\theta_6)+3.2929$$

$$Ab_1 = Ba_1 = 0.45162\theta_3 - 1.5843\times10^{-5} cos(\theta_2+\theta_4+\theta_5)+1.5061\times10^{-6} cos(\theta_4+\theta_5+\theta_6)$$
$$-9.9776\times10^{-6} sin(\theta_2+\theta_4+\theta_5)+2.3139\times10^{-6} sin(\theta_4+\theta_5+\theta_6)$$
$$-6.8831\times10^{-6} cos(\theta_2+\theta_4+\theta_5-\theta_6)-2.625\times10^{-7} cos(\theta_2+\theta_4+\theta_5-2\theta_6)$$
$$+2.625\times10^{-7} cos(\theta_2+\theta_4+\theta_5+2\theta_6)-4.4801\times10^{-6} sin(\theta_2+\theta_4+\theta_5-\theta_6)$$
$$-5.9289\times10^{-7} sin(\theta_2+\theta_4+\theta_5-2\theta_6)-5.9289\times10^{-7} sin(\theta_2+\theta_4+\theta_5+2\theta_6)$$
$$+5.7673\times10^{-4} cos(q1-\theta_2)-8.399\times10^{-6} cos(\theta_2-\theta_6)$$
$$-2.3139\times10^{-6} cos(2\theta_2+\theta_6)-1.3731\times10^{-6} sin(\theta_2-\theta_6)$$
$$+1.5061\times10^{-6} sin(2\theta_2+\theta_6)-0.023736 cos(2\theta_2)+0.0024823 sin(2\theta_2)$$
$$+4.3027\times10^{-6} cos(\theta_2+\theta_4+\theta_5+\theta_6)+0.0057659 cos(3\theta_2)$$
$$-2.8005\times10^{-6} sin(\theta_2+\theta_4+\theta_5+\theta_6)+0.29764 sin(3\theta_2)$$
$$+5.7673\times10^{-4} cos(q1+\theta_2)-1.3047\times10^{-5} cos(\theta_2+\theta_4)$$
$$-4.6558\times10^{-6} cos(\theta_2+\theta_6)+4.6166\times10^{-6} cos(\theta_4+\theta_5)$$
$$+7.124\times10^{-6} sin(\theta_2+\theta_6)-6.5547\times10^{-6} sin(\theta_4+\theta_5)$$
$$+1.5061\times10^{-6} cos(\theta_4+\theta_5-\theta_6)-2.3139\times10^{-6} sin(\theta_4+\theta_5-\theta_6)$$
$$+5.5\times10^{-10} cos(q1)+0.10873 cos(\theta_2)-2.3139\times10^{-6} cos(2\theta_2-\theta_6)$$
$$-0.0065577 sin(q1)-0.88941 sin(\theta_2)-6.008\times10^{-6} sin(\theta_4)$$
$$-1.5061\times10^{-6} sin(2\theta_2-\theta_6)+6.5153\times10^{-6}\theta_3 cos(\theta_2-\theta_6)$$
$$-1.001\times10^{-5}\theta_3 sin(\theta_2-\theta_6)-6.5153\times10^{-6}\theta_3 cos(\theta_2+\theta_6)$$
$$-1.001\times10^{-5}\theta_3 sin(\theta_2+\theta_6)-0.19608\theta_3 sin(\theta_2)-0.12791$$

$$Ac_1 = Ca_1 = 1.001\times10^{-5} cos(\theta_2-\theta_6)+6.5153\times10^{-6} sin(\theta_2-\theta_6)-0.22581 sin(2\theta_2)$$
$$+1.001\times10^{-5} cos(\theta_2+\theta_6)-6.5153\times10^{-6} sin(\theta_2+\theta_6)+0.19608 cos(\theta_2)$$

$$Ad_1 = Da_1 = 7.5304\times10^{-7} cos(\theta_4+\theta_5+\theta_6)-1.5843\times10^{-5} cos(\theta_2+\theta_4+\theta_5)$$
$$-9.9776\times10^{-6} sin(\theta_2+\theta_4+\theta_5)+1.157\times10^{-6} sin(\theta_4+\theta_5+\theta_6)$$
$$-6.8831\times10^{-6} cos(\theta_2+\theta_4+\theta_5-\theta_6)-2.625\times10^{-7} cos(\theta_2+\theta_4+\theta_5-2\theta_6)$$
$$+2.625\times10^{-7} cos(\theta_2+\theta_4+\theta_5+2\theta_6)-7.5304\times10^{-7} cos(2\theta_2+\theta_4+\theta_5+\theta_6)$$
$$-4.4801\times10^{-6} sin(\theta_2+\theta_4+\theta_5-\theta_6)-5.9289\times10^{-7} sin(\theta_2+\theta_4+\theta_5-2\theta_6)$$
$$-5.9289\times10^{-7} sin(\theta_2+\theta_4+\theta_5+2\theta_6)-1.157\times10^{-6} sin(2\theta_2+\theta_4+\theta_5+\theta_6)$$
$$+3.004\times10^{-6} sin(2\theta_2+\theta_4)+4.3027\times10^{-6} cos(\theta_2+\theta_4+\theta_5+\theta_6)$$
$$-2.8005\times10^{-6} sin(\theta_2+\theta_4+\theta_5+\theta_6)-1.3047\times10^{-5} cos(\theta_2+\theta_4)$$
$$+2.3083\times10^{-6} cos(\theta_4+\theta_5)-3.2774\times10^{-6} sin(\theta_4+\theta_5)$$
$$-2.3083\times10^{-6} cos(2\theta_2+\theta_4+\theta_5)+7.5304\times10^{-7} cos(\theta_4+\theta_5-\theta_6)$$
$$+3.2774\times10^{-6} sin(2\theta_2+\theta_4+\theta_5)-1.157\times10^{-6} sin(\theta_4+\theta_5-\theta_6)$$
$$-7.5304\times10^{-7} cos(2\theta_2+\theta_4+\theta_5-\theta_6)+1.157\times10^{-6} sin(2\theta_2+\theta_4+\theta_5-\theta_6)$$
$$+1.0\times10^{-11} sin(\theta_1)-3.004\times10^{-6} sin(\theta_4)$$

$$Ae_1 = Ea_1 = 7.5304\times10^{-7} cos(\theta_4+\theta_5+\theta_6)-1.5843\times10^{-5} cos(\theta_2+\theta_4+\theta_5)$$
$$-9.9776\times10^{-6} sin(\theta_2+\theta_4+\theta_5)+1.157\times10^{-6} sin(\theta_4+\theta_5+\theta_6)$$
$$-6.8831\times10^{-6} cos(\theta_2+\theta_4+\theta_5-\theta_6)-2.625\times10^{-7} cos(\theta_2+\theta_4+\theta_5-2\theta_6)$$
$$+2.625\times10^{-7} cos(\theta_2+\theta_4+\theta_5+2\theta_6)-7.5304\times10^{-7} cos(2\theta_2+\theta_4+\theta_5+\theta_6)$$
$$-4.4801\times10^{-6} sin(\theta_2+\theta_4+\theta_5-\theta_6)-5.9289\times10^{-7} sin(\theta_2+\theta_4+\theta_5-2\theta_6)$$
$$-5.9289\times10^{-7} sin(\theta_2+\theta_4+\theta_5+2\theta_6)-1.157\times10^{-6} sin(2\theta_2+\theta_4+\theta_5+\theta_6)$$
$$+4.3027\times10^{-6} cos(\theta_2+\theta_4+\theta_5+\theta_6)-2.8005\times10^{-6} sin(\theta_2+\theta_4+\theta_5+\theta_6)$$
$$+2.3083\times10^{-6} cos(\theta_4+\theta_5)-3.2774\times10^{-6} sin(\theta_4+\theta_5)$$

$$-2.3083\times10^{-6}\cos(2\theta_2+\theta_4+\theta_5)+7.5304\times10^{-7}\cos(\theta_4+\theta_5-\theta_6)$$
$$+3.2774\times10^{-6}\sin(2\theta_2+\theta_4+\theta_5)-1.157\times10^{-6}\sin(\theta_4+\theta_5-\theta_6)$$
$$-7.5304\times10^{-7}\cos(2\theta_2+\theta_4+\theta_5-\theta_6)+1.157\times10^{-6}\sin(2\theta_2+\theta_4+\theta_5-\theta_6)$$
$$+1.0\times10^{-11}\sin(\theta_1)$$

$$Af_1 = Fa_1 = 2.5941\times10^{-6}\cos(\theta_2+\theta_4+\theta_5)+7.5304\times10^{-7}\cos(\theta_4+\theta_5+\theta_6)$$
$$+1.157\times10^{-6}\sin(\theta_4+\theta_5+\theta_6)+4.3027\times10^{-6}\cos(\theta_2+\theta_4+\theta_5-\theta_6)$$
$$-7.5304\times10^{-7}\cos(2\theta_2+\theta_4+\theta_5+\theta_6)+1.5\times10^{-11}\sin(\theta_2-\theta_1+\theta_4+\theta_5)$$
$$+2.8005\times10^{-6}\sin(\theta_2+\theta_4+\theta_5-\theta_6)-1.157\times10^{-6}\sin(2\theta_2+\theta_4+\theta_5+\theta_6)$$
$$-8.399\times10^{-6}\cos(\theta_2-\theta_6)+1.157\times10^{-6}\cos(2\theta_2+\theta_6)$$
$$-1.3731\times10^{-6}\sin(\theta_2-\theta_6)-7.5304\times10^{-7}\sin(2\theta_2+\theta_6)$$
$$+6.8831\times10^{-6}\cos(\theta_2+\theta_4+\theta_5+\theta_6)+1.5\times10^{-11}\sin(\theta_1+\theta_2+\theta_4+\theta_5)$$
$$-4.4801\times10^{-6}\sin(\theta_2+\theta_4+\theta_5+\theta_6)+4.6558\times10^{-6}\cos(\theta_2+\theta_6)$$
$$-7.124\times10^{-6}\sin(\theta_2+\theta_6)-7.5304\times10^{-7}\cos(\theta_4+\theta_5-\theta_6)$$
$$+1.157\times10^{-6}\sin(\theta_4+\theta_5-\theta_6)+7.5304\times10^{-7}\cos(2\theta_2+\theta_4+\theta_5-\theta_6)$$
$$-1.157\times10^{-6}\sin(2\theta_2+\theta_4+\theta_5-\theta_6)-1.157\times10^{-6}\cos(2\theta_2-\theta_6)$$
$$-7.5304\times10^{-7}\sin(2\theta_2-\theta_6)+6.5153\times10^{-6}\theta_3\cos(\theta_2-\theta_6)$$
$$-1.001\times10^{-5}\theta_3\sin(\theta_2-\theta_6)+6.5153\times10^{-6}\theta_3\cos(\theta_2+\theta_6)$$
$$+1.001\times10^{-5}\theta_3\sin(\theta_2+\theta_6)$$

$$Bb_1 = 2.7462\times10^{-6}\sin(\theta_4+\theta_5+\theta_6)-1.6798\times10^{-5}\cos(\theta_4+\theta_5+\theta_6)-1.1224\theta_3$$
$$-4.6278\times10^{-6}\cos(\theta_4-\theta_2+\theta_5+\theta_6)+3.0122\times10^{-6}\sin(\theta_4-\theta_2+\theta_5+\theta_6)$$
$$+0.0011535\cos(\theta_1-\theta_2)+1.2016\times10^{-5}\cos(\theta_2-\theta_4)+5.7673\times10^{-4}\sin(\theta_1-2\theta_2)$$
$$-5.7673\times10^{-4}\sin(\theta_1+2\theta_2)+0.02481\sin(2\theta_1+\theta_2)+0.010922\cos(2\theta_1)$$
$$+0.58247\cos(2\theta_2)-5.2501\times10^{-7}\cos(2\theta_6)+3.335\times10^{-8}\sin(2\theta_1)$$
$$-0.011532\sin(2\theta_2)+1.1858\times10^{-6}\sin(2\theta_6)-0.0011535\cos(\theta_1+\theta_2)$$
$$+2.5507\times10^{-5}\cos(\theta_4+\theta_5)+4.2338\times10^{-5}\sin(\theta_4+\theta_5)$$
$$+1.3109\times10^{-5}\cos(\theta_4-\theta_2+\theta_5)+9.3117\times10^{-6}\cos(\theta_4+\theta_5-\theta_6)$$
$$+9.2333\times10^{-6}\sin(\theta_4-\theta_2+\theta_5)+1.4248\times10^{-5}\sin(\theta_4+\theta_5-\theta_6)$$
$$+4.6278\times10^{-6}\cos(\theta_2-\theta_4-\theta_5+\theta_6)+3.4975\cos(\theta_2)+3.3897\times10^{-5}\cos(\theta_4)$$
$$-3.0122\times10^{-6}\sin(\theta_2-\theta_4-\theta_5+\theta_6)-0.0062026\cos(2\theta_1-2\theta_2)$$
$$-0.0062026\cos(2\theta_1+2\theta_2)+0.25582\sin(\theta_2)+1.4932\times10^{-5}\sin(\theta_4)$$
$$+0.02481\sin(2\theta_1-\theta_2)+3.9943\times10^{-5}\theta_3\cos(\theta_4+\theta_5)$$
$$-5.6712\times10^{-5}\theta_3\sin(\theta_4+\theta_5)+1.3031\times10^{-5}\theta_3\cos(\theta_4+\theta_5-\theta_6)$$
$$-2.002\times10^{-5}\theta_3\sin(\theta_4+\theta_5-\theta_6)-0.90323\theta_3\sin(\theta_2)-5.1982\times10^{-5}\theta_3\sin(\theta_4)$$
$$+1.9537{\theta_3}^2+1.3031\times10^{-5}\theta_3\cos(\theta_4+\theta_5+\theta_6)+2.002\times10^{-5}\theta_3\sin(\theta_4+\theta_5+\theta_6)$$
$$+6.7862$$

$$Bc_1 = Cb_1 = 1.001\times10^{-5}\cos(\theta_4+\theta_5+\theta_6)-6.5153\times10^{-6}\sin(\theta_4+\theta_5+\theta_6)$$
$$-2.8356\times10^{-5}\cos(\theta_4+\theta_5)-1.9972\times10^{-5}\sin(\theta_4+\theta_5)$$
$$-1.001\times10^{-5}\cos(\theta_4+\theta_5-\theta_6)-6.5153\times10^{-6}\sin(\theta_4+\theta_5-\theta_6)$$
$$-0.45162\cos(\theta_2)-2.5991\times10^{-5}\cos(\theta_4)-1.3717$$

$$Bd_1 = Db_1 = 1.3731\times10^{-6}\sin(\theta_4+\theta_5+\theta_6)-8.399\times10^{-6}\cos(\theta_4+\theta_5+\theta_6)$$
$$-2.3139\times10^{-6}\cos(\theta_4-\theta_2+\theta_5+\theta_6)+1.5061\times10^{-6}\sin(\theta_4-\theta_2+\theta_5+\theta_6)$$
$$+6.008\times10^{-6}\cos(\theta_2-\theta_4)+6.2\times10^{-10}\cos(2\theta_1)-5.2501\times10^{-7}\cos(2\theta_6)$$
$$+1.1858\times10^{-6}\sin(2\theta_6)+1.2753\times10^{-5}\cos(\theta_4+\theta_5)$$
$$+2.1169\times10^{-5}\sin(\theta_4+\theta_5)+6.5547\times10^{-6}\cos(\theta_4-\theta_2+\theta_5)$$

$$+4.6558\times10^{-6}\cos(\theta_4+\theta_5-\theta_6)+4.6166\times10^{-6}\sin(\theta_4-\theta_2+\theta_5)$$
$$+7.124\times10^{-6}\sin(\theta_4+\theta_5-\theta_6)+2.3139\times10^{-6}\cos(\theta_2-\theta_4-\theta_5+\theta_6)$$
$$+1.6948\times10^{-5}\cos(\theta_4)-1.5061\times10^{-6}\sin(\theta_2-\theta_4-\theta_5+\theta_6)$$
$$+7.4661\times10^{-6}\sin(\theta_4)+1.9972\times10^{-5}\theta_3\cos(\theta_4+\theta_5)$$
$$-2.8356\times10^{-5}\theta_3\sin(\theta_4+\theta_5)+6.5153\times10^{-6}\theta_3\cos(\theta_4+\theta_5-\theta_6)$$
$$-1.001\times10^{-5}\theta_3\sin(\theta_4+\theta_5-\theta_6)-2.5991\times10^{-5}\theta_3\sin(\theta_4)$$
$$+6.5153\times10^{-6}\theta_3\cos(\theta_4+\theta_5+\theta_6)+1.001\times10^{-5}\theta_3\sin(\theta_4+\theta_5+\theta_6)$$
$$+7.4087\times10^{-6}$$

$Be_1 = Eb_1 =$
$$1.3731\times10^{-6}\sin(\theta_4+\theta_5+\theta_6)-8.399\times10^{-6}\cos(\theta_4+\theta_5+\theta_6)$$
$$-2.3139\times10^{-6}\cos(\theta_4-\theta_2+\theta_5+\theta_6)+1.5061\times10^{-6}\sin(\theta_4-\theta_2+\theta_5+\theta_6)$$
$$+8.7\times10^{-10}\cos(2\theta_1)-5.2501\times10^{-7}\cos(2\theta_6)+1.1858\times10^{-6}\sin(2\theta_6)$$
$$+1.2753\times10^{-5}\cos(\theta_4+\theta_5)+2.1169\times10^{-5}\sin(\theta_4+\theta_5)$$
$$+6.5547\times10^{-6}\cos(\theta_4-\theta_2+\theta_5)+4.6558\times10^{-6}\cos(\theta_4+\theta_5-\theta_6)$$
$$+4.6166\times10^{-6}\sin(\theta_4-\theta_2+\theta_5)+7.124\times10^{-6}\sin(\theta_4+\theta_5-\theta_6)$$
$$+2.3139\times10^{-6}\cos(\theta_2-\theta_4-\theta_5+\theta_6)-1.5061\times10^{-6}\sin(\theta_2-\theta_4-\theta_5+\theta_6)$$
$$+1.9972\times10^{-5}\theta_3\cos(\theta_4+\theta_5)-2.8356\times10^{-5}\theta_3\sin(\theta_4+\theta_5)$$
$$+6.5153\times10^{-6}\theta_3\cos(\theta_4+\theta_5-\theta_6)-1.001\times10^{-5}\theta_3\sin(\theta_4+\theta_5-\theta_6)$$
$$+6.5153\times10^{-6}\theta_3\cos(\theta_4+\theta_5+\theta_6)+1.001\times10^{-5}\theta_3\sin(\theta_4+\theta_5+\theta_6)$$
$$+5.8693\times10^{-6}$$

$Bf_1 = Fb_1 =$
$$1.3731\times10^{-6}\sin(\theta_4+\theta_5+\theta_6)-8.399\times10^{-6}\cos(\theta_4+\theta_5+\theta_6)$$
$$-4.75\times10^{-11}\cos(\theta_2-2\theta_1+\theta_4+\theta_5)+4.75\times10^{-11}\cos(2\theta_1+\theta_2+\theta_4+\theta_5)$$
$$-2.3139\times10^{-6}\cos(\theta_4-\theta_2+\theta_5+\theta_6)+1.5\times10^{-11}\sin(\theta_2-\theta_1+\theta_4+\theta_5)$$
$$+1.5061\times10^{-6}\sin(\theta_4-\theta_2+\theta_5+\theta_6)+1.5061\times10^{-6}\cos(\theta_2-\theta_6)$$
$$-2.3139\times10^{-6}\sin(\theta_2-\theta_6)-1.5\times10^{-11}\sin(\theta_1+\theta_2+\theta_4+\theta_5)$$
$$+1.5061\times10^{-6}\cos(\theta_2+\theta_6)+2.3139\times10^{-6}\sin(\theta_2+\theta_6)$$
$$-4.6558\times10^{-6}\cos(\theta_4+\theta_5-\theta_6)-7.124\times10^{-6}\sin(\theta_4+\theta_5-\theta_6)$$
$$-2.3139\times10^{-6}\cos(\theta_2-\theta_4-\theta_5+\theta_6)-2.5804\times10^{-6}\cos(\theta_6)$$
$$+1.5061\times10^{-6}\sin(\theta_2-\theta_4-\theta_5+\theta_6)+1.6795\times10^{-6}\sin(\theta_6)$$
$$-6.5153\times10^{-6}\theta_3\cos(\theta_4+\theta_5-\theta_6)+1.001\times10^{-5}\theta_3\sin(\theta_4+\theta_5-\theta_6)$$
$$+6.5153\times10^{-6}\theta_3\cos(\theta_4+\theta_5+\theta_6)+1.001\times10^{-5}\theta_3\sin(\theta_4+\theta_5+\theta_6)$$

$Cc_1 =$ 1.9537

$Cd_1 = Dc_1 =$
$$1.001\times10^{-5}\cos(\theta_4+\theta_5+\theta_6)-6.5153\times10^{-6}\sin(\theta_4+\theta_5+\theta_6)$$
$$-2.8356\times10^{-5}\cos(\theta_4+\theta_5)-1.9972\times10^{-5}\sin(\theta_4+\theta_5)$$
$$-1.001\times10^{-5}\cos(\theta_4+\theta_5-\theta_6)-6.5153\times10^{-6}\sin(\theta_4+\theta_5-\theta_6)$$
$$-2.5991\times10^{-5}\cos(\theta_4)$$

$Ce_1 = Ec_1 =$
$$1.001\times10^{-5}\cos(\theta_4+\theta_5+\theta_6)-6.5153\times10^{-6}\sin(\theta_4+\theta_5+\theta_6)$$
$$-2.8356\times10^{-5}\cos(\theta_4+\theta_5)-1.9972\times10^{-5}\sin(\theta_4+\theta_5)$$
$$-1.001\times10^{-5}\cos(\theta_4+\theta_5-\theta_6)-6.5153\times10^{-6}\sin(\theta_4+\theta_5-\theta_6)$$

$Cf_1 = Fc_1 =$
$$1.001\times10^{-5}\cos(\theta_4+\theta_5+\theta_6)-6.5153\times10^{-6}\sin(\theta_4+\theta_5+\theta_6)$$
$$+1.001\times10^{-5}\cos(\theta_4+\theta_5-\theta_6)+6.5153\times10^{-6}\sin(\theta_4+\theta_5-\theta_6)$$

$Dd_1 =$
$$6.2\times10^{-10}\cos(2\theta_1)-5.2501\times10^{-7}\cos(2\theta_6)+1.1858\times10^{-6}\sin(2\theta_6)$$
$$+7.4087\times10^{-6}$$

$De_1 = Ed_1 =$
$$8.7\times10^{-10}\cos(2\theta_1)-5.2501\times10^{-7}\cos(2\theta_6)$$
$$+1.1858\times10^{-6}\sin(2\theta_6)+5.8693\times10^{-6}$$

$$Df_1 = Fd_1 = 4.75\times10^{-11}\cos(2\theta_1+\theta_2+\theta_4+\theta_5)-4.75\times10^{-11}\cos(\theta_2-2\theta_1+\theta_4+\theta_5)$$
$$+1.5\times10^{-11}\sin(\theta_2-2\theta_1+\theta_4+\theta_5)-1.5\times10^{-11}\sin(\theta_1+\theta_2+\theta_4+\theta_5)-$$
$$2.5804\times10^{-6}\cos(\theta_6)+1.6795\times10^{-6}\sin(\theta_6)$$
$$Ee_1 = 8.7\times10^{-10}\cos(2\theta_1)-5.2501\times10^{-7}\cos(2\theta_6)+1.1858\times10^{-6}\sin(2\theta_6)$$
$$+5.8693\times10^{-6}$$
$$Ef_1 = Fe_1 = 4.75\times10^{-11}\cos(2\theta_1+\theta_2+\theta_4+\theta_5)-4.75\times10^{-11}\cos(\theta_2-2\theta_1+\theta_4+\theta_5)$$
$$+1.5\times10^{-11}\sin(\theta_2-\theta_1+\theta_4+\theta_5)-1.5\times10^{-11}\sin(\theta_1+\theta_2+\theta_4+\theta_5)$$
$$-2.5804\times10^{-6}\cos(\theta_6)+1.6795\times10^{-6}\sin(\theta_6)$$
$$Ff_1 = 1.5\times10^{-11}\sin(2\theta_2-\theta_1+2\theta_4+2\theta_5)-2.375\times10^{-11}\cos(2\theta_1+2\theta_2+2\theta_4+2\theta_5)$$
$$-2.375\times10^{-11}\cos(2\theta_2 2\theta_1+2\theta_4+2\theta_5)+4.75\times10^{-11}\cos(2\theta_1)$$
$$+1.5\times10^{-11}\sin(\theta_1+2\theta_2+2\theta_4+2\theta_5)-1.8325\times10^{-9}\cos(2\theta_2+2\theta_4+2\theta_5)$$
$$+2.596\times10^{-6}$$

$$Aa_2 = 5.7673\times10^{-4}\dot{\theta}_2\sin(\theta_1-\theta_2)-1.5\times10^{-11}\dot{\theta}_6\cos(\theta_1+\theta_2+\theta_4+\theta_5)$$
$$+5.7673\times10^{-4}\dot{\theta}_2\sin(\theta_1+\theta_2)+0.0065577\dot{\theta}_2\cos(\theta_1)-1.0\times10^{-11}\dot{\theta}_4\cos(\theta_1)$$
$$-1.0\times10^{-11}\dot{\theta}_5\cos(\theta_1)+5.5\times10^{-10}\dot{\theta}_2\sin(\theta_1)+1.5\times10^{-11}\dot{\theta}_6\cos(\theta_2-\theta_1+\theta_4+\theta_5)$$
$$Ab_2 = 9.5\times10^{-11}\dot{\theta}_6\sin(\theta_2-2\theta_1+\theta_4+\theta_5)+9.5\times10^{-11}\dot{\theta}_6\sin(2\theta_1+\theta_2+\theta_4+\theta_5)$$
$$+1.24\times10^{-9}\dot{\theta}_4\sin(2\theta_1)+1.74\times10^{-9}\dot{\theta}_5\sin(2\theta_1)$$
$$+1.510^{-11}\dot{\theta}_6\cos(\theta_1+\theta_2+\theta_4+\theta_5)-\dot{\theta}_2(2.8837\times10^{-4}\cos(\theta_1-2\theta_2)$$
$$-2.8837\times10^{-4}\cos(\theta_1+2\theta_2)+0.02481\cos(2\theta_1+\theta_2)$$
$$-5.7673\times10^{-4}\sin(\theta_1-\theta_2)+3.335\times10^{-8}\cos(2\theta_1)-0.010922\sin(2\theta_1)$$
$$+5.7673\times10^{-4}\sin(\theta_1+\theta_2)+0.02481\cos(2\theta_1-\theta_2)+0.0062026\sin(2\theta_1-2\theta_2)$$
$$+0.0062026\sin(2\theta_1+2\theta_2))+1.5\times10^{-11}\dot{\theta}_6\cos(\theta_2-\theta_1+\theta_4+\theta_5)$$
$$Ad_2 = 9.5\times10^{-11}\dot{\theta}_6\sin(\theta_2-2\theta_1+\theta_4+\theta_5)+9.5\times10^{-11}\dot{\theta}_6\sin(2\theta_1+\theta_2+\theta_4+\theta_5)$$
$$+6.2\times10^{-10}\dot{\theta}_4\sin(2\theta_1)+1.74\times10^{-9}\dot{\theta}_5\sin(2\theta_1)$$
$$+1.5\times10^{-11}\dot{\theta}_6\cos(\theta_1+\theta_2+\theta_4+\theta_5)+1.5\times10^{-11}\dot{\theta}_6\cos(\theta_2-\theta_1+\theta_4+\theta_5)$$
$$Ae_2 = 9.5\times10^{-11}\dot{\theta}_6\sin(\theta_2-2\theta_1+\theta_4+\theta_5)+9.5\times10^{-11}\dot{\theta}_6\sin(2\theta_1+\theta_2+\theta_4+\theta_5)$$
$$+8.7\times10^{-10}\dot{\theta}_5\sin(2\theta_1)+1.5\times10^{-11}\dot{\theta}_6\cos(\theta_1+\theta_2+\theta_4+\theta_5)$$
$$+1.5\times10^{-11}\dot{\theta}_6\cos(\theta_2-\theta_1+\theta_4+\theta_5)$$
$$Ba_2 = 2.625\times10^{-7}\dot{\theta}_2\sin(\theta_2+\theta_4+\theta_5+2\theta_6)-2.625\times10^{-7}\dot{\theta}_2\sin(\theta_2+\theta_4+\theta_5-2\theta_6)$$
$$-6.8831\times10^{-6}\dot{\theta}_2\sin(\theta_2+\theta_4+\theta_5-\theta_6)-6.8831\times10^{-6}\dot{\theta}_4\sin(\theta_2+\theta_4+\theta_5-\theta_6)$$
$$-2.625\times10^{-7}\dot{\theta}_4\sin(\theta_2+\theta_4+\theta_5-2\theta_6)+2.625\times10^{-7}\dot{\theta}_4\sin(\theta_2+\theta_4+\theta_5+2\theta_6)$$
$$-1.5061\times10^{-6}\dot{\theta}_4\sin(2\theta_2+\theta_4+\theta_5+\theta_6)-6.8831\times10^{-6}\dot{\theta}_5\sin(\theta_2+\theta_4+\theta_5-\theta_6)$$
$$-2.625\times10^{-7}\dot{\theta}_5\sin(\theta_2+\theta_4+\theta_5-2\theta_6)+2.625\times10^{-7}\dot{\theta}_5\sin(\theta_2+\theta_4+\theta_5+2\theta_6)$$
$$-1.5061\times10^{-6}\dot{\theta}_5\sin(2\theta_2+\theta_4+\theta_5+\theta_6)+4.3027\times10^{-6}\dot{\theta}_6\sin(\theta_2+\theta_4+\theta_5-\theta_6)$$
$$-1.5061\times10^{-6}\dot{\theta}_6\sin(2\theta_2+\theta_4+\theta_5+\theta_6)+1.3731\times10^{-6}\dot{\theta}_2\cos(\theta_2-\theta_6)$$
$$-3.0122\times10^{-6}\dot{\theta}_2\cos(2\theta_2+\theta_6)-6.5153\times10^{-6}\dot{\theta}_3\cos(\theta_2-\theta_6)$$
$$-6.008\times10^{-6}\dot{\theta}_4\cos(2\theta_2+\theta_4)+1.3731\times10^{-6}\dot{\theta}_6\cos(\theta_2-\theta_6)$$
$$+1.5061\times10^{-6}\dot{\theta}_6\cos(2\theta_2+\theta_6)-5.7673\times10^{-4}\dot{\theta}_2\sin(\theta_1-\theta_2)$$
$$-8.399\times10^{-6}\dot{\theta}_2\sin(\theta_2-\theta_6)-4.6278\times10^{-6}\dot{\theta}_2\sin(2\theta_2+\theta_6)$$
$$+1.001\times10^{-5}\dot{\theta}_3\sin(\theta_2-\theta_6)-8.399\times10^{-6}\dot{\theta}_6\sin(\theta_2-\theta_6)$$
$$+2.3139\times10^{-6}\dot{\theta}_6\sin(2\theta_2+\theta_6)-0.0049646\dot{\theta}_2\cos(2\theta_2)+0.45162\dot{\theta}_3\cos(2\theta_2)$$

$$+\dot{\theta}_1(8.3976\times10^{-7}\,cos(2\theta_2+2\theta_4+2\theta_5-\theta_6)-7.2573\times10^{-7}\,sin(2\theta_2+2\theta_4+2\theta_5)$$
$$+2.9645\times10^{-7}\,cos(2\theta_2+2\theta_4+2\theta_5-2\theta_6)$$
$$-2.9645\times10^{-7}\,cos(2\theta_2+2\theta_4+2\theta_5+2\theta_6)-1.2902\times10^{-6}\,sin(2\theta_2+2\theta_4+2\theta_5-\theta_6)$$
$$-1.3125\times10^{-7}\,sin(2\theta_2+2\theta_4+2\theta_5-2\theta_6)-1.3125\times10^{-7}\,sin(2\theta_2+2\theta_4+2\theta_5+2\theta_6)$$
$$+3.7652\times10^{-7}\,cos(\theta_4-\theta_2+\theta_5+\theta_6)+7.124\times10^{-6}\,cos(2\theta_2+\theta_4+\theta_5+\theta_6)$$
$$+5.7848\times10^{-7}\,sin(\theta_4-\theta_2+\theta_5+\theta_6)+4.6558\times10^{-6}\,sin(2\theta_2+\theta_4+\theta_5+\theta_6)$$
$$-7.4661\times10^{-6}\,cos(2\theta_2+\theta_4)+2.3139\times10^{-6}\,cos(\theta_2-\theta_6)$$
$$+1.1296\times10^{-6}\,cos(3\theta_2+\theta_4+\theta_5+\theta_6)+1.502\times10^{-6}\,sin(\theta_2-\theta_4)$$
$$-1.6948\times10^{-5}\,sin(2\theta_2+\theta_4)+1.5061\times10^{-6}\,sin(\theta_2-\theta_6)$$
$$+1.7354\times10^{-6}\,sin(3\theta_2+\theta_4+\theta_5+\theta_6)+8.3976\times10^{-7}\,cos(2\theta_2+2\theta_4+2\theta_5+\theta_6)$$
$$-0.3998\,cos(2\theta_2)-0.0057659\,cos(4\theta_2)-4.506\times10^{-6}\,sin(3\theta_2+\theta_4)$$
$$+1.2902\times10^{-6}\,sin(2\theta_2+2\theta_4+2\theta_5+\theta_6)-2.7897\,sin(2\theta_2)-0.29764\,sin(4\theta_2)$$
$$-0.098665\,cos(3\theta_2)-1.3116\,sin(3\theta_2)+2.3139\times10^{-6}\,cos(\theta_2+\theta_6)$$
$$-1.5061\times10^{-6}\,sin(\theta_2+\theta_6)+1.1542\times10^{-6}\,cos(\theta_4-\theta_2+\theta_5)$$
$$+4.8778\times10^{-6}\,cos(2\theta_2+\theta_4+\theta_5)-1.6387\times10^{-6}\,sin(\theta_4-\theta_2+\theta_5)$$
$$-2.4228\times10^{-5}\,sin(2\theta_2+\theta_4+\theta_5)+3.7652\times10^{-7}\,cos(\theta_2-\theta_4-\theta_5+\theta_6)$$
$$+1.3731\times10^{-6}\,cos(2\theta_2+\theta_4+\theta_5-\theta_6)-0.0073298\,cos(\theta_2)$$
$$+3.4625\times10^{-6}\,cos(3\theta_2+\theta_4+\theta_5)+5.7848\times10^{-7}\,sin(\theta_2-\theta_4-\theta_5+\theta_6)$$
$$-8.399\times10^{-6}\,sin(2\theta_2+\theta_4+\theta_5-\theta_6)+0.43471\,sin(\theta_2)$$
$$-4.916\times10^{-6}\,sin(3\theta_2+\theta_4+\theta_5)+1.1296\times10^{-6}\,cos(3\theta_2+\theta_4+\theta_5-\theta_6)$$
$$-7.6764\times10^{-7}\,sin(2\theta_2+2\theta_4)-1.7354\times10^{-6}\,sin(3\theta_2+\theta_4+\theta_5-\theta_6)$$
$$+6.5153\times10^{-6}\theta_3\,sin(2\theta_2+\theta_4+\theta_5+\theta_6)+2.5991\times10^{-5}\theta_3\,cos(2\theta_2+\theta_4)$$
$$+1.3717\theta_3\,cos(2\theta_2)-0.56122\theta_3\,sin(2\theta_2)+0.33871\theta_3\,cos(3\theta_2)$$
$$+2.8356\times10^{-5}\theta_3\,cos(2\theta_2+\theta_4+\theta_5)+1.9972\times10^{-5}\theta_3\,sin(2\theta_2+\theta_4+\theta_5)$$
$$+1.001\times10^{-5}\theta_3\,cos(2\theta_2+\theta_4+\theta_5-\theta_6)+0.1129\theta_3\,cos(\theta_2)$$
$$+6.5153\times10^{-6}\theta_3\,sin(2\theta_2+\theta_4+\theta_5-\theta_6)+0.97685{\theta_3}^2\,sin(2\theta_2)-1.001\times$$
$$10^{-5}\theta_3\,cos(2\theta_2+\theta_4+\theta_5+\theta_6))-0.047473\dot{\theta}_2\,sin(2\theta_2)$$
$$-1.5\times10^{-11}\dot{\theta}_6\,cos(\theta_1+\theta_2+\theta_4+\theta_5)+2.8005\times10^{-6}\dot{\theta}_2\,cos(\theta_2+\theta_4+\theta_5+\theta_6)$$
$$+2.8005\times10^{-6}\dot{\theta}_4\,cos(\theta_2+\theta_4+\theta_5+\theta_6)+2.8005\times10^{-6}\dot{\theta}_5\,cos(\theta_2+\theta_4+\theta_5+\theta_6)$$
$$+4.4801\times10^{-6}\dot{\theta}_6\,cos(\theta_2+\theta_4+\theta_5+\theta_6)-0.89292\dot{\theta}_2\,cos(3\theta_2)$$
$$+4.3027\times10^{-6}\dot{\theta}_2\,sin(\theta_2+\theta_4+\theta_5+\theta_6)+4.3027\times10^{-6}\dot{\theta}_4\,sin(\theta_2+\theta_4+\theta_5+\theta_6)$$
$$+4.3027\times10^{-6}\dot{\theta}_5\,sin(\theta_2+\theta_4+\theta_5+\theta_6)+6.8831\times10^{-6}\dot{\theta}_6\,sin(\theta_2+\theta_4+\theta_5+\theta_6)$$
$$+0.017298\dot{\theta}_2\,sin(3\theta_2)-7.124\times10^{-6}\dot{\theta}_2\,cos(\theta_2+\theta_6)+6.5153\times10^{-6}\dot{\theta}_3\,cos(\theta_2+\theta_6)$$
$$+7.124\times10^{-6}\dot{\theta}_6\,cos(\theta_2+\theta_6)+5.7673\times10^{-4}\dot{\theta}_2\,sin(\theta_1+\theta_2)$$
$$-1.3047\times10^{-5}\dot{\theta}_2\,sin(\theta_2+\theta_4)-4.6558\times10^{-6}\dot{\theta}_2\,sin(\theta_2+\theta_6)$$
$$-1.3047\times10^{-5}\dot{\theta}_4\,sin(\theta_2+\theta_4)+1.001\times10^{-5}\dot{\theta}_3\,sin(\theta_2+\theta_6)$$
$$+4.6558\times10^{-6}\dot{\theta}_6\,sin(\theta_2+\theta_6)-6.5547\times10^{-6}\dot{\theta}_4\,cos(2\theta_2+\theta_4+\theta_5)$$
$$-6.5547\times10^{-6}\dot{\theta}_5\,cos(2\theta_2+\theta_4+\theta_5)-4.6166\times10^{-6}\dot{\theta}_4\,sin(2\theta_2+\theta_4+\theta_5)$$
$$-4.6166\times10^{-6}\dot{\theta}_5\,sin(2\theta_2+\theta_4+\theta_5)-2.3139\times10^{-6}\dot{\theta}_4\,cos(2\theta_2+\theta_4+\theta_5-\theta_6)$$
$$-2.3139\times10^{-6}\dot{\theta}_5\,cos(2\theta_2+\theta_4+\theta_5-\theta_6)+2.3139\times10^{-6}\dot{\theta}_6\,cos(2\theta_2+\theta_4+\theta_5-\theta_6)$$
$$+0.88941\dot{\theta}_2\,cos(\theta_2)-1.5061\times10^{-6}\dot{\theta}_4\,sin(2\theta_2+\theta_4+\theta_5-\theta_6)$$
$$-1.5061\times10^{-6}\dot{\theta}_5\,sin(2\theta_2+\theta_4+\theta_5-\theta_6)+1.5061\times10^{-6}\dot{\theta}_6\,sin(2\theta_2+\theta_4+\theta_5-\theta_6)$$
$$+3.0122\times10^{-6}\dot{\theta}_2\,cos(2\theta_2-\theta_6)+1.5061\times10^{-6}\dot{\theta}_6\,cos(2\theta_2-\theta_6)$$

$$+0.10873\dot{\theta}_2 sin(\theta_2)+0.19608\dot{\theta}_3 sin(\theta_2)-4.6278\times10^{-6}\dot{\theta}_2 sin(2\theta_2-\theta_6)$$
$$-2.3139\times10^{-6}\dot{\theta}_6 sin(2\theta_2-\theta_6)+9.9776\times10^{-6}\dot{\theta}_2 cos(\theta_2+\theta_4+\theta_5)$$
$$+9.9776\times10^{-6}\dot{\theta}_4 cos(\theta_2+\theta_4+\theta_5)+9.9776\times10^{-6}\dot{\theta}_5 cos(\theta_2+\theta_4+\theta_5)$$
$$-1.5843\times10^{-5}\dot{\theta}_2 sin(\theta_2+\theta_4+\theta_5)-1.5843\times10^{-5}\dot{\theta}_4 sin(\theta_2+\theta_4+\theta_5)$$
$$-1.5843\times10^{-5}\dot{\theta}_5 sin(\theta_2+\theta_4+\theta_5)+2.5941\times10^{-6}\dot{\theta}_6 sin(\theta_2+\theta_4+\theta_5)$$
$$-1.5\times10^{-11}\dot{\theta}_6 cos(\theta_2-\theta_1+\theta_4+\theta_5)+4.4801\times10^{-6}\dot{\theta}_2 cos(\theta_2+\theta_4+\theta_5-\theta_6)$$
$$+5.9289\times10^{-7}\dot{\theta}_2 cos(\theta_2+\theta_4+\theta_5-2\theta_6)+5.9289\times10^{-7}\dot{\theta}_2 cos(\theta_2+\theta_4+\theta_5+2\theta_6)$$
$$+4.4801\times10^{-6}\dot{\theta}_4 cos(\theta_2+\theta_4+\theta_5-\theta_6)+5.9289\times10^{-7}\dot{\theta}_4 cos(\theta_2+\theta_4+\theta_5-2\theta_6)$$
$$+5.9289\times10^{-7}\dot{\theta}_4 cos(\theta_2+\theta_4+\theta_5+2\theta_6)+2.3139\times10^{-6}\dot{\theta}_4 cos(2\theta_2+\theta_4+\theta_5+\theta_6)$$
$$+4.4801\times10^{-6}\dot{\theta}_5 cos(\theta_2+\theta_4+\theta_5-\theta_6)+5.9289\times10^{-7}\dot{\theta}_5 cos(\theta_2+\theta_4+\theta_5-2\theta_6)$$
$$+5.9289\times10^{-7}\dot{\theta}_5 cos(\theta_2+\theta_4+\theta_5+2\theta_6)+2.3139\times10^{-6}\dot{\theta}_5 cos(2\theta_2+\theta_4+\theta_5+\theta_6)$$
$$-2.8005\times10^{-6}\dot{\theta}_6 cos(\theta_2+\theta_4+\theta_5-\theta_6)+2.3139\times10^{-6}\dot{\theta}_6 cos(2\theta_2+\theta_4+\theta_5+\theta_6)$$
$$+0.19608\theta_3\dot{\theta}_2 cos(\theta_2)+1.001\times10^{-5}\theta_3\dot{\theta}_2 cos(\theta_2-\theta_6)$$
$$+1.001\times10^{-5}\theta_3\dot{\theta}_6 cos(\theta_2-\theta_6)+6.5153\times10^{-6}\theta_3\dot{\theta}_2 sin(\theta_2-\theta_6)$$
$$+6.5153\times10^{-6}\theta_3\dot{\theta}_6 sin(\theta_2-\theta_6)+1.001\times10^{-5}\theta_3\dot{\theta}_2 cos(\theta_2+\theta_6)$$
$$-1.001\times10^{-5}\theta_3\dot{\theta}_6 cos(\theta_2+\theta_6)-6.5153\times10^{-6}\theta_3\dot{\theta}_2 sin(\theta_2+\theta_6)$$
$$+6.5153\times10^{-6}\theta_3\dot{\theta}_6 sin(\theta_2+\theta_6)$$

$$Bb_2 = 4.75\times10^{-11}\dot{\theta}_6 sin(2\theta_1+\theta_2+\theta_4+\theta_5)-4.75\times10^{-11}\dot{\theta}_6 sin(\theta_2-2\theta_1+\theta_4+\theta_5)$$
$$+2.3139\times10^{-6}\dot{\theta}_4 sin(\theta_4-\theta_2+\theta_5+\theta_6)+2.3139\times10^{-6}\dot{\theta}_5 sin(\theta_4-\theta_2+\theta_5+\theta_6)$$
$$+2.3139\times10^{-6}\dot{\theta}_6 sin(\theta_4-\theta_2+\theta_5+\theta_6)+2.3139\times10^{-6}\dot{\theta}_6 cos(\theta_2-\theta_6)$$
$$+\dot{\theta}_2(1.5061\times10^{-6} cos(\theta_4-\theta_2+\theta_5+\theta_6)+2.3139\times10^{-6} sin(\theta_4-\theta_2+\theta_5+\theta_6)$$
$$+5.7673\times10^{-4} cos(\theta_1-2\theta_2)+5.7673\times10^{-4} cos(\theta_1+2\theta_2)$$
$$-0.012405 cos(2\theta_1+\theta_2)-5.7673\times10^{-4} sin(\theta_1-\theta_2)+6.008\times10^{-6} sin(\theta_2-\theta_4)$$
$$+0.011532 cos(2\theta_2)+0.58247 sin(2\theta_2)-5.7673\times10^{-4} sin(\theta_1+\theta_2)$$
$$+4.6166\times10^{-6} cos(\theta_4-\theta_2+\theta_5)-6.5547\times10^{-6} sin(\theta_4-\theta_2+\theta_5)$$
$$+1.5061\times10^{-6} cos(\theta_2-\theta_4-\theta_5+\theta_6)-0.12791 cos(\theta_2)$$
$$+2.3139\times10^{-6} sin(\theta_2-\theta_4-\theta_5+\theta_6)+0.012405 cos(2\theta_1-\theta_2)+1.7488 sin(\theta_2)$$
$$+0.0062026 sin(2\theta_1-2\theta_2)-0.0062026 sin(2\theta_1+2\theta_2)+0.45162\theta_3 cos(\theta_2))$$
$$+6.008\times10^{-6}\dot{\theta}_4 sin(\theta_2-\theta_4)+1.5061\times10^{-6}\dot{\theta}_6 sin(\theta_2-\theta_6)$$
$$+1.5\times10^{-11}\dot{\theta}_6 cos(\theta_1+\theta_2+\theta_4+\theta_5)-2.3139\times10^{-6}\dot{\theta}_6 cos(\theta_2+\theta_6)$$
$$+1.5061\times10^{-6}\dot{\theta}_6 sin(\theta_2+\theta_6)+4.6166\times10^{-6}\dot{\theta}_4 cos(\theta_4-\theta_2+\theta_5)$$
$$+4.6166\times10^{-6}\dot{\theta}_5 cos(\theta_4-\theta_2+\theta_5)-6.5547\times10^{-6}\dot{\theta}_4 sin(\theta_4-\theta_2+\theta_5)$$
$$-6.5547\times10^{-6}\dot{\theta}_5 sin(\theta_4-\theta_2+\theta_5)+1.5061\times10^{-6}\dot{\theta}_4 cos(\theta_2-\theta_4-\theta_5+\theta_6)$$
$$+1.5061\times10^{-6}\dot{\theta}_5 cos(\theta_2-\theta_4-\theta_5+\theta_6)-1.5061\times10^{-6}\dot{\theta}_6 cos(\theta_2-\theta_4-\theta_5+\theta_6)$$
$$+2.3139\times10^{-6}\dot{\theta}_4 sin(\theta_2-\theta_4-\theta_5+\theta_6)+2.3139\times10^{-6}\dot{\theta}_5 sin(\theta_2-\theta_4-\theta_5+\theta_6)$$
$$-2.3139\times10^{-6}\dot{\theta}_6 sin(\theta_2-\theta_4-\theta_5+\theta_6)-0.45162\dot{\theta}_3 sin(\theta_2)$$
$$-1.5\times10^{-11}\dot{\theta}_6 cos(\theta_2-\theta_1+\theta_4+\theta_5)+1.5061\times10^{-6}\dot{\theta}_4 cos(\theta_4-\theta_2+\theta_5+\theta_6)$$
$$+1.5061\times10^{-6}\dot{\theta}_5 cos(\theta_4-\theta_2+\theta_5+\theta_6)+1.5061\times10^{-6}\dot{\theta}_6 cos(\theta_4-\theta_2+\theta_5+\theta_6)$$

$$Bd_2 = Be_2 = 4.75\times10^{-11}\dot{\theta}_6 sin(2\theta_1+\theta_2+\theta_4+\theta_5)-4.75\times10^{-11}\dot{\theta}_6 sin(\theta_2-2\theta_1+\theta_4+\theta_5)$$
$$+1.5\times10^{-11}\dot{\theta}_6 cos(\theta_1+\theta_2+\theta_4+\theta_5)-1.5\times10^{-11}\dot{\theta}_6 cos(\theta_2-\theta_1+\theta_4+\theta_5)$$

$$Ca_2 = 1.001\times10^{-5}\dot{\theta}_2 sin(\theta_2-\theta_6)-6.5153\times10^{-6}\dot{\theta}_2 cos(\theta_2-\theta_6)$$
$$-6.5153\times10^{-6}\dot{\theta}_6 cos(\theta_2-\theta_6)-0.45162\dot{\theta}_2+1.001\times10^{-5}\dot{\theta}_6 sin(\theta_2-\theta_6)$$

$$+\dot{\theta}_1(1.2995\times10^{-5}sin(2\theta_2+\theta_4)-3.2577\times10^{-6}cos(\theta_4+\theta_5+\theta_6)$$
$$-5.005\times10^{-6}sin(\theta_4+\theta_5+\theta_6)-3.2577\times10^{-6}cos(2\theta_2+\theta_4+\theta_5+\theta_6)$$
$$-5.005\times10^{-6}sin(2\theta_2+\theta_4+\theta_5+\theta_6)-0.97685\theta_3+0.28061cos(2\theta_2)$$
$$+0.68585sin(2\theta_2)+0.1129sin(3\theta_2)-9.9858\times10^{-6}cos(\theta_4+\theta_5)$$
$$+1.4178\times10^{-5}sin(\theta_4+\theta_5)-9.9858\times10^{-6}cos(2\theta_2+\theta_4+\theta_5)$$
$$-3.2577\times10^{-6}cos(\theta_4+\theta_5-\theta_6)+1.4178\times10^{-5}sin(2\theta_2+\theta_4+\theta_5)$$
$$+5.005\times10^{-6}sin(\theta_4+\theta_5-\theta_6)-3.2577\times10^{-6}cos(2\theta_2+\theta_4+\theta_5-\theta_6)$$
$$+5.005\times10^{-6}sin(2\theta_2+\theta_4+\theta_5-\theta_6)+0.1129sin(\theta_2)+1.2995\times10^{-5}sin(\theta_4)$$
$$-0.97685\theta_3cos(2\theta_2)+0.28061)+6.5153\times10^{-6}\dot{\theta}_2cos(\theta_2+\theta_6)$$
$$-6.5153\times10^{-6}\dot{\theta}_6cos(\theta_2+\theta_6)+1.001\times10^{-5}\dot{\theta}_2sin(\theta_2+\theta_6)$$
$$-1.001\times10^{-5}\dot{\theta}_6sin(\theta_2+\theta_6)+0.19608\dot{\theta}_2sin(\theta_2)$$

$$Cb_2=2.8356\times10^{-5}sin(\theta_4+\theta_5)-6.5153\times10^{-6}cos(\theta_4+\theta_5+\theta_6)$$
$$-1.001\times10^{-5}sin(\theta_4+\theta_5+\theta_6)-1.9972\times10^{-5}cos(\theta_4+\theta_5)-1.9537\theta_3$$
$$-6.5153\times10^{-6}cos(\theta_4+\theta_5-\theta_6)+1.001\times10^{-5}sin(\theta_4+\theta_5-\theta_6)+0.45162sin(\theta_2)$$
$$+2.5991\times10^{-5}sin(\theta_4)+0.56122$$

$$Cd_2=.8356\times10^{-5}sin(\theta_4+\theta_5)-6.5153\times10^{-6}cos(\theta_4+\theta_5+\theta_6)$$
$$-1.001\times10^{-5}sin(\theta_4+\theta_5+\theta_6)-1.9972\times10^{-5}cos(\theta_4+\theta_5)-1.9537\theta_3$$
$$-6.5153\times10^{-6}cos(\theta_4+\theta_5-\theta_6)+1.001\times10^{-5}sin(\theta_4+\theta_5-\theta_6)+0.45162sin(\theta_2)$$
$$+2.5991\times10^{-5}sin(\theta_4)+0.56122$$

$$Ce_2=2.8356\times10^{-5}sin(\theta_4+\theta_5)-1.001\times10^{-5}sin(\theta_4+\theta_5+\theta_6)$$
$$-1.9972\times10^{-5}cos(\theta_4+\theta_5)-6.5153\times10^{-6}cos(\theta_4+\theta_5+\theta_6)$$
$$-6.5153\times10^{-6}cos(\theta_4+\theta_5-\theta_6)+1.001\times10^{-5}sin(\theta_4+\theta_5-\theta_6)$$

$$Cf_2=6.5153\times10^{-6}cos(\theta_4+\theta_5-\theta_6)-1.001\times10^{-5}sin(\theta_4+\theta_5+\theta_6)$$
$$-6.5153\times10^{-6}cos(\theta_4+\theta_5+\theta_6)-1.001\times10^{-5}sin(\theta_4+\theta_5-\theta_6)$$

$$Da_2=2.625\times10^{-7}\dot{\theta}_2sin(\theta_2+\theta_4+\theta_5+2\theta_6)-2.625\times10^{-7}\dot{\theta}_2sin(\theta_2+\theta_4+\theta_5-2\theta_6)$$
$$-6.8831\times10^{-6}\dot{\theta}_2sin(\theta_2+\theta_4+\theta_5-\theta_6)-6.8831\times10^{-6}\dot{\theta}_4sin(\theta_2+\theta_4+\theta_5-\theta_6)$$
$$-2.625\times10^{-7}\dot{\theta}_4sin(\theta_2+\theta_4+\theta_5-2\theta_6)+2.625\times10^{-7}\dot{\theta}_4sin(\theta_2+\theta_4+\theta_5+2\theta_6)$$
$$-7.5304\times10^{-7}\dot{\theta}_4sin(2\theta_2+\theta_4+\theta_5+\theta_6)-6.8831\times10^{-6}\dot{\theta}_5sin(\theta_2+\theta_4+\theta_5-\theta_6)$$
$$-2.625\times10^{-7}\dot{\theta}_5sin(\theta_2+\theta_4+\theta_5-2\theta_6)+2.625\times10^{-7}\dot{\theta}_5sin(\theta_2+\theta_4+\theta_5+2\theta_6)$$
$$-7.5304\times10^{-7}\dot{\theta}_5sin(2\theta_2+\theta_4+\theta_5+\theta_6)+4.3027\times10^{-6}\dot{\theta}_6sin(\theta_2+\theta_4+\theta_5-\theta_6)$$
$$-7.5304\times10^{-7}\dot{\theta}_6sin(2\theta_2+\theta_4+\theta_5+\theta_6)-3.004\times10^{-6}\dot{\theta}_4cos(2\theta_2+\theta_4)$$
$$+\dot{\theta}_1(8.3976\times10^{-7}cos(2\theta_2+2\theta_4+2\theta_5-\theta_6)-7.2573\times10^{-7}sin(2\theta_2+2\theta_4+2\theta_5)$$
$$+2.9645\times10^{-7}cos(2\theta_2+2\theta_4+2\theta_5-2\theta_6)\ -1.3125\times10^{-7}sin(2\theta_2+2\theta_4+2\theta_5-2\theta_6)$$
$$-2.9645\times10^{-7}cos(2\theta_2+2\theta_4+2\theta_5+2\theta_6)-1.2902\times10^{-6}sin(2\theta_2+2\theta_4+2\theta_5-\theta_6)$$
$$-1.3125\times10^{-7}sin(2\theta_2+2\theta_4+2\theta_5+2\theta_6)-6.8654\times10^{-7}cos(\theta_4+\theta_5+\theta_6)$$
$$-4.1995\times10^{-6}sin(\theta_4+\theta_5+\theta_6)-3.7652\times10^{-7}cos(\theta_4-\theta_2+\theta_5+\theta_6)$$
$$+3.562\times10^{-6}cos(2\theta_2+\theta_4+\theta_5+\theta_6)-5.7848\times10^{-7}sin(\theta_4-\theta_2+\theta_5+\theta_6)$$
$$+2.3279\times10^{-6}sin(2\theta_2+\theta_4+\theta_5+\theta_6)-3.7331\times10^{-6}cos(2\theta_2+\theta_4)$$
$$+3.7652\times10^{-7}cos(3\theta_2+\theta_4+\theta_5+\theta_6)-1.502\times10^{-6}sin(\theta_2-\theta_4)$$
$$-8.4742\times10^{-6}sin(2\theta_2+\theta_4)+5.7848\times10^{-7}sin(3\theta_2+\theta_4+\theta_5+\theta_6)$$
$$+8.3976\times10^{-7}cos(2\theta_2+2\theta_4+2\theta_5+\theta_6)-1.502\times10^{-6}sin(3\theta_2+\theta_4)$$
$$+1.2902\times10^{-6}sin(2\theta_2+2\theta_4+2\theta_5+\theta_6)-1.0584\times10^{-5}cos(\theta_4+\theta_5)$$
$$+6.3767\times10^{-6}sin(\theta_4+\theta_5)-1.1542\times10^{-6}cos(\theta_4-\theta_2+\theta_5)$$

$$+2.4389\times10^{-6}cos(2\theta_2+\theta_4+\theta_5)-3.562\times10^{-6}cos(\theta_4+\theta_5-\theta_6)$$
$$+1.6387\times10^{-6}sin(\theta_4-\theta_2+\theta_5)-1.2114\times10^{-5}sin(2\theta_2+\theta_4+\theta_5)$$
$$+2.3279\times10^{-6}sin(\theta_4+\theta_5-\theta_6)-3.7652\times10^{-7}cos(\theta_2-\theta_4-\theta_5+\theta_6)$$
$$+6.8654\times10^{-7}cos(2\theta_2+\theta_4+\theta_5-\theta_6)-3.7331\times10^{-6}cos(\theta_4)$$
$$+1.1542\times10^{-6}cos(3\theta_2+\theta_4+\theta_5)-5.7848\times10^{-7}sin(\theta_2-\theta_4-\theta_5+\theta_6)$$
$$-4.1995\times10^{-6}sin(2\theta_2+\theta_4+\theta_5-\theta_6)+8.4742\times10^{-6}sin(\theta_4)$$
$$-1.6387\times10^{-6}sin(3\theta_2+\theta_4+\theta_5)+3.7652\times10^{-7}cos(3\theta_2+\theta_4+\theta_5-\theta_6)$$
$$-7.6764\times10^{-7}sin(2\theta_2+2\theta_4)-5.7848\times10^{-7}sin(3\theta_2+\theta_4+\theta_5-\theta_6)$$
$$+3.2577\times10^{-6}\theta_3 sin(2\theta_2+\theta_4+\theta_5+\theta_6)+1.2995\times10^{-5}\theta_3 cos(2\theta_2+\theta_4)$$
$$+1.4178\times10^{-5}\theta_3 cos(\theta_4+\theta_5)+9.9858\times10^{-6}\theta_3 sin(\theta_4+\theta_5)$$
$$+1.4178\times10^{-5}\theta_3 cos(2\theta_2+\theta_4+\theta_5)+5.005\times10^{-6}\theta_3 cos(\theta_4+\theta_5-\theta_6)$$
$$+9.9858\times10^{-6}\theta_3 sin(2\theta_2+\theta_4+\theta_5)+3.2577\times10^{-6}\theta_3 sin(\theta_4+\theta_5-\theta_6)$$
$$+5.005\times10^{-6}\theta_3 cos(2\theta_2+\theta_4+\theta_5-\theta_6)+1.2995\times10^{-5}\theta_3 cos(\theta_4)$$
$$+3.2577\times10^{-6}\theta_3 sin(2\theta_2+\theta_4+\theta_5-\theta_6)-5.005\times10^{-6}\theta_3 cos(\theta_4+\theta_5+\theta_6)$$
$$+3.2577\times10^{-6}\theta_3 sin(\theta_4+\theta_5+\theta_6)-5.005\times10^{-6}\theta_3 cos(2\theta_2+\theta_4+\theta_5+\theta_6))$$
$$-1.5\times10^{-11}\dot{\theta}_6 cos(\theta_1+\theta_2+\theta_4+\theta_5)+2.8005\times10^{-6}\dot{\theta}_2 cos(\theta_2+\theta_4+\theta_5+\theta_6)$$
$$+2.8005\times10^{-6}\dot{\theta}_4 cos(\theta_2+\theta_4+\theta_5+\theta_6)+2.8005\times10^{-6}\dot{\theta}_5 cos(\theta_2+\theta_4+\theta_5+\theta_6)$$
$$+4.4801\times10^{-6}\dot{\theta}_6 cos(\theta_2+\theta_4+\theta_5+\theta_6)+4.3027\times10^{-6}\dot{\theta}_2 sin(\theta_2+\theta_4+\theta_5+\theta_6)$$
$$+4.3027\times10^{-6}\dot{\theta}_4 sin(\theta_2+\theta_4+\theta_5+\theta_6)+4.3027\times10^{-6}\dot{\theta}_5 sin(\theta_2+\theta_4+\theta_5+\theta_6)$$
$$+6.8831\times10^{-6}\dot{\theta}_6 sin(\theta_2+\theta_4+\theta_5+\theta_6)+6.5547\times10^{-6}\dot{\theta}_2 cos(\theta_4+\theta_5)$$
$$+3.2774\times10^{-6}\dot{\theta}_4 cos(\theta_4+\theta_5)+3.2774\times10^{-6}\dot{\theta}_5 cos(\theta_4+\theta_5)$$
$$-1.3047\times10^{-5}\dot{\theta}_2 sin(\theta_2+\theta_4)-1.3047\times10^{-5}\dot{\theta}_4 sin(\theta_2+\theta_4)$$
$$+4.6166\times10^{-6}\dot{\theta}_2 sin(\theta_4+\theta_5)+2.3083\times10^{-6}\dot{\theta}_4 sin(\theta_4+\theta_5)$$
$$+2.3083\times10^{-6}\dot{\theta}_5 sin(\theta_4+\theta_5)-3.2774\times10^{-6}\dot{\theta}_4 cos(2\theta_2+\theta_4+\theta_5)$$
$$+2.3139\times10^{-6}\dot{\theta}_2 cos(\theta_4+\theta_5-\theta_6)-3.2774\times10^{-6}\dot{\theta}_5 cos(2\theta_2+\theta_4+\theta_5)$$
$$+1.157\times10^{-6}\dot{\theta}_4 cos(\theta_4+\theta_5-\theta_6)+1.157\times10^{-6}\dot{\theta}_5 cos(\theta_4+\theta_5-\theta_6)$$
$$-1.157\times10^{-6}\dot{\theta}_6 cos(\theta_4+\theta_5-\theta_6)-2.3083\times10^{-6}\dot{\theta}_4 sin(2\theta_2+\theta_4+\theta_5)$$
$$+1.5061\times10^{-6}\dot{\theta}_2 sin(\theta_4+\theta_5-\theta_6)-2.3083\times10^{-6}\dot{\theta}_5 sin(2\theta_2+\theta_4+\theta_5)$$
$$+7.5304\times10^{-7}\dot{\theta}_4 sin(\theta_4+\theta_5-\theta_6)+7.5304\times10^{-7}\dot{\theta}_5 sin(\theta_4+\theta_5-\theta_6)$$
$$-7.5304\times10^{-7}\dot{\theta}_6 sin(\theta_4+\theta_5-\theta_6)-1.157\times10^{-6}\dot{\theta}_4 cos(2\theta_2+\theta_4+\theta_5-\theta_6)$$
$$-1.157\times10^{-6}\dot{\theta}_5 cos(2\theta_2+\theta_4+\theta_5-\theta_6)+1.157\times10^{-6}\dot{\theta}_6 cos(2\theta_2+\theta_4+\theta_5-\theta_6)$$
$$+6.008\times10^{-6}\dot{\theta}_2 cos(\theta_4)+3.004\times10^{-6}\dot{\theta}_4 cos(\theta_4)$$
$$-7.5304\times10^{-7}\dot{\theta}_4 sin(2\theta_2+\theta_4+\theta_5-\theta_6)-7.5304\times10^{-7}\dot{\theta}_5 sin(2\theta_2+\theta_4+\theta_5-\theta_6)$$
$$+7.5304\times10^{-7}\dot{\theta}_6 sin(2\theta_2+\theta_4+\theta_5-\theta_6)+9.9776\times10^{-6}\dot{\theta}_2 cos(\theta_2+\theta_4+\theta_5)$$
$$+9.9776\times10^{-6}\dot{\theta}_4 cos(\theta_2+\theta_4+\theta_5)+9.9776\times10^{-6}\dot{\theta}_5 cos(\theta_2+\theta_4+\theta_5)$$
$$-2.3139\times10^{-6}\dot{\theta}_2 cos(\theta_4+\theta_5+\theta_6)-1.157\times10^{-6}\dot{\theta}_4 cos(\theta_4+\theta_5+\theta_6)$$
$$-1.157\times10^{-6}\dot{\theta}_5 cos(\theta_4+\theta_5+\theta_6)-1.157\times10^{-6}\dot{\theta}_6 cos(\theta_4+\theta_5+\theta_6)$$
$$-1.5843\times10^{-5}\dot{\theta}_2 sin(\theta_2+\theta_4+\theta_5)-1.5843\times10^{-5}\dot{\theta}_4 sin(\theta_2+\theta_4+\theta_5)$$
$$-1.5843\times10^{-5}\dot{\theta}_5 sin(\theta_2+\theta_4+\theta_5)+1.5061\times10^{-6}\dot{\theta}_2 sin(\theta_4+\theta_5+\theta_6)$$
$$+2.5941\times10^{-6}\dot{\theta}_6 sin(\theta_2+\theta_4+\theta_5)+7.5304\times10^{-7}\dot{\theta}_4 sin(\theta_4+\theta_5+\theta_6)$$
$$+7.5304\times10^{-7}\dot{\theta}_5 sin(\theta_4+\theta_5+\theta_6)+7.5304\times10^{-7}\dot{\theta}_6 sin(\theta_4+\theta_5+\theta_6)$$
$$-1.5\times10^{-11}\dot{\theta}_6 cos(\theta_2-\theta_1+\theta_4+\theta_5)+4.4801\times10^{-6}\dot{\theta}_2 cos(\theta_2+\theta_4+\theta_5-\theta_6)$$

$$
\begin{aligned}
&+5.9289\times10^{-7}\dot{\theta}_2 cos(\theta_2+\theta_4+\theta_5-2\theta_6)+5.9289\times10^{-7}\dot{\theta}_2 cos(\theta_2+\theta_4+\theta_5+2\theta_6)\\
&+4.4801\times10^{-6}\dot{\theta}_4 cos(\theta_2+\theta_4+\theta_5-\theta_6)+5.9289\times10^{-7}\dot{\theta}_4 cos(\theta_2+\theta_4+\theta_5-2\theta_6)\\
&+5.9289\times10^{-7}\dot{\theta}_4 cos(\theta_2+\theta_4+\theta_5+2\theta_6)+1.157\times10^{-6}\dot{\theta}_4 cos(2\theta_2+\theta_4+\theta_5+\theta_6)\\
&+4.4801\times10^{-6}\dot{\theta}_5 cos(\theta_2+\theta_4+\theta_5-\theta_6)+5.9289\times10^{-7}\dot{\theta}_5 cos(\theta_2+\theta_4+\theta_5-2\theta_6)\\
&+5.9289\times10^{-7}\dot{\theta}_5 cos(\theta_2+\theta_4+\theta_5+2\theta_6)+1.157\times10^{-6}\dot{\theta}_5 cos(2\theta_2+\theta_4+\theta_5+\theta_6)\\
&-2.8005\times10^{-6}\dot{\theta}_6 cos(\theta_2+\theta_4+\theta_5-\theta_6)+1.157\times10^{-6}\dot{\theta}_6 cos(2\theta_2+\theta_4+\theta_5+\theta_6)\\
Db_2=\ &4.75\times10^{-11}\dot{\theta}_6 sin(2\theta_1+\theta_2+\theta_4+\theta_5)-4.75\times10^{-11}\dot{\theta}_6 sin(\theta_2-2\theta_1+\theta_4+\theta_5)\\
&-2.3139\times10^{-6}\dot{\theta}_4 sin(\theta_4-\theta_2+\theta_5+\theta_6)-2.3139\times10^{-6}\dot{\theta}_5 sin(\theta_4-\theta_2+\theta_5+\theta_6)\\
&-2.3139\times10^{-6}\dot{\theta}_6 sin(\theta_4-\theta_2+\theta_5+\theta_6)-\dot{\theta}_2(1.3731\times10^{-6} cos(\theta_4+\theta_5+\theta_6)\\
&+8.399\times10^{-6} sin(\theta_4+\theta_5+\theta_6)+1.5061\times10^{-6} cos(\theta_4-\theta_2+\theta_5+\theta_6)\\
&+2.3139\times10^{-6} sin(\theta_4-\theta_2+\theta_5+\theta_6)+6.008\times10^{-6} sin(\theta_2-\theta_4)\\
&+2.1169\times10^{-5} cos(\theta_4+\theta_5)-1.2753\times10^{-5} sin(\theta_4+\theta_5)\\
&+4.6166\times10^{-6} cos(\theta_4-\theta_2+\theta_5)+7.124\times10^{-6} cos(\theta_4+\theta_5-\theta_6)\\
&-6.5547\times10^{-6} sin(\theta_4-\theta_2+\theta_5)-4.6558\times10^{-6} sin(\theta_4+\theta_5-\theta_6)\\
&+1.5061\times10^{-6} cos(\theta_2-\theta_4-\theta_5+\theta_6)+7.4661\times10^{-6} cos(\theta_4)\\
&+2.3139\times10^{-6} sin(\theta_2-\theta_4-\theta_5+\theta_6)-1.6948\times10^{-5} sin(\theta_4)\\
&-2.8356\times10^{-5}\theta_3 cos(\theta_4+\theta_5)-1.9972\times10^{-5}\theta_3 sin(\theta_4+\theta_5)\\
&-1.001\times10^{-5}\theta_3 cos(\theta_4+\theta_5-\theta_6)-6.5153\times10^{-6}\theta_3 sin(\theta_4+\theta_5-\theta_6)\\
&-2.5991\times10^{-5}\theta_3 cos(\theta_4)+1.001\times10^{-5}\theta_3 cos(\theta_4+\theta_5+\theta_6)\\
&-6.5153\times10^{-6}\theta_3 sin(\theta_4+\theta_5+\theta_6))-6.008\times10^{-6}\dot{\theta}_4 sin(\theta_2-\theta_4)\\
&+1.5\times10^{-11}\dot{\theta}_6 cos(\theta_1+\theta_2+\theta_4+\theta_5)+1.9972\times10^{-5}\dot{\theta}_3 cos(\theta_4+\theta_5)\\
&-2.1169\times10^{-5}\dot{\theta}_4 cos(\theta_4+\theta_5)-2.1169\times10^{-5}\dot{\theta}_5 cos(\theta_4+\theta_5)\\
&-2.8356\times10^{-5}\dot{\theta}_3 sin(\theta_4+\theta_5)+1.2753\times10^{-5}\dot{\theta}_4 sin(\theta_4+\theta_5)\\
&+1.2753\times10^{-5}\dot{\theta}_5 sin(\theta_4+\theta_5)-4.6166\times10^{-6}\dot{\theta}_4 cos(\theta_4-\theta_2+\theta_5)\\
&-4.6166\times10^{-6}\dot{\theta}_5 cos(\theta_4-\theta_2+\theta_5)+6.5153\times10^{-6}\dot{\theta}_3 cos(\theta_4+\theta_5-\theta_6)\\
&-7.124\times10^{-6}\dot{\theta}_4 cos(\theta_4+\theta_5-\theta_6)-7.124\times10^{-6}\dot{\theta}_5 cos(\theta_4+\theta_5-\theta_6)\\
&+7.124\times10^{-6}\dot{\theta}_6 cos(\theta_4+\theta_5-\theta_6)+6.5547\times10^{-6}\dot{\theta}_4 sin(\theta_4-\theta_2+\theta_5)\\
&+6.5547\times10^{-6}\dot{\theta}_5 sin(\theta_4-\theta_2+\theta_5)-1.001\times10^{-5}\dot{\theta}_3 sin(\theta_4+\theta_5-\theta_6)\\
&+4.6558\times10^{-6}\dot{\theta}_4 sin(\theta_4+\theta_5-\theta_6)+4.6558\times10^{-6}\dot{\theta}_5 sin(\theta_4+\theta_5-\theta_6)\\
&-4.6558\times10^{-6}\dot{\theta}_6 sin(\theta_4+\theta_5-\theta_6)-1.5061\times10^{-6}\dot{\theta}_4 cos(\theta_2-\theta_4-\theta_5+\theta_6)\\
&-1.5061\times10^{-6}\dot{\theta}_5 cos(\theta_2-\theta_4-\theta_5+\theta_6)+1.5061\times10^{-6}\dot{\theta}_6 cos(\theta_2-\theta_4-\theta_5+\theta_6)\\
&-7.4661\times10^{-6}\dot{\theta}_4 cos(\theta_4)-2.3139\times10^{-6}\dot{\theta}_4 sin(\theta_2-\theta_4-\theta_5+\theta_6)\\
&-2.3139\times10^{-6}\dot{\theta}_5 sin(\theta_2-\theta_4-\theta_5+\theta_6)+2.3139\times10^{-6}\dot{\theta}_6 sin(\theta_2-\theta_4-\theta_5+\theta_6)\\
&-2.5991\times10^{-5}\dot{\theta}_3 sin(\theta_4)+1.6948\times10^{-5}\dot{\theta}_4 sin(\theta_4)\\
&+6.5153\times10^{-6}\dot{\theta}_3 cos(\theta_4+\theta_5+\theta_6)-1.3731\times10^{-6}\dot{\theta}_4 cos(\theta_4+\theta_5+\theta_6)\\
&-1.3731\times10^{-6}\dot{\theta}_5 cos(\theta_4+\theta_5+\theta_6)-1.3731\times10^{-6}\dot{\theta}_6 cos(\theta_4+\theta_5+\theta_6)\\
&+1.001\times10^{-5}\dot{\theta}_3 sin(\theta_4+\theta_5+\theta_6)-8.399\times10^{-6}\dot{\theta}_4 sin(\theta_4+\theta_5+\theta_6)\\
&-8.399\times10^{-6}\dot{\theta}_5 sin(\theta_4+\theta_5+\theta_6)-8.399\times10^{-6}\dot{\theta}_6 sin(\theta_4+\theta_5+\theta_6)\\
&-1.5\times10^{-11}\dot{\theta}_6 cos(\theta_2-\theta_1+\theta_4+\theta_5)-1.5061\times10^{-6}\dot{\theta}_4 cos(\theta_4-\theta_2+\theta_5+\theta_6)\\
&-1.5061\times10^{-6}\dot{\theta}_5 cos(\theta_4-\theta_2+\theta_5+\theta_6)-1.5061\times10^{-6}\dot{\theta}_6 cos(\theta_4-\theta_2+\theta_5+\theta_6)\\
&+6.5153\times10^{-6}\theta_3\dot{\theta}_4 sin(\theta_4+\theta_5-\theta_6)+6.5153\times10^{-6}\theta_3\dot{\theta}_5 sin(\theta_4+\theta_5-\theta_6)\\
&-6.5153\times10^{-6}\theta_3\dot{\theta}_6 sin(\theta_4+\theta_5-\theta_6)+2.5991\times10^{-5}\theta_3\dot{\theta}_4 cos(\theta_4)
\end{aligned}
$$

$$
\begin{aligned}
&-1.001\times10^{-5}\theta_3\dot{\theta}_4 cos(\theta_4+\theta_5+\theta_6)-1.001\times10^{-5}\theta_3\dot{\theta}_5 cos(\theta_4+\theta_5+\theta_6)\\
&-1.001\times10^{-5}\theta_3\dot{\theta}_6 cos(\theta_4+\theta_5+\theta_6)+6.5153\times10^{-6}\theta_3\dot{\theta}_4 sin(\theta_4+\theta_5+\theta_6)\\
&+6.5153\times10^{-6}\theta_3\dot{\theta}_5 sin(\theta_4+\theta_5+\theta_6)+6.5153\times10^{-6}\theta_3\dot{\theta}_6 sin(\theta_4+\theta_5+\theta_6)\\
&+2.8356\times10^{-5}\theta_3\dot{\theta}_4 cos(\theta_4+\theta_5)+2.8356\times10^{-5}\theta_3\dot{\theta}_5 cos(\theta_4+\theta_5)\\
&+1.9972\times10^{-5}\theta_3\dot{\theta}_4 sin(\theta_4+\theta_5)+1.9972\times10^{-5}\theta_3\dot{\theta}_5 sin(\theta_4+\theta_5)\\
&+1.001\times10^{-5}\theta_3\dot{\theta}_4 cos(\theta_4+\theta_5-\theta_6)+1.001\times10^{-5}\theta_3\dot{\theta}_5 cos(\theta_4+\theta_5-\theta_6)\\
&-1.001\times10^{-5}\theta_3\dot{\theta}_6 cos(\theta_4+\theta_5-\theta_6)
\end{aligned}
$$

$$
\begin{aligned}
Dc_2=\ &1.9972\times10^{-5}\dot{\theta}_4 cos(\theta_4+\theta_5)+1.9972\times10^{-5}\dot{\theta}_5 cos(\theta_4+\theta_5)\\
&-2.8356\times10^{-5}\dot{\theta}_4 sin(\theta_4+\theta_5)-2.8356\times10^{-5}\dot{\theta}_5 sin(\theta_4+\theta_5)\\
&+6.5153\times10^{-6}\dot{\theta}_4 cos(\theta_4+\theta_5-\theta_6)+6.5153\times10^{-6}\dot{\theta}_5 cos(\theta_4+\theta_5-\theta_6)\\
&-6.5153\times10^{-6}\dot{\theta}_6 cos(\theta_4+\theta_5-\theta_6)-1.001\times10^{-5}\dot{\theta}_4 sin(\theta_4+\theta_5-\theta_6)\\
&-1.001\times10^{-5}\dot{\theta}_5 sin(\theta_4+\theta_5-\theta_6)+1.001\times10^{-5}\dot{\theta}_6 sin(\theta_4+\theta_5-\theta_6)\\
&-2.5991\times10^{-5}\dot{\theta}_4 sin(\theta_4)+6.5153\times10^{-6}\dot{\theta}_4 cos(\theta_4+\theta_5+\theta_6)\\
&+6.5153\times10^{-6}\dot{\theta}_5 cos(\theta_4+\theta_5+\theta_6)+6.5153\times10^{-6}\dot{\theta}_6 cos(\theta_4+\theta_5+\theta_6)\\
&+1.001\times10^{-5}\dot{\theta}_4 sin(\theta_4+\theta_5+\theta_6)+1.001\times10^{-5}\dot{\theta}_5 sin(\theta_4+\theta_5+\theta_6)\\
&+1.001\times10^{-5}\dot{\theta}_6 sin(\theta_4+\theta_5+\theta_6)
\end{aligned}
$$

$$
\begin{aligned}
Dd_2=De_2=\ &4.75\times10^{-11}\dot{\theta}_6 sin(2\theta_1+\theta_2+\theta_4+\theta_5)-4.75\times10^{-11}\dot{\theta}_6 sin(\theta_2-2\theta_1+\theta_4+\theta_5)\\
&+1.5\times10^{-11}\dot{\theta}_6 cos(\theta_1+\theta_2+\theta_4+\theta_5)-1.5\times10^{-11}\dot{\theta}_6 cos(\theta_2-\theta_1+\theta_4+\theta_5)
\end{aligned}
$$

$$
\begin{aligned}
Ea_2=\ &2.625\times10^{-7}\dot{\theta}_2 sin(\theta_2+\theta_4+\theta_5+2\theta_6)-2.625\times10^{-7}\dot{\theta}_2 sin(\theta_2+\theta_4+\theta_5-2\theta_6)\\
&-6.8831\times10^{-6}\dot{\theta}_2 sin(\theta_2+\theta_4+\theta_5-\theta_6)-6.8831\times10^{-6}\dot{\theta}_4 sin(\theta_2+\theta_4+\theta_5-\theta_6)\\
&-2.625\times10^{-7}\dot{\theta}_4 sin(\theta_2+\theta_4+\theta_5-2\theta_6)+2.625\times10^{-7}\dot{\theta}_4 sin(\theta_2+\theta_4+\theta_5+2\theta_6)\\
&-7.5304\times10^{-7}\dot{\theta}_4 sin(2\theta_2+\theta_4+\theta_5+\theta_6)-6.8831\times10^{-6}\dot{\theta}_5 sin(\theta_2+\theta_4+\theta_5-\theta_6)\\
&-2.625\times10^{-7}\dot{\theta}_5 sin(\theta_2+\theta_4+\theta_5-2\theta_6)+2.625\times10^{-7}\dot{\theta}_5 sin(\theta_2+\theta_4+\theta_5+2\theta_6)\\
&-7.5304\times10^{-7}\dot{\theta}_5 sin(2\theta_2+\theta_4+\theta_5+\theta_6)+4.3027\times10^{-6}\dot{\theta}_6 sin(\theta_2+\theta_4+\theta_5-\theta_6)\\
&-7.5304\times10^{-7}\dot{\theta}_6 sin(2\theta_2+\theta_4+\theta_5+\theta_6)-1.5\times10^{-11}\dot{\theta}_6 cos(\theta_1+\theta_2+\theta_4+\theta_5)\\
&+2.8005\times10^{-6}\dot{\theta}_2 cos(\theta_2+\theta_4+\theta_5+\theta_6)+2.8005\times10^{-6}\dot{\theta}_4 cos(\theta_2+\theta_4+\theta_5+\theta_6)\\
&+2.8005\times10^{-6}\dot{\theta}_5 cos(\theta_2+\theta_4+\theta_5+\theta_6)+4.4801\times10^{-6}\dot{\theta}_6 cos(\theta_2+\theta_4+\theta_5+\theta_6)\\
&+\dot{\theta}_1(8.3976\times10^{-7} cos(2\theta_2+2\theta_4+2\theta_5-\theta_6)-7.2573\times10^{-7} sin(2\theta_2+2\theta_4+2\theta_5)\\
&+2.9645\times10^{-7} cos(2\theta_2+2\theta_4+2\theta_5-2\theta_6)\\
&-2.9645\times10^{-7} cos(2\theta_2+2\theta_4+2\theta_5+2\theta_6)-1.2902\times10^{-6} sin(2\theta_2+2\theta_4+2\theta_5-\theta_6)\\
&-1.3125\times10^{-7} sin(2\theta_2+2\theta_4+2\theta_5-2\theta_6)-1.3125\times10^{-7} sin(2\theta_2+2\theta_4+2\theta_5+2\theta_6)\\
&-6.8654\times10^{-7} cos(\theta_4+\theta_5+\theta_6)-4.1995\times10^{-6} sin(\theta_4+\theta_5+\theta_6)\\
&-3.7652\times10^{-7} cos(\theta_4-\theta_2+\theta_5+\theta_6)+3.562\times10^{-6} cos(2\theta_2+\theta_4+\theta_5+\theta_6)\\
&-5.7848\times10^{-7} sin(\theta_4-\theta_2+\theta_5+\theta_6)+2.3279\times10^{-6} sin(2\theta_2+\theta_4+\theta_5+\theta_6)\\
&+3.7652\times10^{-7} cos(3\theta_2+\theta_4+\theta_5+\theta_6)+5.7848\times10^{-7} sin(3\theta_2+\theta_4+\theta_5+\theta_6)\\
&+8.3976\times10^{-7} cos(2\theta_2+2\theta_4+2\theta_5+\theta_6)+1.2902\times10^{-6} sin(2\theta_2+2\theta_4+2\theta_5+\theta_6)\\
&-1.0584\times10^{-5} cos(\theta_4+\theta_5)+6.3767\times10^{-6} sin(\theta_4+\theta_5)\\
&-1.1542\times10^{-6} cos(\theta_4-\theta_2+\theta_5)+2.4389\times10^{-6} cos(2\theta_2+\theta_4+\theta_5)\\
&-3.562\times10^{-6} cos(\theta_4+\theta_5-\theta_6)+1.6387\times10^{-6} sin(\theta_4-\theta_2+\theta_5)\\
&-1.2114\times10^{-5} sin(2\theta_2+\theta_4+\theta_5)+2.3279\times10^{-6} sin(\theta_4+\theta_5-\theta_6)\\
&-3.7652\times10^{-7} cos(\theta_2-\theta_4-\theta_5+\theta_6)+6.8654\times10^{-7} cos(2\theta_2+\theta_4+\theta_5-\theta_6)\\
&+1.1542\times10^{-6} cos(3\theta_2+\theta_4+\theta_5)-5.7848\times10^{-7} sin(\theta_2-\theta_4-\theta_5+\theta_6)
\end{aligned}
$$

$$
\begin{aligned}
&-4.1995\times10^{-6}\sin(2\theta_2+\theta_4+\theta_5-\theta_6)-1.6387\times10^{-6}\sin(3\theta_2+\theta_4+\theta_5)+3.7652\times\\
&10^{-7}\cos(3\theta_2+\theta_4+\theta_5-\theta_6)-5.7848\times10^{-7}\sin(3\theta_2+\theta_4+\theta_5-\theta_6)+3.2577\times\\
&10^{-6}\theta_3\sin(2\theta_2+\theta_4+\theta_5+\theta_6)+1.4178\times10^{-5}\theta_3\cos(\theta_4+\theta_5)+9.9858\times\\
&10^{-6}\theta_3\sin(\theta_4+\theta_5)+1.4178\times10^{-5}\theta_3\cos(2\theta_2+\theta_4+\theta_5)+5.005\times\\
&10^{-6}\theta_3\cos(\theta_4+\theta_5-\theta_6)+9.9858\times10^{-6}\theta_3\sin(2\theta_2+\theta_4+\theta_5)\\
&+3.2577\times10^{-6}\theta_3\sin(\theta_4+\theta_5-\theta_6)+5.005\times10^{-6}\theta_3\cos(2\theta_2+\theta_4+\theta_5-\theta_6)\\
&+3.2577\times10^{-6}\theta_3\sin(2\theta_2+\theta_4+\theta_5-\theta_6)-5.005\times10^{-6}\theta_3\cos(\theta_4+\theta_5+\theta_6)\\
&+3.2577\times10^{-6}\theta_3\sin(\theta_4+\theta_5+\theta_6)-5.005\times10^{-6}\theta_3\cos(2\theta_2+\theta_4+\theta_5+\theta_6))\\
&+4.3027\times10^{-6}\dot{\theta}_2\sin(\theta_2+\theta_4+\theta_5+\theta_6)+4.3027\times10^{-6}\dot{\theta}_4\sin(\theta_2+\theta_4+\theta_5+\theta_6)\\
&+4.3027\times10^{-6}\dot{\theta}_5\sin(\theta_2+\theta_4+\theta_5+\theta_6)+6.8831\times10^{-6}\dot{\theta}_6\sin(\theta_2+\theta_4+\theta_5+\theta_6)\\
&+6.5547\times10^{-6}\dot{\theta}_2\cos(\theta_4+\theta_5)+3.2774\times10^{-6}\dot{\theta}_4\cos(\theta_4+\theta_5)\\
&+3.2774\times10^{-6}\dot{\theta}_5\cos(\theta_4+\theta_5)+4.6166\times10^{-6}\dot{\theta}_2\sin(\theta_4+\theta_5)\\
&+2.3083\times10^{-6}\dot{\theta}_4\sin(\theta_4+\theta_5)+2.3083\times10^{-6}\dot{\theta}_5\sin(\theta_4+\theta_5)\\
&-3.2774\times10^{-6}\dot{\theta}_4\cos(2\theta_2+\theta_4+\theta_5)+2.3139\times10^{-6}\dot{\theta}_2\cos(\theta_4+\theta_5-\theta_6)\\
&-3.2774\times10^{-6}\dot{\theta}_5\cos(2\theta_2+\theta_4+\theta_5)+1.157\times10^{-6}\dot{\theta}_4\cos(\theta_4+\theta_5-\theta_6)\\
&+1.157\times10^{-6}\dot{\theta}_5\cos(\theta_4+\theta_5-\theta_6)-1.157\times10^{-6}\dot{\theta}_6\cos(\theta_4+\theta_5-\theta_6)\\
&-2.3083\times10^{-6}\dot{\theta}_4\sin(2\theta_2+\theta_4+\theta_5)+1.5061\times10^{-6}\dot{\theta}_2\sin(\theta_4+\theta_5-\theta_6)\\
&-2.3083\times10^{-6}\dot{\theta}_5\sin(2\theta_2+\theta_4+\theta_5)+7.5304\times10^{-7}\dot{\theta}_4\sin(\theta_4+\theta_5-\theta_6)\\
&+7.5304\times10^{-7}\dot{\theta}_5\sin(\theta_4+\theta_5-\theta_6)-7.5304\times10^{-7}\dot{\theta}_6\sin(\theta_4+\theta_5-\theta_6)\\
&-1.157\times10^{-6}\dot{\theta}_4\cos(2\theta_2+\theta_4+\theta_5-\theta_6)-1.157\times10^{-6}\dot{\theta}_5\cos(2\theta_2+\theta_4+\theta_5-\theta_6)\\
&+1.157\times10^{-6}\dot{\theta}_6\cos(2\theta_2+\theta_4+\theta_5-\theta_6)-7.5304\times10^{-7}\dot{\theta}_4\sin(2\theta_2+\theta_4+\theta_5-\theta_6)\\
&-7.5304\times10^{-7}\dot{\theta}_5\sin(2\theta_2+\theta_4+\theta_5-\theta_6)+7.5304\times10^{-7}\dot{\theta}_6\sin(2\theta_2+\theta_4+\theta_5-\theta_6)\\
&+9.9776\times10^{-6}\dot{\theta}_2\cos(\theta_2+\theta_4+\theta_5)+9.9776\times10^{-6}\dot{\theta}_4\cos(\theta_2+\theta_4+\theta_5)\\
&+9.9776\times10^{-6}\dot{\theta}_5\cos(\theta_2+\theta_4+\theta_5)-2.3139\times10^{-6}\dot{\theta}_2\cos(\theta_4+\theta_5+\theta_6)\\
&-1.157\times10^{-6}\dot{\theta}_4\cos(\theta_4+\theta_5+\theta_6)-1.157\times10^{-6}\dot{\theta}_5\cos(\theta_4+\theta_5+\theta_6)\\
&-1.157\times10^{-6}\dot{\theta}_6\cos(\theta_4+\theta_5+\theta_6)-1.5843\times10^{-5}\dot{\theta}_2\sin(\theta_2+\theta_4+\theta_5)\\
&-1.5843\times10^{-5}\dot{\theta}_4\sin(\theta_2+\theta_4+\theta_5)-1.5843\times10^{-5}\dot{\theta}_5\sin(\theta_2+\theta_4+\theta_5)\\
&+1.5061\times10^{-6}\dot{\theta}_2\sin(\theta_4+\theta_5+\theta_6)+2.5941\times10^{-6}\dot{\theta}_6\sin(\theta_2+\theta_4+\theta_5)\\
&+7.5304\times10^{-7}\dot{\theta}_4\sin(\theta_4+\theta_5+\theta_6)+7.5304\times10^{-7}\dot{\theta}_5\sin(\theta_4+\theta_5+\theta_6)\\
&+7.5304\times10^{-7}\dot{\theta}_6\sin(\theta_4+\theta_5+\theta_6)-1.5\times10^{-11}\dot{\theta}_6\cos(\theta_2-\theta_1+\theta_4+\theta_5)\\
&+4.4801\times10^{-6}\dot{\theta}_2\cos(\theta_2+\theta_4+\theta_5-\theta_6)+5.9289\times10^{-7}\dot{\theta}_2\cos(\theta_2+\theta_4+\theta_5-2\theta_6)\\
&+5.9289\times10^{-7}\dot{\theta}_2\cos(\theta_2+\theta_4+\theta_5+2\theta_6)+4.4801\times10^{-6}\dot{\theta}_4\cos(\theta_2+\theta_4+\theta_5-\theta_6)\\
&+5.9289\times10^{-7}\dot{\theta}_4\cos(\theta_2+\theta_4+\theta_5-2\theta_6)+5.9289\times10^{-7}\dot{\theta}_4\cos(\theta_2+\theta_4+\theta_5+2\theta_6)\\
&+1.157\times10^{-6}\dot{\theta}_4\cos(2\theta_2+\theta_4+\theta_5+\theta_6)+4.4801\times10^{-6}\dot{\theta}_5\cos(\theta_2+\theta_4+\theta_5-\theta_6)\\
&+5.9289\times10^{-7}\dot{\theta}_5\cos(\theta_2+\theta_4+\theta_5-2\theta_6)+5.9289\times10^{-7}\dot{\theta}_5\cos(\theta_2+\theta_4+\theta_5+2\theta_6)\\
&+1.157\times10^{-6}\dot{\theta}_5\cos(2\theta_2+\theta_4+\theta_5+\theta_6)-2.8005\times10^{-6}\dot{\theta}_6\cos(\theta_2+\theta_4+\theta_5-\theta_6)\\
&+1.157\times10^{-6}\dot{\theta}_6\cos(2\theta_2+\theta_4+\theta_5+\theta_6)
\end{aligned}
$$

$$
\begin{aligned}
Eb_2=\ &4.75\times10^{-11}\dot{\theta}_6\sin(2\theta_1+\theta_2+\theta_4+\theta_5)-4.75\times10^{-11}\dot{\theta}_6\sin(\theta_2-2\theta_1+\theta_4+\theta_5)\\
&-2.3139\times10^{-6}\dot{\theta}_4\sin(\theta_4-\theta_2+\theta_5+\theta_6)-2.3139\times10^{-6}\dot{\theta}_5\sin(\theta_4-\theta_2+\theta_5+\theta_6)\\
&-2.3139\times10^{-6}\dot{\theta}_6\sin(\theta_4-\theta_2+\theta_5+\theta_6)+1.5\times10^{-11}\dot{\theta}_6\cos(\theta_1+\theta_2+\theta_4+\theta_5)\\
&+1.9972\times10^{-5}\dot{\theta}_3\cos(\theta_4+\theta_5)-2.1169\times10^{-5}\dot{\theta}_4\cos(\theta_4+\theta_5)\\
&-2.1169\times10^{-5}\dot{\theta}_5\cos(\theta_4+\theta_5)-2.8356\times10^{-5}\dot{\theta}_3\sin(\theta_4+\theta_5)
\end{aligned}
$$

$$+1.2753\times10^{-5}\dot{\theta}_4 sin(\theta_4+\theta_5)+1.2753\times10^{-5}\dot{\theta}_5 sin(\theta_4+\theta_5)$$
$$-4.6166\times10^{-6}\dot{\theta}_4 cos(\theta_4-\theta_2+\theta_5)-4.6166\times10^{-6}\dot{\theta}_5 cos(\theta_4-\theta_2+\theta_5)$$
$$+6.5153\times10^{-6}\dot{\theta}_3 cos(\theta_4+\theta_5-\theta_6)-7.124\times10^{-6}\dot{\theta}_4 cos(\theta_4+\theta_5-\theta_6)$$
$$-7.124\times10^{-6}\dot{\theta}_5 cos(\theta_4+\theta_5-\theta_6)+7.124\times10^{-6}\dot{\theta}_6 cos(\theta_4+\theta_5-\theta_6)$$
$$+6.5547\times10^{-6}\dot{\theta}_4 sin(\theta_4-\theta_2+\theta_5)+6.5547\times10^{-6}\dot{\theta}_5 sin(\theta_4-\theta_2+\theta_5)$$
$$-1.001\times10^{-5}\dot{\theta}_3 sin(\theta_4+\theta_5-\theta_6)+4.6558\times10^{-6}\dot{\theta}_4 sin(\theta_4+\theta_5-\theta_6)$$
$$+4.6558\times10^{-6}\dot{\theta}_5 sin(\theta_4+\theta_5-\theta_6)-4.6558\times10^{-6}\dot{\theta}_6 sin(\theta_4+\theta_5-\theta_6)$$
$$-1.5061\times10^{-6}\dot{\theta}_4 cos(\theta_2-\theta_4-\theta_5+\theta_6)-1.5061\times10^{-6}\dot{\theta}_5 cos(\theta_2-\theta_4-\theta_5+\theta_6)$$
$$+1.5061\times10^{-6}\dot{\theta}_6 cos(\theta_2-\theta_4-\theta_5+\theta_6)-2.3139\times10^{-6}\dot{\theta}_4 sin(\theta_2-\theta_4-\theta_5+\theta_6)$$
$$-2.3139\times10^{-6}\dot{\theta}_5 sin(\theta_2-\theta_4-\theta_5+\theta_6)+2.3139\times10^{-6}\dot{\theta}_6 sin(\theta_2-\theta_4-\theta_5+\theta_6)$$
$$-\dot{\theta}_2(1.3731\times10^{-6} cos(\theta_4+\theta_5+\theta_6)+8.399\times10^{-6} sin(\theta_4+\theta_5+\theta_6)$$
$$+1.5061\times10^{-6} cos(\theta_4-\theta_2+\theta_5+\theta_6)+2.3139\times10^{-6} sin(\theta_4-\theta_2+\theta_5+\theta_6)$$
$$+2.1169\times10^{-5} cos(\theta_4+\theta_5)-1.2753\times10^{-5} sin(\theta_4+\theta_5)$$
$$+4.6166\times10^{-6} cos(\theta_4-\theta_2+\theta_5)+7.124\times10^{-6} cos(\theta_4+\theta_5-\theta_6)$$
$$-6.5547\times10^{-6} sin(\theta_4-\theta_2+\theta_5)-4.6558\times10^{-6} sin(\theta_4+\theta_5-\theta_6)$$
$$+1.5061\times10^{-6} cos(\theta_2-\theta_4-\theta_5+\theta_6)+2.3139\times10^{-6} sin(\theta_2-\theta_4-\theta_5+\theta_6)$$
$$-2.8356\times10^{-5}\theta_3 cos(\theta_4+\theta_5)-1.9972\times10^{-5}\theta_3 sin(\theta_4+\theta_5)$$
$$-1.001\times10^{-5}\theta_3 cos(\theta_4+\theta_5-\theta_6)-6.5153\times10^{-6}\theta_3 sin(\theta_4+\theta_5-\theta_6)$$
$$+1.001\times10^{-5}\theta_3 cos(\theta_4+\theta_5+\theta_6)-6.5153\times10^{-6}\theta_3 sin(\theta_4+\theta_5+\theta_6))$$
$$+6.5153\times10^{-6}\dot{\theta}_3 cos(\theta_4+\theta_5+\theta_6)-1.3731\times10^{-6}\dot{\theta}_4 cos(\theta_4+\theta_5+\theta_6)$$
$$-1.3731\times10^{-6}\dot{\theta}_5 cos(\theta_4+\theta_5+\theta_6)-1.3731\times10^{-6}\dot{\theta}_6 cos(\theta_4+\theta_5+\theta_6)$$
$$+1.001\times10^{-5}\dot{\theta}_3 sin(\theta_4+\theta_5+\theta_6)-8.399\times10^{-6}\dot{\theta}_4 sin(\theta_4+\theta_5+\theta_6)$$
$$-8.399\times10^{-6}\dot{\theta}_5 sin(\theta_4+\theta_5+\theta_6)-8.399\times10^{-6}\dot{\theta}_6 sin(\theta_4+\theta_5+\theta_6)-1.5\times$$
$$10^{-11}\dot{\theta}_6 cos(\theta_2-\theta_1+\theta_4+\theta_5)-1.5061\times10^{-6}\dot{\theta}_4 cos(\theta_4-\theta_2+\theta_5+\theta_6)-1.5061\times$$
$$10^{-6}\dot{\theta}_5 cos(\theta_4-\theta_2+\theta_5+\theta_6)-1.5061\times10^{-6}\dot{\theta}_6 cos(\theta_4-\theta_2+\theta_5+\theta_6)+6.5153\times$$
$$10^{-6}\theta_3\dot{\theta}_4 sin(\theta_4+\theta_5-\theta_6)+6.5153\times10^{-6}\theta_3\dot{\theta}_5 sin(\theta_4+\theta_5-\theta_6)-6.5153\times$$
$$10^{-6}\theta_3\dot{\theta}_6 sin(\theta_4+\theta_5-\theta_6)-1.001\times10^{-5}\theta_3\dot{\theta}_4 cos(\theta_4+\theta_5+\theta_6)$$
$$-1.001\times10^{-5}\theta_3\dot{\theta}_5 cos(\theta_4+\theta_5+\theta_6)-1.001\times10^{-5}\theta_3\dot{\theta}_6 cos(\theta_4+\theta_5+\theta_6)$$
$$+6.5153\times10^{-6}\theta_3\dot{\theta}_4 sin(\theta_4+\theta_5+\theta_6)+6.5153\times10^{-6}\theta_3\dot{\theta}_5 sin(\theta_4+\theta_5+\theta_6)$$
$$+6.5153\times10^{-6}\theta_3\dot{\theta}_6 sin(\theta_4+\theta_5+\theta_6)+2.8356\times10^{-5}\theta_3\dot{\theta}_4 cos(\theta_4+\theta_5)$$
$$+2.8356\times10^{-5}\theta_3\dot{\theta}_5 cos(\theta_4+\theta_5)+1.9972\times10^{-5}\theta_3\dot{\theta}_4 sin(\theta_4+\theta_5)$$
$$+1.9972\times10^{-5}\theta_3\dot{\theta}_5 sin(\theta_4+\theta_5)+1.001\times10^{-5}\theta_3\dot{\theta}_4 cos(\theta_4+\theta_5-\theta_6)$$
$$+1.001\times10^{-5}\theta_3\dot{\theta}_5 cos(\theta_4+\theta_5-\theta_6)-1.001\times10^{-5}\theta_3\dot{\theta}_6 cos(\theta_4+\theta_5-\theta_6)$$

$$Ec_2= 1.9972\times10^{-5}\dot{\theta}_4 cos(\theta_4+\theta_5)+1.9972\times10^{-5}\dot{\theta}_5 cos(\theta_4+\theta_5)$$
$$-2.8356\times10^{-5}\dot{\theta}_4 sin(\theta_4+\theta_5)-2.8356\times10^{-5}\dot{\theta}_5 sin(\theta_4+\theta_5)$$
$$+6.5153\times10^{-6}\dot{\theta}_4 cos(\theta_4+\theta_5-\theta_6)+6.5153\times10^{-6}\dot{\theta}_5 cos(\theta_4+\theta_5-\theta_6)$$
$$-6.5153\times10^{-6}\dot{\theta}_6 cos(\theta_4+\theta_5-\theta_6)-1.001\times10^{-5}\dot{\theta}_4 sin(\theta_4+\theta_5-\theta_6)$$
$$-1.001\times10^{-5}\dot{\theta}_5 sin(\theta_4+\theta_5-\theta_6)+1.001\times10^{-5}\dot{\theta}_6 sin(\theta_4+\theta_5-\theta_6)$$
$$+6.5153\times10^{-6}\dot{\theta}_4 cos(\theta_4+\theta_5+\theta_6)+6.5153\times10^{-6}\dot{\theta}_5 cos(\theta_4+\theta_5+\theta_6)$$
$$+6.5153\times10^{-6}\dot{\theta}_6 cos(\theta_4+\theta_5+\theta_6)+1.001\times10^{-5}\dot{\theta}_4 sin(\theta_4+\theta_5+\theta_6)$$
$$+1.001\times10^{-5}\dot{\theta}_5 sin(\theta_4+\theta_5+\theta_6)+1.001\times10^{-5}\dot{\theta}_6 sin(\theta_4+\theta_5+\theta_6)$$

$$Ed_2= Ee_2= 4.75\times10^{-11}\dot{\theta}_6 sin(2\theta_1+\theta_2+\theta_4+\theta_5)-4.75\times10^{-11}\dot{\theta}_6 sin(\theta_2-2\theta_1+\theta_4+\theta_5)$$

$$
\begin{aligned}
Fa_2 = {} & +1.5\times10^{-11}\dot{\theta}_6 cos(\theta_1+\theta_2+\theta_4+\theta_5)-1.5\times10^{-11}\dot{\theta}_6 cos(\theta_2-\theta_1+\theta_4+\theta_5) \\
& 6.8831\times10^{-6}\dot{\theta}_2 sin(\theta_2+\theta_4+\theta_5-\theta_6)+5.2501\times10^{-7}\dot{\theta}_2 sin(\theta_2+\theta_4+\theta_5-2\theta_6) \\
& +5.2501\times10^{-7}\dot{\theta}_2 sin(\theta_2+\theta_4+\theta_5+2\theta_6)+6.8831\times10^{-6}\dot{\theta}_4 sin(\theta_2+\theta_4+\theta_5-\theta_6) \\
& +5.2501\times10^{-7}\dot{\theta}_4 sin(\theta_2+\theta_4+\theta_5-2\theta_6)+5.2501\times10^{-7}\dot{\theta}_4 sin(\theta_2+\theta_4+\theta_5+2\theta_6) \\
& -7.5304\times10^{-7}\dot{\theta}_4 sin(2\theta_2+\theta_4+\theta_5+\theta_6)+6.8831\times10^{-6}\dot{\theta}_5 sin(\theta_2+\theta_4+\theta_5-\theta_6) \\
& +5.2501\times10^{-7}\dot{\theta}_5 sin(\theta_2+\theta_4+\theta_5-2\theta_6)+5.2501\times10^{-7}\dot{\theta}_5 sin(\theta_2+\theta_4+\theta_5+2\theta_6) \\
& -7.5304\times10^{-7}\dot{\theta}_5 sin(2\theta_2+\theta_4+\theta_5+\theta_6)-4.3027\times10^{-6}\dot{\theta}_6 sin(\theta_2+\theta_4+\theta_5-\theta_6) \\
& -7.5304\times10^{-7}\dot{\theta}_6 sin(2\theta_2+\theta_4+\theta_5+\theta_6)-1.3731\times10^{-6}\dot{\theta}_2 cos(\theta_2-\theta_6) \\
& -1.5061\times10^{-6}\dot{\theta}_2 cos(2\theta_2+\theta_6)+6.5153\times10^{-6}\dot{\theta}_3 cos(\theta_2-\theta_6) \\
& -1.3731\times10^{-6}\dot{\theta}_6 cos(\theta_2-\theta_6)+7.5304\times10^{-7}\dot{\theta}_6 cos(2\theta_2+\theta_6) \\
& +8.399\times10^{-6}\dot{\theta}_2 sin(\theta_2-\theta_6)-2.3139\times10^{-6}\dot{\theta}_2 sin(2\theta_2+\theta_6)-\dot{\theta}_3 sin(\theta_2-\theta_6) \\
& +8.399\times10^{-6}\dot{\theta}_6 sin(\theta_2-\theta_6)+1.157\times10^{-6}\dot{\theta}_6 sin(2\theta_2+\theta_6) \\
& +2.8005\times10^{-6}\dot{\theta}_2 cos(\theta_2+\theta_4+\theta_5+\theta_6)+2.8005\times10^{-6}\dot{\theta}_4 cos(\theta_2+\theta_4+\theta_5+\theta_6) \\
& +2.8005\times10^{-6}\dot{\theta}_5 cos(\theta_2+\theta_4+\theta_5+\theta_6)+4.4801\times10^{-6}\dot{\theta}_6 cos(\theta_2+\theta_4+\theta_5+\theta_6) \\
& -\dot{\theta}_1(4.1988\times10^{-7} cos(2\theta_2+2\theta_4+2\theta_5-\theta_6) \\
& +2.9645\times10^{-7} cos(2\theta_2+2\theta_4+2\theta_5-2\theta_6) \\
& +2.9645\times10^{-7} cos(2\theta_2+2\theta_4+2\theta_5+2\theta_6)-6.4509\times10^{-7} sin(2\theta_2+2\theta_4+2\theta_5-\theta_6) \\
& -1.3125\times10^{-7} sin(2\theta_2+2\theta_4+2\theta_5-2\theta_6)+1.3125\times10^{-7} sin(2\theta_2+2\theta_4+2\theta_5+2\theta_6) \\
& +6.8654\times10^{-7} cos(\theta_4+\theta_5+\theta_6)+4.1995\times10^{-6} sin(\theta_4+\theta_5+\theta_6) \\
& +3.7652\times10^{-7} cos(\theta_4-\theta_2+\theta_5+\theta_6)-3.562\times10^{-6} cos(2\theta_2+\theta_4+\theta_5+\theta_6) \\
& +5.7848\times10^{-7} sin(\theta_4-\theta_2+\theta_5+\theta_6)-2.3279\times10^{-6} sin(2\theta_2+\theta_4+\theta_5+\theta_6) \\
& +2.3139\times10^{-6} cos(\theta_2-\theta_6)-3.7652\times10^{-7} cos(3\theta_2+\theta_4+\theta_5+\theta_6) \\
& +1.5061\times10^{-6} sin(\theta_2-\theta_6)-5.7848\times10^{-7} sin(3\theta_2+\theta_4+\theta_5+\theta_6) \\
& -4.1988\times10^{-7} cos(2\theta_2+2\theta_4+2\theta_5+\theta_6)-5.9289\times10^{-7} cos(2\theta_6) \\
& -6.4509\times10^{-7} sin(2\theta_2+2\theta_4+2\theta_5+\theta_6)-2.625\times10^{-7} sin(2\theta_6) \\
& -2.3139\times10^{-6} cos(\theta_2+\theta_6)+1.5061\times10^{-6} sin(\theta_2+\theta_6) \\
& -3.562\times10^{-6} cos(\theta_4+\theta_5-\theta_6)+2.3279\times10^{-6} sin(\theta_4+\theta_5-\theta_6) \\
& -3.7652\times10^{-7} cos(\theta_2-\theta_4-\theta_5+\theta_6)+6.8654\times10^{-7} cos(2\theta_2+\theta_4+\theta_5-\theta_6) \\
& -7.2806\times10^{-6} cos(\theta_6)-5.7848\times10^{-7} sin(\theta_2-\theta_4-\theta_5+\theta_6) \\
& -4.1995\times10^{-6} sin(2\theta_2+\theta_4+\theta_5-\theta_6)-1.1186\times10^{-5} sin(\theta_6) \\
& +3.7652\times10^{-7} cos(3\theta_2+\theta_4+\theta_5-\theta_6)-5.7848\times10^{-7} sin(3\theta_2+\theta_4+\theta_5-\theta_6) \\
& -3.2577\times10^{-6}\theta_3 sin(2\theta_2+\theta_4+\theta_5+\theta_6)+5.005\times10^{-6}\theta_3 cos(\theta_4+\theta_5-\theta_6) \\
& +3.2577\times10^{-6}\theta_3 sin(\theta_4+\theta_5-\theta_6)+5.005\times10^{-6}\theta_3 cos(2\theta_2+\theta_4+\theta_5-\theta_6) \\
& +3.2577\times10^{-6}\theta_3 sin(2\theta_2+\theta_4+\theta_5-\theta_6)+5.005\times10^{-6}\theta_3 cos(\theta_4+\theta_5+\theta_6) \\
& -3.2577\times10^{-6}\theta_3 sin(\theta_4+\theta_5+\theta_6)+5.005\times10^{-6}\theta_3 cos(2\theta_2+\theta_4+\theta_5+\theta_6)) \\
& +4.3027\times10^{-6}\dot{\theta}_2 sin(\theta_2+\theta_4+\theta_5+\theta_6)+4.3027\times10^{-6}\dot{\theta}_4 sin(\theta_2+\theta_4+\theta_5+\theta_6) \\
& +4.3027\times10^{-6}\dot{\theta}_5 sin(\theta_2+\theta_4+\theta_5+\theta_6)+6.8831\times10^{-6}\dot{\theta}_6 sin(\theta_2+\theta_4+\theta_5+\theta_6) \\
& -7.124\times10^{-6}\dot{\theta}_2 cos(\theta_2+\theta_6)+6.5153\times10^{-6}\dot{\theta}_3 cos(\theta_2+\theta_6) \\
& +7.124\times10^{-6}\dot{\theta}_6 cos(\theta_2+\theta_6)-4.6558\times10^{-6}\dot{\theta}_2 sin(\theta_2+\theta_6)+\dot{\theta}_3 sin(\theta_2+\theta_6) \\
& +4.6558\times10^{-6}\dot{\theta}_6 sin(\theta_2+\theta_6)-2.3139\times10^{-6}\dot{\theta}_2 cos(\theta_4+\theta_5-\theta_6) \\
& -1.157\times10^{-6}\dot{\theta}_4 cos(\theta_4+\theta_5-\theta_6)-1.157\times10^{-6}\dot{\theta}_5 cos(\theta_4+\theta_5-\theta_6) \\
& +1.157\times10^{-6}\dot{\theta}_6 cos(\theta_4+\theta_5-\theta_6)-1.5061\times10^{-6}\dot{\theta}_2 sin(\theta_4+\theta_5-\theta_6) \\
& -7.5304\times10^{-7}\dot{\theta}_4 sin(\theta_4+\theta_5-\theta_6)-7.5304\times10^{-7}\dot{\theta}_5 sin(\theta_4+\theta_5-\theta_6)
\end{aligned}
$$

$$
\begin{aligned}
&+7.5304\times10^{-7}\dot{\theta}_6 sin(\theta_4+\theta_5-\theta_6)+1.157\times10^{-6}\dot{\theta}_4 cos(2\theta_2+\theta_4+\theta_5-\theta_6)\\
&+1.157\times10^{-6}\dot{\theta}_5 cos(2\theta_2+\theta_4+\theta_5-\theta_6)-1.157\times10^{-6}\dot{\theta}_6 cos(2\theta_2+\theta_4+\theta_5-\theta_6)\\
&+7.5304\times10^{-7}\dot{\theta}_4 sin(2\theta_2+\theta_4+\theta_5-\theta_6)+7.5304\times10^{-7}\dot{\theta}_5 sin(2\theta_2+\theta_4+\theta_5-\theta_6)\\
&-7.5304\times10^{-7}\dot{\theta}_6 sin(2\theta_2+\theta_4+\theta_5-\theta_6)-1.5061\times10^{-6}\dot{\theta}_2 cos(2\theta_2-\theta_6)\\
&-7.5304\times10^{-7}\dot{\theta}_6 cos(2\theta_2-\theta_6)+2.3139\times10^{-6}\dot{\theta}_2 sin(2\theta_2-\theta_6)\\
&+1.157\times10^{-6}\dot{\theta}_6 sin(2\theta_2-\theta_6)-2.3139\times10^{-6}\dot{\theta}_2 cos(\theta_4+\theta_5+\theta_6)\\
&-1.157\times10^{-6}\dot{\theta}_4 cos(\theta_4+\theta_5+\theta_6)-1.157\times10^{-6}\dot{\theta}_5 cos(\theta_4+\theta_5+\theta_6)\\
&-1.157\times10^{-6}\dot{\theta}_6 cos(\theta_4+\theta_5+\theta_6)+1.5061\times10^{-6}\dot{\theta}_2 sin(\theta_4+\theta_5+\theta_6)\\
&+7.5304\times10^{-7}\dot{\theta}_4 sin(\theta_4+\theta_5+\theta_6)+7.5304\times10^{-7}\dot{\theta}_5 sin(\theta_4+\theta_5+\theta_6)\\
&+7.5304\times10^{-7}\dot{\theta}_6 sin(\theta_4+\theta_5+\theta_6)-4.4801\times10^{-6}\dot{\theta}_2 cos(\theta_2+\theta_4+\theta_5-\theta_6)\\
&-1.1858\times10^{-6}\dot{\theta}_2 cos(\theta_2+\theta_4+\theta_5-2\theta_6)+1.1858\times10^{-6}\dot{\theta}_2 cos(\theta_2+\theta_4+\theta_5+2\theta_6)\\
&-4.4801\times10^{-6}\dot{\theta}_4 cos(\theta_2+\theta_4+\theta_5-\theta_6)-1.1858\times10^{-6}\dot{\theta}_4 cos(\theta_2+\theta_4+\theta_5-2\theta_6)\\
&+1.1858\times10^{-6}\dot{\theta}_4 cos(\theta_2+\theta_4+\theta_5+2\theta_6)+1.157\times10^{-6}\dot{\theta}_4 cos(2\theta_2+\theta_4+\theta_5+\theta_6)\\
&-4.4801\times10^{-6}\dot{\theta}_5 cos(\theta_2+\theta_4+\theta_5-\theta_6)-1.1858\times10^{-6}\dot{\theta}_5 cos(\theta_2+\theta_4+\theta_5-2\theta_6)\\
&+1.1858\times10^{-6}\dot{\theta}_5 cos(\theta_2+\theta_4+\theta_5+2\theta_6)+1.157\times10^{-6}\dot{\theta}_5 cos(2\theta_2+\theta_4+\theta_5+\theta_6)\\
&+2.8005\times10^{-6}\dot{\theta}_6 cos(\theta_2+\theta_4+\theta_5-\theta_6)+1.157\times10^{-6}\dot{\theta}_6 cos(2\theta_2+\theta_4+\theta_5+\theta_6)\\
&-\theta_3\dot{\theta}_2 cos(\theta_2-\theta_6)-\theta_3\dot{\theta}_6 cos(\theta_2-\theta_6)-6.5153\times10^{-6}\theta_3\dot{\theta}_2 sin(\theta_2-\theta_6)\\
&-6.5153\times10^{-6}\theta_3\dot{\theta}_6 sin(\theta_2-\theta_6)+\theta_3\dot{\theta}_2 cos(\theta_2+\theta_6)-\theta_3\dot{\theta}_6 cos(\theta_2+\theta_6)\\
&-6.5153\times10^{-6}\theta_3\dot{\theta}_2 sin(\theta_2+\theta_6)+6.5153\times10^{-6}\theta_3\dot{\theta}_6 sin(\theta_2+\theta_6)\\
Fb_2=\ &1.5061\times10^{-6}\dot{\theta}_6 sin(\theta_2+\theta_6)-2.3139\times10^{-6}\dot{\theta}_5 sin(\theta_4-\theta_2+\theta_5+\theta_6)\\
&-2.3139\times10^{-6}\dot{\theta}_6 sin(\theta_4-\theta_2+\theta_5+\theta_6)-2.3139\times10^{-6}\dot{\theta}_6 cos(\theta_2-\theta_6)\\
&-1.5061\times10^{-6}\dot{\theta}_6 sin(\theta_2-\theta_6)-2.3716\times10^{-6}\dot{\theta}_4 cos(2\theta_6)\\
&-2.3716\times10^{-6}\dot{\theta}_5 cos(2\theta_6)-1.05\times10^{-6}\dot{\theta}_4 sin(2\theta_6)-1.05\times10^{-6}\dot{\theta}_5 sin(2\theta_6)\\
&-\dot{\theta}_2(1.3731\times10^{-6} cos(\theta_4+\theta_5+\theta_6)+8.399\times10^{-6} sin(\theta_4+\theta_5+\theta_6)\\
&+1.5061\times10^{-6} cos(\theta_4-\theta_2+\theta_5+\theta_6)+2.3139\times10^{-6} sin(\theta_4-\theta_2+\theta_5+\theta_6)\\
&+1.1858\times10^{-6} cos(2\theta_6)+5.2501\times10^{-7} sin(2\theta_6)-7.124\times10^{-6} cos(\theta_4+\theta_5-\theta_6)\\
&+4.6558\times10^{-6} sin(\theta_4+\theta_5-\theta_6)-1.5061\times10^{-6} cos(\theta_2-\theta_4-\theta_5+\theta_6)\\
&-2.3139\times10^{-6} sin(\theta_2-\theta_4-\theta_5+\theta_6)+1.001\times10^{-5}\theta_3 cos(\theta_4+\theta_5-\theta_6)\\
&+6.5153\times10^{-6}\theta_3 sin(\theta_4+\theta_5-\theta_6)+1.001\times10^{-5}\theta_3 cos(\theta_4+\theta_5+\theta_6)\\
&-6.5153\times10^{-6}\theta_3 sin(\theta_4+\theta_5+\theta_6))-2.3139\times10^{-6}\dot{\theta}_6 cos(\theta_2+\theta_6)\\
&-2.3139\times10^{-6}\dot{\theta}_4 sin(\theta_4-\theta_2+\theta_5+\theta_6)-6.5153\times10^{-6}\dot{\theta}_3 cos(\theta_4+\theta_5-\theta_6)\\
&+7.124\times10^{-6}\dot{\theta}_4 cos(\theta_4+\theta_5-\theta_6)+7.124\times10^{-6}\dot{\theta}_5 cos(\theta_4+\theta_5-\theta_6)\\
&-7.124\times10^{-6}\dot{\theta}_6 cos(\theta_4+\theta_5-\theta_6)+1.001\times10^{-5}\dot{\theta}_3 sin(\theta_4+\theta_5-\theta_6)\\
&-4.6558\times10^{-6}\dot{\theta}_4 sin(\theta_4+\theta_5-\theta_6)-4.6558\times10^{-6}\dot{\theta}_5 sin(\theta_4+\theta_5-\theta_6)\\
&+4.6558\times10^{-6}\dot{\theta}_6 sin(\theta_4+\theta_5-\theta_6)+1.5061\times10^{-6}\dot{\theta}_4 cos(\theta_2-\theta_4-\theta_5+\theta_6)\\
&+1.5061\times10^{-6}\dot{\theta}_5 cos(\theta_2-\theta_4-\theta_5+\theta_6)-1.5061\times10^{-6}\dot{\theta}_6 cos(\theta_2-\theta_4-\theta_5+\theta_6)\\
&-1.6795\times10^{-6}\dot{\theta}_6 cos(\theta_6)+2.3139\times10^{-6}\dot{\theta}_4 sin(\theta_2-\theta_4-\theta_5+\theta_6)\\
&+2.3139\times10^{-6}\dot{\theta}_5 sin(\theta_2-\theta_4-\theta_5+\theta_6)-2.3139\times10^{-6}\dot{\theta}_6 sin(\theta_2-\theta_4-\theta_5+\theta_6)\\
&-2.5804\times10^{-6}\dot{\theta}_6 sin(\theta_6)+6.5153\times10^{-6}\dot{\theta}_3 cos(\theta_4+\theta_5+\theta_6)\\
&-1.3731\times10^{-6}\dot{\theta}_4 cos(\theta_4+\theta_5+\theta_6)-1.3731\times10^{-6}\dot{\theta}_5 cos(\theta_4+\theta_5+\theta_6)\\
&-1.3731\times10^{-6}\dot{\theta}_6 cos(\theta_4+\theta_5+\theta_6)+1.001\times10^{-5}\dot{\theta}_3 sin(\theta_4+\theta_5+\theta_6)\\
&-8.399\times10^{-6}\dot{\theta}_4 sin(\theta_4+\theta_5+\theta_6)-8.399\times10^{-6}\dot{\theta}_5 sin(\theta_4+\theta_5+\theta_6)
\end{aligned}
$$

$$
\begin{aligned}
&-8.399\times10^{-6}\dot{\theta}_6 sin(\theta_4+\theta_5+\theta_6)-1.5061\times10^{-6}\dot{\theta}_4 cos(\theta_4-\theta_2+\theta_5+\theta_6)\\
&-1.5061\times10^{-6}\dot{\theta}_5 cos(\theta_4-\theta_2+\theta_5+\theta_6)-1.5061\times10^{-6}\dot{\theta}_6 cos(\theta_4-\theta_2+\theta_5+\theta_6)\\
&-6.5153\times10^{-6}\theta_3\dot{\theta}_4 sin(\theta_4+\theta_5-\theta_6)-6.5153\times10^{-6}\theta_3\dot{\theta}_5 sin(\theta_4+\theta_5-\theta_6)\\
&+6.5153\times10^{-6}\theta_3\dot{\theta}_6 sin(\theta_4+\theta_5-\theta_6)-1.001\times10^{-5}\theta_3\dot{\theta}_4 cos(\theta_4+\theta_5+\theta_6)\\
&-1.001\times10^{-5}\theta_3\dot{\theta}_5 cos(\theta_4+\theta_5+\theta_6)-1.001\times10^{-5}\theta_3\dot{\theta}_6 cos(\theta_4+\theta_5+\theta_6)\\
&+6.5153\times10^{-6}\theta_3\dot{\theta}_4 sin(\theta_4+\theta_5+\theta_6)+6.5153\times10^{-6}\theta_3\dot{\theta}_5 sin(\theta_4+\theta_5+\theta_6)\\
&+6.5153\times10^{-6}\theta_3\dot{\theta}_6 sin(\theta_4+\theta_5+\theta_6)-1.001\times10^{-5}\theta_3\dot{\theta}_4 cos(\theta_4+\theta_5-\theta_6)\\
&-1.001\times10^{-5}\theta_3\dot{\theta}_5 cos(\theta_4+\theta_5-\theta_6)+1.001\times10^{-5}\theta_3\dot{\theta}_6 cos(\theta_4+\theta_5-\theta_6)
\end{aligned}
$$

$$
\begin{aligned}
Fc_2 = {} & 6.5153\times10^{-6}\dot{\theta}_6 cos(\theta_4+\theta_5-\theta_6)-6.5153\times10^{-6}\dot{\theta}_5 cos(\theta_4+\theta_5-\theta_6)\\
&-6.5153\times10^{-6}\dot{\theta}_4 cos(\theta_4+\theta_5-\theta_6)+1.001\times10^{-5}\dot{\theta}_4 sin(\theta_4+\theta_5-\theta_6)\\
&+1.001\times10^{-5}\dot{\theta}_5 sin(\theta_4+\theta_5-\theta_6)-1.001\times10^{-5}\dot{\theta}_6 sin(\theta_4+\theta_5-\theta_6)\\
&+6.5153\times10^{-6}\dot{\theta}_4 cos(\theta_4+\theta_5+\theta_6)+6.5153\times10^{-6}\dot{\theta}_5 cos(\theta_4+\theta_5+\theta_6)\\
&+6.5153\times10^{-6}\dot{\theta}_6 cos(\theta_4+\theta_5+\theta_6)+1.001\times10^{-5}\dot{\theta}_4 sin(\theta_4+\theta_5+\theta_6)\\
&+1.001\times10^{-5}\dot{\theta}_5 sin(\theta_4+\theta_5+\theta_6)+1.001\times10^{-5}\dot{\theta}_6 sin(\theta_4+\theta_5+\theta_6)
\end{aligned}
$$

$$
\begin{aligned}
Fd_2 = {} & -2.3716\times10^{-6}\dot{\theta}_5 cos(2\theta_6)-1.05\times10^{-6}\dot{\theta}_5 sin(2\theta_6)-\dot{\theta}_4(1.1858\times10^{-6} cos(2\theta_6)\\
&+5.2501\times10^{-7} sin(2\theta_6))-1.6795\times10^{-6}\dot{\theta}_6 cos(\theta_6)-2.5804\times10^{-6}\dot{\theta}_6 sin(\theta_6)
\end{aligned}
$$

$$
Fe_2 = -1.1858\times10^{-6} cos(2\theta_6)-5.2501\times10^{-7} sin(2\theta_6)
$$

$$
Ff_2 = -1.6795\times10^{-6} cos(\theta_6)-2.5804\times10^{-6} sin(\theta_6)
$$

$$
\begin{aligned}
A = {} & 7.5\times10^{-12} cos(2\theta_2-\theta_1+2\theta_4+2\theta_5)+2.375\times10^{-11} sin(2\theta_2-2\theta_1+2\theta_4+2\theta_5)\\
&-2.375\times10^{-11} sin(2\theta_1+2\theta_2+2\theta_4+2\theta_5)-7.5\times10^{-12} cos(\theta_1+2\theta_2+2\theta_4+2\theta_5)\\
&+4.75\times10^{-11} sin(2\theta_1)
\end{aligned}
$$

$$
\begin{aligned}
B = D = E = {} & -1.8325\times10^{-9} sin(2\theta_2+2\theta_4+2\theta_5)-1.5\times10^{-11} cos(2\theta_2-\theta_1+2\theta_4+2\theta_5)\\
&-2.375\times10^{-11} sin(2\theta_2-2\theta_1+2\theta_4+2\theta_5)\\
&-2.375\times10^{-11} sin(2\theta_1+2\theta_2+2\theta_4+2\theta_5)-1.5\times10^{-11} cos(\theta_1+2\theta_2+2\theta_4+2\theta_5)
\end{aligned}
$$

$$
Ac_2 = Af_2 = Cc_2 = Bf_2 = Cc_2 = Df_2 = Ef_2 = C = F = 0
$$